ROLE OF DAMAGE AND DAMAGE GROWTH ON DYNAMIC LOAD TRANSFER IN PARTICULATE MEDIA

(Final Report)

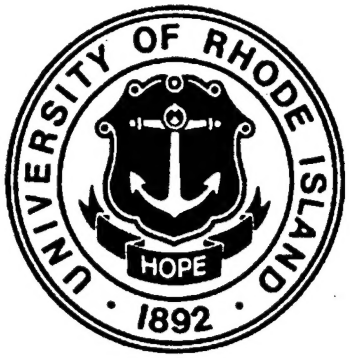

by

Arun Shukla and Martin H. Sadd

Prepared for U.S. Air Force Office of Scientific Research
Under Contract No. F49620-93-1-0475
Bolling Air Force Base

Department of Mechanical Engineering and Applied Mechanics
University of Rhode Island
Kingston, RI 02881

September 1997

REPORT DOCUMENTATION PAGE

Form Approved
OMB No. 0704-0188

1. AGENCY USE ONLY (Leave blank)	2. REPORT DATE	3. REPORT TYPE AND DATES COVERED
	9/30/97	Final, July 93 to August 97

4. TITLE AND SUBTITLE

Role of Damage and Damage Growth on Dynamic Load Transfer in Particulate Media

5. FUNDING NUMBERS

F496209310475

6. AUTHOR(S)

Arun Shukla and Martin H. Sadd

7. PERFORMING ORGANIZATION NAME(S) AND ADDRESS(ES)

Department of Mechanical Engineering
and Applied Mechanics
University of Rhode Island
Kingston, Rhode Island 02881

8. PERFORMING ORGANIZATION REPORT NUMBER

AFOSR97

9. SPONSORING/MONITORING AGENCY NAME(S) AND ADDRESS(ES)

Air Force Office of Scientific Research
Particulate Mechanics Program
Bolling Air Force Base
Washington, DC 20332

10. SPONSORING/MONITORING AGENCY REPORT NUMBER

11. SUPPLEMENTARY NOTES

12a. DISTRIBUTION/AVAILABILITY STATEMENT

Approved for public release: Distribution is unlimited.

12b. DISTRIBUTION CODE

13. ABSTRACT *(Maximum 200 words)*

An experimental study was conducted to investigate dynamic load transfer and wave propagation in particulate assemblies containing damaged particles. The assembly was simulated by a one-dimensional array of circular disks, and the damage itself, by a natural crack or drilled holes. The assembly was explosively loaded and the dynamic load transfer process observed using dynamic photoelasticity and strain gages. Attention was focused on the influence of damage size and orientation on the group wave velocity, wave dispersion, and peak contact load attenuation of the stress wave pulse Damage growth occurring from the interaction of the stress wave with the crack tip was also studied. The results demonstrate that the inclusion of a damaged particle greatly influences the load transfer process, both locally and in the far field. The degree to which the damaged particle modified the load transfer process is more dependent upon the orientation of the crack than upon the size of the crack. Moreover, damage growth within the damaged partices is also a strong function of the orientation of the crack. Experiments with drilled disks showed that the stress wave propagation was influenced by the amount as well as the orientation of the pores.

14. SUBJECT TERMS	15. NUMBER OF PAGES
Particulate media, wave propagation, dynamic contact load, dynamic photoelasticity, wave velocity, explosive loading, straingage, damage growth.	137
	16. PRICE CODE

17. SECURITY CLASSIFICATION OF REPORT	18. SECURITY CLASSIFICATION OF THIS PAGE	19. SECURITY CLASSIFICATION OF ABSTRACT	20. LIMITATION OF ABSTRACT
Unclassified	Unclassified	Unclassified	

TABLE OF CONTENTS

CHAPTER 1

EFFECT OF FLAWS ON THE STRESS WAVE PROPAGATION IN PARTICULATE AGGREGATES: NEAR AND FAR FIELD OBSERVATIONS.

ABSTRACT

An experimental study is conducted using dynamic photoelasticity and strain gage techniques to investigate transient stress fields in aggregate assemblies of circular disks. In particular, attention is focused on the effect of damage and damage growth in the particles on the dynamic load transfer process. The experimental data is analyzed to obtain the wave velocity, contact load profiles, peak load attenuation, wave dispersion and other changes in the stress fields as the dynamic load transfer process takes place. Both near and far field effects due to the presence of a flaw on the load transfer process are studied. The results show that the size and the orientation of the flaw greatly influences the load transfer process locally. However, in the far field the flaw only affects the attenuation of the peak loads without changing the wavelength of the loading pulse.

1.1 INTRODUCTION

A granular medium is discrete in nature, and its response under the application of explosive loading is a highly complex dynamic process involving the local microstructural arrangement of particles, their material properties and the contact mechanisms. These processes are best studied by performing simple controlled experiments in which the load transfer information is obtained for the whole assembly of particles and then using this information to develop numerical codes to predict load-time history in more complex assemblies. This paper describes the experimental portion of this study and investigates the dynamic load transfer process in granular assemblies where particle damage is present and/or created during the wave propagation process. Damage in particulate media is interpreted as varying from small amounts of surface damage to the more severe case of particle fracture into two or more pieces. Slight surface damage produces negligible changes in the inter-particle dynamic contact response between adjacent grains. For the more severe cases of larger damage zones or of granular fracture, considerable effects are noted in the attenuation rate since propagational energy is dissipated in the fracture process through the creation of new surfaces and in diffusion of particulate kinetic energy, also, some of the energy is reflected back from the free

surfaces of the open flaws.

The study of wave propagation in granular media is interesting because of its importance to many areas of technology such as soil mechanics, earthquake engineering, powder metallurgy and vibration isolation systems. Investigators have utilized aggregate assemblies of elastic particles interacting through contact mechanisms to model granular materials such as sand, rock, etc. Early work by Iida (1939), Takahashi and Sato (1949), Hughes and Cross (1952), Gassman (1951), and Brant (1952) employed a normal contact force concept, while Duffy and Mindlin (1957) included tangential forces as well. Some of the recent work in this field includes that of Thornton (1985), Zhu et. al. (1991), Dvorkin et. al. (1991), Ting and Corkum (1992), Shukla et. al. (1993), and Sadd et. al. (1993). Results of their efforts have led to initial attempts at predicting stress wave propagation in granular media. However, very few studies have been conducted to investigate media damage as it relates to wave propagation. Shin and Karr (1991) presented a one-dimensional wave propagation study of a viscoelastic medium with a continuum damage evolution model used for boundary and transgranular cracking of polycrystalline ice. A collection of articles in a book edited by Rossmanith (1983) outlines wave propagation in damaged blocky materials. Nonetheless little quantitative information exists on dynamic load transfer in damaged particulate materials.

This paper focuses on the effect of open flaws in particles on the dynamic load transfer process in particulate aggregates. Both dynamic photoelasticity and strain gages are utilized to collect stress and strain information in the bulk of the material and at contact points. The effect of flaws on the group wave propagating in the assembly is evaluated in terms of the peak contact load attenuation and wave dispersion. The results elucidate some of the basic mechanisms of energy dissipation and redistribution during the interaction of stress waves with flaws in particles.

1.2 PHOTOELASTIC EXPERIMENTS

1.2.1 Experimental Procedure

A series of experiments was conducted on single chain assemblies of circular disks which were dynamically loaded by detonating a small amount of explosive lead azide directly on top of the assembly. Figure 1.1 shows such an assembly along with the explosive charge holder. The disks were machined from a brittle, transparent polyester material, Homalite 100, which is birefringent and ideally suited for photoelastic studies. One or more disks with flaws were included in the chain. The flaw was simulated by an "open crack" which was machined using a band-saw. The assembly was

placed in the optical bench of a multiple-spark, high-speed camera. An explosive charge of 20 mg was detonated in a specially designed charge holder. The camera was synchronized to record photographs after a predetermined time from the explosion. A series of intense flashes of light are generated by the camera providing twenty images during the experiment. A typical set of photographs obtained for a single chain assembly with no cracked disk, using this technique, is shown in figure 1.2. During the experiments the size and orientation of the crack was varied, and their effects on the wave propagation process studied.

1.2.2 Analysis Procedure

The experimental data obtained were analyzed using the stress field equations developed by Smith and Liu (1953) coupled with a multipoint non-linear numerical technique proposed by Shukla and Nigam (1985). This technique uses full-field photoelastic data to evaluate the contact stresses and the contact area by utilizing the method of least squares in conjunction with the Newton-Raphson method.

As shown in the coordinate system, provided in figure 1.1, the disk is subjected to a normal distributed load of P Newtons per unit length, which presses it against another disk over a narrow area of contact whose width is *2b*. A lateral distributed load of f Newtons per unit length is also applied to the body. Let P be defined as the friction factor such that f=PP. P will be the coefficient of friction if motion impends. Neglecting far field effects, the stresses a., CY. and (Y. for points close to the contact are given by,

$$\sigma_{zz} = -\frac{b}{\pi\Delta}\left[z\left(b\phi_1 - x\phi_2\right) + \beta z^2\phi_2\right] \tag{1.1}$$

$$\sigma_{xx} = -\frac{b}{\pi\Delta}\left\{z\left(\frac{b^2 + 2z^2 + 2x^2}{b}\phi_1 - \frac{2\pi}{b} - 3x\phi_2\right) + \beta\left[\left(2x^2 - 2b^2 - 2z^2\right)\phi_2 + \frac{2\pi}{b}x + 2x\frac{\left(b^2 - x^2 - z\right)}{b}\phi_2\right]\right\} \tag{1.2}$$

$$\sigma_{xz} = -\frac{b}{\pi\Delta}\left\{z^2\phi_2 + \beta\left[\left(b^2 + 2x^2 + 2z^2\right)\frac{z}{b}\phi_1 - \frac{2\pi}{b}z - 3xz\phi_2\right]\right\} \qquad (1.3)$$

where ϕ_1 and ϕ_2 are

$$\phi_1 = \frac{\pi(M + N)}{MN\sqrt{2MN + 2x^2 + 2z^2 - 2b^2}}, \qquad \phi_2 = \frac{\pi(M - N)}{MN\sqrt{2MN + 2x^2 + 2z^2 - 2b^2}}$$

$$M = \sqrt{(b + x)^2 + z^2}, \qquad N = \sqrt{(b - x)^2 + z^2} \qquad (1.4)$$

$$\Delta = 2R\left(\frac{1 - \nu^2}{E}\right)$$

where R is the Radius of Curvature at the point of contacts, E is the modulus of elasticity and ν is the Poisson's ratio. The two unknowns in the stress field equations are b and β. Other parameters depend on the geometry of the bodies, location coordinates and material properties. Equations (1.1), (2) and (3) are coupled with the stress optic law (Shukla and Nigam, 1985), and the two unknowns, namely the half contact length b and the friction factor β are obtained from the photoelastic data. The stresses thus obtained are integrated to give the contact loads. The wave velocity is obtained by plotting the stress wave front as a function of time. The wavelength of the stress wave pulse is obtained directly from the photographs as shown in figure 1.2. Wave dispersion information is obtained from the load-time profile. The experiment shown in figure 1.2 was used to compare with experiments with flawed particles.

1.3 STRAIN GAGE EXPERIMENTS

1.3.1 Experimental Procedure

Dynamic photoelasticity, in conjunction with high speed photography, allows for full-field visualization and analysis of the stress wave pulse. However, the limited field of view of the camera places restriction on the number of disks that can be observed in one experiment. Strain gages (MicroMeasurements: EA-13-031DE-120) were used to observe the far field effects of including a flawed particle in a long chain assembly of disks. The experimental setup is shown in figure 1.3. The single chain assembly of disks was loaded explosively as in the photoelastic experiments. Eight

separate strain gages, at various locations, were used to monitor the strains resulting from the stress wave propagating in the assembly. The first four strain gages were located at contact points around the cracked disk (disk # 13), as shown in figure 1.3. The other gages were located at various contacts further down the single chain assembly. Data collection and storage was accomplished by dynamic Ectron amplifiers and a LeCroy digital data acquisition system. The frequency response of these systems was adequate for the stress wave propagation experiments. Figure 1.4 shows the strains measured for a single chain assembly containing no flawed particles. This experiment also served as the baseline experiment, for comparison purposes.

1.3.2 Analysis Procedure

For the case of plane stress,

$$\epsilon_{zz} = \frac{1}{E}\left(\sigma_{zz} - \nu\sigma_{xx}\right) \tag{1.5}$$

Hence, from the stress field equations developed by Smith and Liu (1953), the strain, ε_{zz}, along the z-axis (x = 0) for $\beta = 0$, is given as,

$$\epsilon_{zz} = -\frac{1}{E}\left[\frac{(1 - \nu)b^2 - 2\nu z^2}{\Delta\sqrt{b^2 + z^2}} + \frac{2\nu z}{\Delta}\right] \tag{1.6}$$

Using strain gage data, the half contact length, b, is determined from equation 1.5. once this parameter is known, the stresses and the normal contact load are determined as discussed in section 2.2. The velocity and wavelength of the stress wave pulse are determined directly from the strain versus time data.

1.4 RESULTS AND DISCUSSIONS

The results obtained from the series of experiments to study the effect of damage and damage growth on dynamic load transfer in particulate media are discussed in the following sections.

1.4.1. Effect of crack length

A series of dynamic photoelastic experiments were conducted to observe the near field effects of crack length on the stress wave propagation through granular media. In all, three different crack lengths were used and each experiment contained a single flawed particle. The results from all these experiments were analyzed to study the effect of the crack length on dynamic load transfer characteristics, in particular, on the attenuation, dispersion and wave propagation speed. The crack length was varied from zero to seventy-five percent of the disk diameter in increments of twenty-five percent. In all of the cases, the cracked disk was oriented such that the crack was parallel to the tangent plane of contact.

Typical isochromatic fringes obtained for a single chain assembly with no cracked disk are shown in figure 1.2. These photographs were analyzed, and the contact load profiles obtained as a function of time, are shown in figure 1.5. As shown by this figure, the stress wave propagated through the assembly with no dispersion and negligible load attenuation. The average wave velocity and wavelength were determined to be 1050 m/s and four disk diameters respectively. Both remained constant throughout the propagation of the wave. Consequently each contact point was loaded for about 100 μs.

A series of typical isochromatic patterns obtained for the twenty-five, fifty and seventy five percent crack assemblies are shown in figures 1.6, 1.7 and 1.8, respectively. These photographs clearly indicate that the crack influenced stress wave propagation and also the stress field distribution within the cracked disk. However, the nature of the stress field in the uncracked disks was not affected, and the Hertz contact theory, as discussed before, could still be used for analysis. The contact load profiles obtained from these experiments are shown in figures 1.9, 1.10 and 1.11. The effect of the crack on the dynamic load transfer characteristics became more pronounced as the crack length was increased. The presence of a crack not only influenced existing load transfer mechanisms from particle to particle but also introduced some new mechanisms. Some of these effects are discussed in detail below.

As the stress wave encountered the cracked disk both reflection off the free surfaces of the open crack and scattering at the crack tip took place. When compressive parts of the stress wave pulse impinged on the free surface of the crack, they were reflected as tensile. These tensile reflections interacted with the preceding contact. As a result, part of the compressive loading at this contact was neutralized, and energy was transmitted back up the chain. This resulted in a 25 percent

attenuation in the contact load at the preceding contact (for the seventy five percent crack case) even before the pulse had propagated through the cracked disk. The energy transmitted back up the chain was observed as a back reflected pulse as shown in the 19th and 20th frames in figure 1.7.

The interaction of the stress wave with the crack also resulted in dynamic loading of the crack. The 19th frame in figure 1.7 shows typical isochromatic fringes in the cracked disk as one would expect for a crack under mode-1 loading. The dynamic nature of this loading was evident from the lack of any contact stresses between the cracked disk and its adjoining disks. For the seventy-five percent crack case, interaction of the stress wave with the crack resulted in extremely high stresses within the cracked disk as shown by the high density of isochromatic fringes in the 12th, 15th and 19th frames in figure 1.8. These high stresses resulted in crack closure causing the crack surfaces to come into contact. Rapid closure of the crack surface for two seventy-five percent crack experiments is plotted in figure 1.12. The crack closed to 80 percent of its total length at a rapid rate of 450 m/s. This crack closure speed is higher than the terminal crack speeds observed normally in this material. The crack remained partially closed for the duration of the experiment, and exhibited oscillations in the closure length. The oscillations were expected because of the oscillatory nature of the stress field. The crack behaved as a barrier, blocking the path of the stress wave pulse. As the crack closed, for example in the seventy-five percent crack case, some energy was allowed to transfer across the contacting crack surfaces. However, most of the stress wave was subjected to many more reflections within the cracked disk before it could reach the next contact point. These multiple reflections resulted in elongation of the stress wave pulse. As the pulse propagated through the cracked disk, it elongated from an input duration of 90 μs to a much greater duration. The complete elongated pulse was not observed in the photoelastic experiments because of the limited field of view of the camera. Varying the crack length had no effect on the average velocity of the stress wave pulse. This is consistent because the group wave velocity for a given particulate media depends primarily on the contact geometry.

A series of strain gage experiments was conducted with the same assemblies to observe wavelength elongation and peak load attenuation of the stress wave as it propagated through the cracked disk. Figure 1.13, 1.14 and 1.15 show the strain versus time plots for a single chain-assembly containing twenty-five, fifty and seventy-five percent cracked disks. Many new features were observed in these experiments. In addition, certain features observed in the photoelastic experiments were also confirmed, such as the presence of a strong back reflected pulse. The back

reflected pulses, for the seventy-five percent crack case, are shown in figures 1.15a and 1.15b. Similar features were observed in all the experiments. For brevity only the results from the seventy-five percent crack assembly are presented as follows.

As the stress wave pulse passed through the cracked disk (disk #13) many non linear stress wave effects were observed. The duration of the loading pulse was almost tripled from 120 μs to 330 μs. Moreover, the pulse profile immediately following the cracked disk was jagged and rough (see figure 1.15c) as compared to the smooth input pulse. The jaggedness of the pulse profile was a result of increased reflections that the stress wave was subjected to as it propagated through the cracked disk. These perturbations in the pulse were an indication of high frequency components now present in the wave profile. Some of these high frequency components were rapidly dissipated by the granular medium resulting in smoothening of the elongated pulse profile. This occurred as soon as the pulse propagated through a single disk, as evidenced by the much smoother pulse profile shown in figure 1.15d. The elongated pulse shown in figure 1.15d had a duration of 360 μs, which represented twelve disk diameters. As this elongated pulse propagated further, it quickly separated into four wavelets with average peak separations of 90 μs (see figures 1.15d, 1.15e and 1.15f). The separation of the elongated pulse into several wavelets was a result of redistribution of energy associated with a ringing phenomenon which produces oscillations within long wavelength pulse. During this redistribution of energy the primary wavelet gathered some of the energy from the elongated pulse and registered an increase in amplitude. The separation between the various wavelets increased with propagation distance as the wavelets traveled with different velocities. As shown in figure 1.16 the average velocity decreased from 950 m/s for the first wavelet to 760 m/s for the fourth wavelet. The separated wavelets had a specific wavelength to disk diameter ratio of about four, which was equivalent to the wavelength of the input pulse. This implies that this single chain assembly can support only those stress wave pulses that have a wavelength to disk diameter ratio of about four. Stress wave pulses with such a wavelength propagate with no dispersion and small attenuation. Whereas, longer wavelengths separate into wavelets with the same specific wavelength to disk diameter ratio of about four. With further propagation down the single chain assembly, the secondary wavelets were rapidly dissipated resulting in a far field stress wave pulse that resembled the input pulse. The property of a single chain assembly to support only those pulses with a specific wavelength to disk diameter ratio of four can be explained in terms of the modal characteristics of the granular medium. This phenomenon has been observed earlier and the details are presented by

Shukla et. al.(1993).

The inclusion of a cracked disk in the single chain assembly resulted in large far field attenuation of the peak contact load. Figure 1.17 shows the peak contact load attenuation as a function of distance propagated. The peak contact load attenuation increased from 20 percent for the no crack case to 55 percent for the seventy-five percent crack case in one meter distance of travel. This increase in attenuation was a result of energy being reflected back up the chain and energy being lost from the dissipation of secondary wavelets. Figure 1.17 also shows the local drop in the peak contact load due to pulse elongation and subsequent increase in the peak contact load associated with the ringing phenomenon.

The average velocity of the stress wave pulse was determined to be 950 m/s, for all the crack assemblies, which remained constant throughout the propagation of the stress wave pulse. This was in good agreement with the photoelastic data.

1.4.2. Effect of Crack Orientation

A series of dynamic photoelastic experiments was conducted to observe the near field effects of crack orientation on stress wave propagation through granular media. To investigate the dynamic load transfer characteristics, seven different single chain assemblies were studied. The crack orientation was varied from -90° to +90° in increments of 30°, where the angle was measured from the tangent plane of contact. In all the assemblies, the crack length was maintained constant at fifty percent of the disk diameter.

Typical isochromatic fringes obtained for the -60° and +60° crack orientations are shown in figures 18 and 19, respectively. As observed in earlier experiments, the presence of a crack influenced stress wave propagation through the assembly. However, in crack orientation assemblies, the relative angle of the crack with respect to the incoming stress wave pulse also influenced the interaction of the stress wave with the crack surfaces and the crack tip. For the +60° orientation, the incoming stress wave pulse interacted with the crack surface at grazing incidence, causing both longitudinal and shear waves to be reflected off the crack surface. The shear component in the reflections was substantial due to the specific angle of inclination of the crack. Interaction of these shear waves, with the preceding contact, resulted in an oscillatory shear loading at the contact as evident from the change in the tilt of the isochromatic fringes shown in figure 1.18. The shear loads at the preceding contact were calculated and are plotted in figure 1.20, for two separate experiments.

The magnitude of the shear loading was quite large with its peak value equal to about 20 percent of the peak normal load. The results also confirmed the oscillatory nature of the shear reflections coming back to the contact point. However, shear loading of the preceding contact was not observed for the -60° orientation case, because of the relative angle of impingement of the stress wave with the crack surfaces.

Interaction of the stress wave pulse with the crack resulted in loading of the crack tip. However, unlike the horizontal case experiments the angled cracks were subjected to mixed mode loading, as observed from the crack tip isochromatic fringes in figures 18 and 19. Moreover, the relative angle of the crack, with respect to the stress wave pulse, governed the nature of stresses at the crack tip. For cracks oriented away from the incoming stress wave pulse, as for the +60° case, most of the reflections occurred only from one surface of the open crack. However, for cracks oriented towards the incoming stress wave pulse, as for the -60° case, reflections occurred from both crack surfaces. Also the more direct impingement of the stress wave on the crack tip for the -60° case, resulted in sufficiently high tensile stresses at the crack tip to cause crack growth, as shown in the 9^{th}, 10^{th} and 11^{th} frames in figure 1.19. The crack in this case was initiated even before the peak of the stress wave pulse had reached the cracked disk. The average crack velocity was determined to be 260 m/s. Post experimental observations indicated a smooth crack surface, which corresponds to a dynamic stress intensity factor, KID, of about 0.5 MPa%rm, for this material. The energy dissipated in the growth of this crack was determined to be 7 x 10-3 J, which was at least an order of magnitude lower than the total energy of the stress wave pulse. Thus, even though crack growth did not result in significant energy dissipation, it caused significant microstructural changes in the granular medium. As shown in the 16^{th} and 20^{th} frames in figure 1.19, the fractured particle had already separated from the single chain assembly by rigid body motion even before the pulse had propagated through the single chain assembly. The various features discussed above were also observed, to a lesser degree, for the +30° and -30° crack orientations. For the sake of brevity, the results from these experiments are not presented.

Despite the new features introduced as a result of varying the crack angle, the nature of the stress field in the uncracked disks was not affected, and the Hertz contact theory could still be used for analysis. The contact load profiles obtained for the +60° and -60° crack orientation experiments are shown in figures 21 and 22, respectively. Cracks oriented away from the incoming stress wave pulse returned more energy up the single chain assembly than cracks oriented towards the incoming

stress wave pulse. This resulted in a 25 percent attenuation in the peak contact load at the preceding contact for the +60° case compared to only 5 percent for the 60° case. The energy reflected back up the chain was also observed as a back reflected pulse as shown in the 16th and 20th frames in figure 1.19.

The crack orientations of +90° and -90° represented special cases of the angled crack experiments. The cracks in these cases were oriented such that one of the contacts occurred at the open end of the crack resulting in a two-point contact. Consequently energy transfer across this contact occurred via two separate paths, as shown in the 1st frame in figure 1.23 and the 9th frame in figure 1.24. Moreover, as the crack surfaces were oriented along the direction of the incoming stress wave pulse, the direct reflections off the crack surfaces were minimized. The stress wave pulse impinged on the crack surfaces only after reflecting off the free boundaries of the cracked disk. These reflections were tensile in nature and were neutralized by the incoming compressive stress wave pulse. Consequently, the crack tips were not loaded until most of the stress wave pulse had propagated through the cracked disk, as shown in figures 23 and 24. After the stress wave pulse had passed through the cracked disk the tensile reflections became dominant causing opening mode loading of the crack tip and subsequent crack growth. Such crack growth was observed for both the orientations. Moreover, the tensile stresses for the -90° case were high enough to cause crack branching. The average velocity of the crack for the +90° case was determined to be 300 m/s. For the -90° case the crack velocities were determined to be 300 m/s and 100 m/s. The slower crack did not have enough energy to propagate and arrested during the experiment. The crack surfaces for the cracks that propagated through the disk were observed to be smooth, as expected.

As for the previous cases, the isochromatic fringes were analyzed and the contact load profiles for the +90° and -90° cases are shown in figures 25 and 26, respectively. The peak contact load attenuation, at contact preceding the cracked disk, was 25 percent for the +90° case as compared to only 10 percent for the -90 case. This was again due to the same reasons as discussed for the +60° and -60° crack orientation experiments.

Pulse elongation was also observed for all the crack orientations, and once again strain gage experiments were conducted to determine the elongation of the pulse as it propagated through the cracked disk. The duration of the stress wave pulse increased from 120 μs to 200 μs , for the +60° and the +90° orientations, and from 120 μs to 170 μs, for the -60° and the -90° orientations as the pulse propagated through the cracked disk. Thus, there was no significant influence of the crack

orientation on the elongation of the stress wave pulse. As this elongated pulse propagated down the chain it was also decomposed into wavelets. The secondary wavelets were dissipated and finally a wave with a characteristic wavelength to disk diameter ratio of four propagated down the assembly. Also the overall attenuation did not change significantly with variation in crack orientation, as shown in figure 1.27. The overall average attenuation in peak contact load was observed to be 35 percent for all the crack orientations for a propagated distance of one meter.

Although the different orientations of the crack did not influence the overall attenuation of the peak contact load, they had a considerable effect on the resulting microstructure of the media. The cracks oriented towards the wave always resulted in the fracture of the particles unlike the cracks oriented away from it. This would greatly affect the subsequent loadings of the media and also loadings from any reflected pulses from the far field boundaries of the container.

1.4.3. Effect of Multiple Cracks

A series of experiments was also conducted to investigate the effect of including more than one cracked disk in the single chain assembly. In these experiments four fifty percent cracked disks were placed adjacent to each other. The choice of four disk was based on the wavelength of the loading pulse in the media. Two separate arrangements were investigated; one with all cracks aligned in the same direction and another with cracks aligned in a staggered fashion. Typical isochromatic fringes obtained for these experiments are shown in figures 28 and 29. As observed from these figures, substantial energy storage occurred within the cracked disks even after the stress wave pulse had propagated through. Each cracked disk was also subjected to tensile energy that was reflected up the chain by the subsequent cracked disks in the assembly. Ibis resulted in sufficiently high tensile loading of the first two cracked disks to cause crack growth as shown in the 11^{th} to 20^{th} frames in figure 1.28 and 11^{th} to 20^{th} frames in figure 1.29. This was in contrast with the single fifty percent cracked disk experiment, for which crack growth was never observed. In certain multiple cracked disk experiments the tensile loading was high enough to cause multiple crack growth within the same disk, as shown in the 18^{th} and 20^{th} frames in figure 1.28. The average crack velocities were determined to be 250 m/s for all these experiments.

As for the earlier experiments, two contacts preceding the cracked disks and two contacts following the cracked disks were analyzed using the photoelastic data. The corresponding contact load profiles for the two multiple cracked disks experiments are shown in figures 30 and 31. The

multiple cracked discs behave like filters. The aligned arrangement of cracks allowed greater energy to transfer across the cracked disks, than the staggered arrangement. This resulted in a 40 percent peak contact load attenuation in the stress wave pulse locally as it propagated through the cracked disks for the staggered arrangement compared to only 30 percent for the aligned assembly. Also both the assemblies resulted in elongation of the loading pulse.

Strain gage experiments were also conducted for these two assembly. The duration of the stress wave pulse increased from 120 μs to 210 μs for both cases, as the pulse propagated through the arrangement of cracked disks. Moreover, the overall attenuation, as determined from strain gage data, was 45 percent for both arrangements for a one meter of travel. This was only a slight increase over the 35 percent attenuation that was observed for a single fifty percent cracked disk assembly.

1.5 SUMMARY

The presence of damaged particles influences stress wave propagation through granular medium. The effects of varying crack length and crack orientation on the transmitted stress wave pulse are summarized as follows.

(1) The stress field in the cracked particle was a superposition of the contact and the crack tip stresses. The crack tip was loaded in pure mode-I or in combined mode-I and mode-II conditions depending on the orientation of the crack. However, the nature of the stresses in the undamaged particles adjacent to the cracked particles were not affected and Hertz stress field equations could still be used for stress analysis of these particles.

(2). As the length of the crack was increased from zero to seventy five percent of the disk diameter the average peak contact load attenuation also increased. This occurred due to the multiple reflections caused by the free surface of the crack. The presence of a crack also caused energy to be reflected back up the chain.

(3). In experiments with a single seventy five percent pre-cracked disk considerable crack closure occurred resulting in substantial strain energy being stored in the cracked particle. This energy was subsequently released causing a large elongation in the stress wave pulse.

(4). As the orientation of the cracked particle was varied the load transfer characteristics changed. However, the far field peak contact load attenuation showed little dependence on the angle between the crack and the tangent plane of contact.

(5). All orientations of the cracks caused local elongation of the loading pulse. As the elongated

pulse traveled, it decomposed into multiple wavelets. The secondary wavelets dissipated within a propagational distance of one meter leaving a wave with a characteristic wavelength of four disc diameters.

(6). The average velocity of the stress wave pulse remained unaffected in these experiments.

(7). Certain crack orientations were found to be more conducive to crack initiation and growth. Crack growth occurs due to tensile loading of the crack tip from multiple reflections of the stress wave pulse within the pre-cracked disk. The tensile loading becomes dominant only towards the tail end of the incoming stress wave pulse, and that is when crack growth was observed. Crack growth results in dissipation of energy and rearrangement of the microstructural fabric of the particulate aggregate.

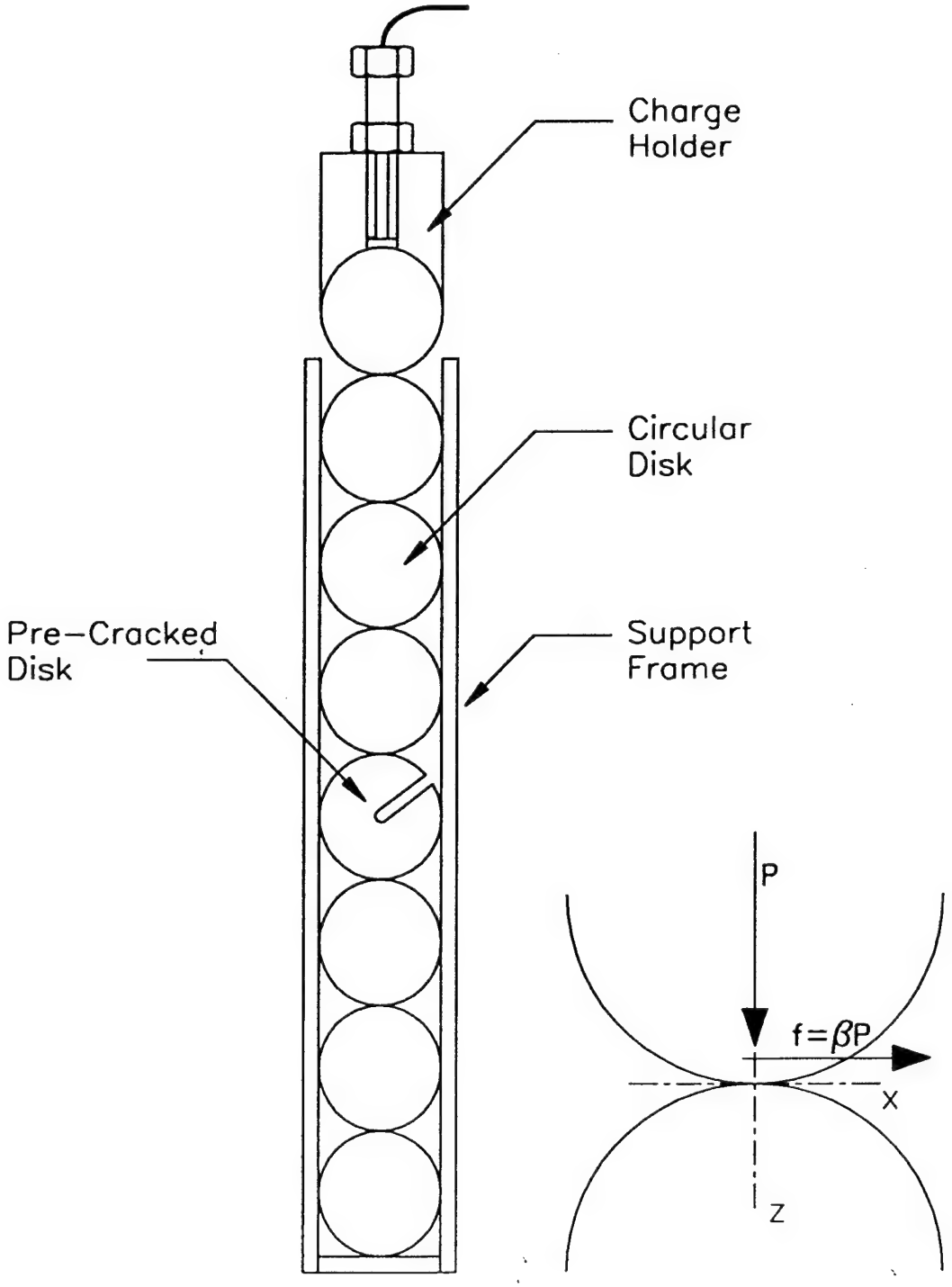

Figure 1.1. Experimental setup for explosive loading of a single chain assembly containing a cracked disk.

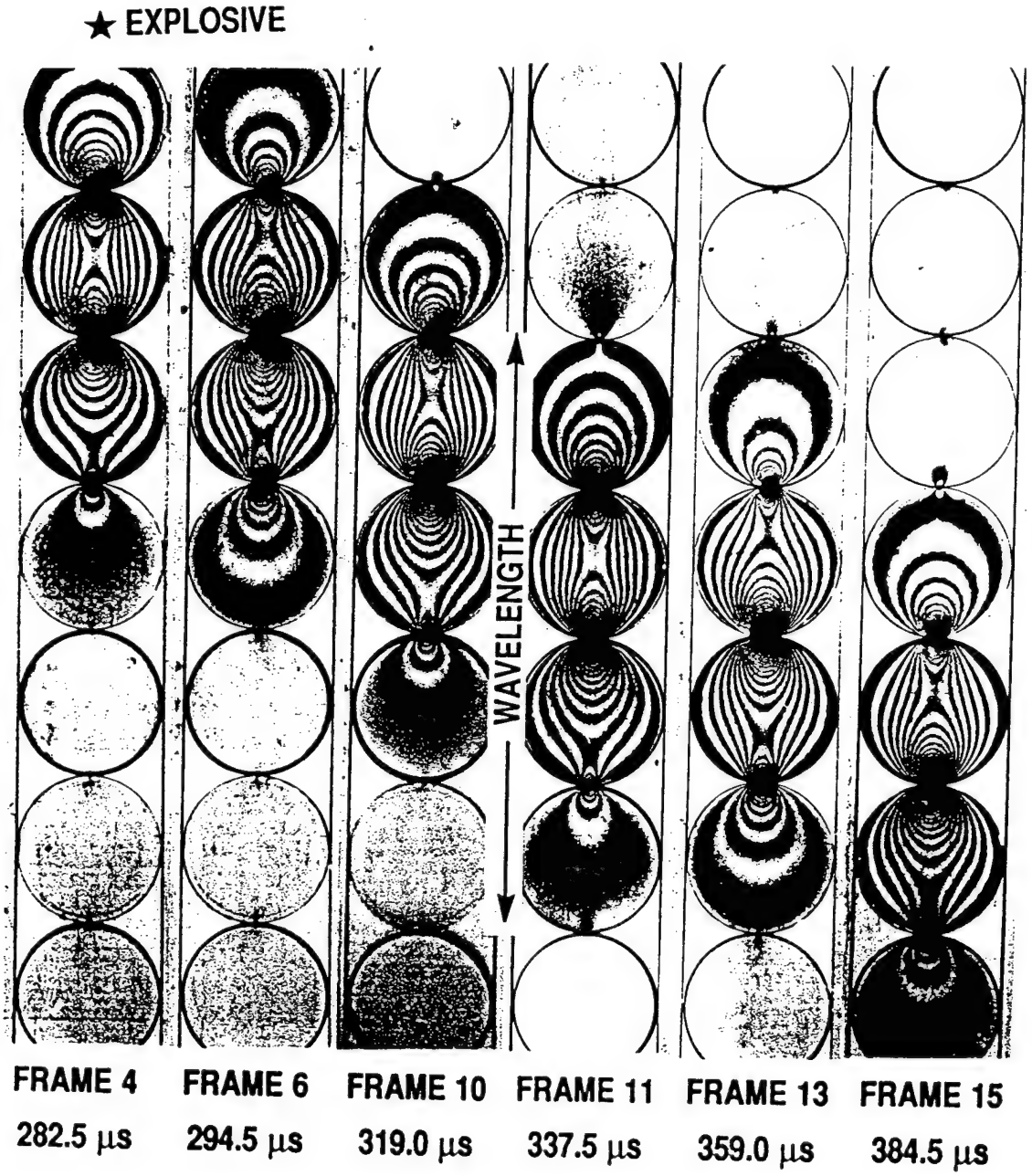

Figure 1.2. Typical isochromatic fringes obtained for a single chain assembly with no cracked disk.

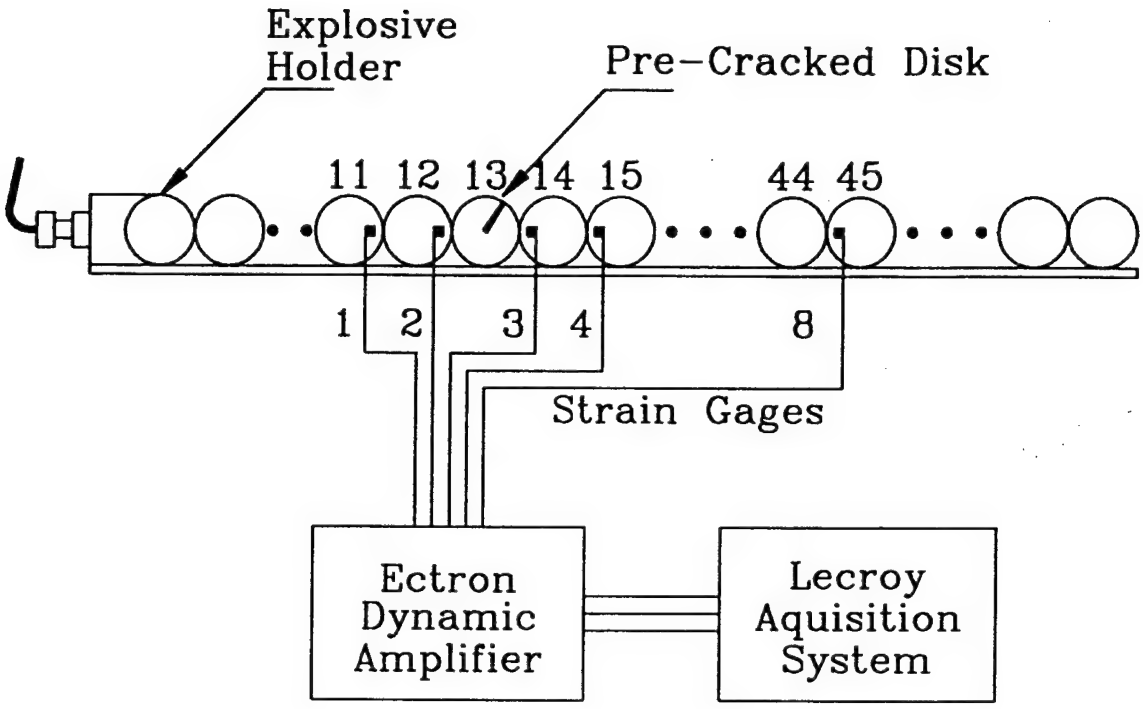

Figure 1.3. Experimental setup for long chain experiments using strain gages.

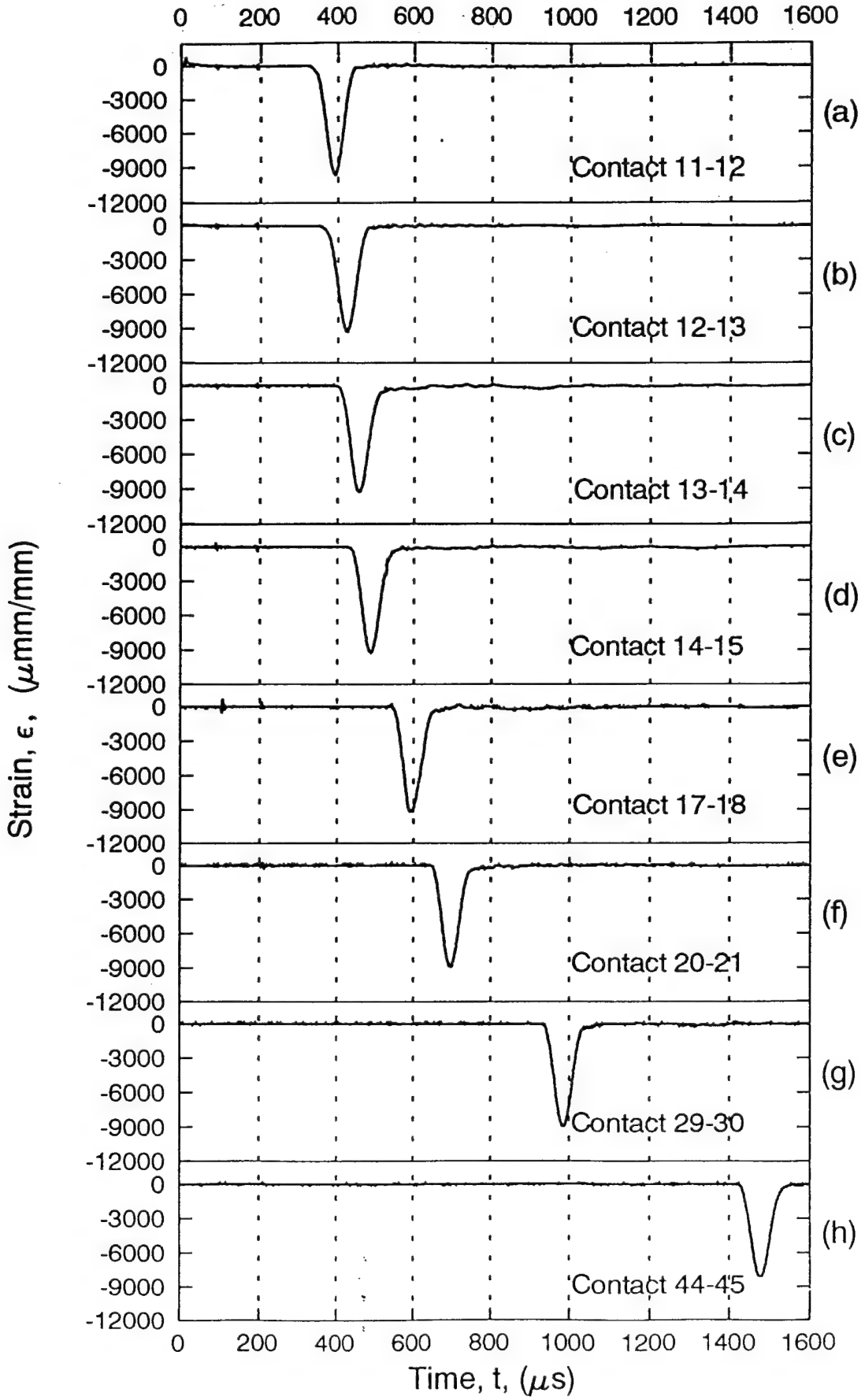

Figure 1.4. Strain gage data for a single chain assembly with no cracked disk.

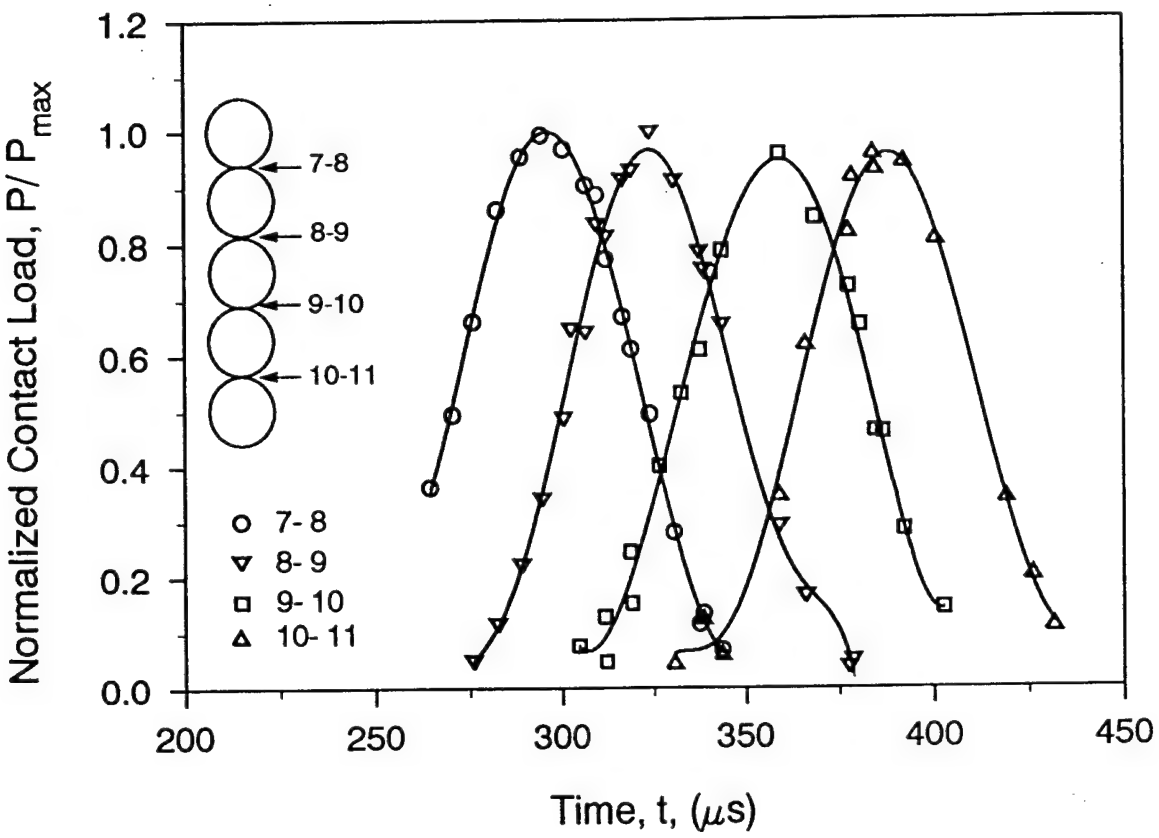

Figure 1.5. Variation of normal contact loads as a function of time for a single chain assembly containing no cracked disk.

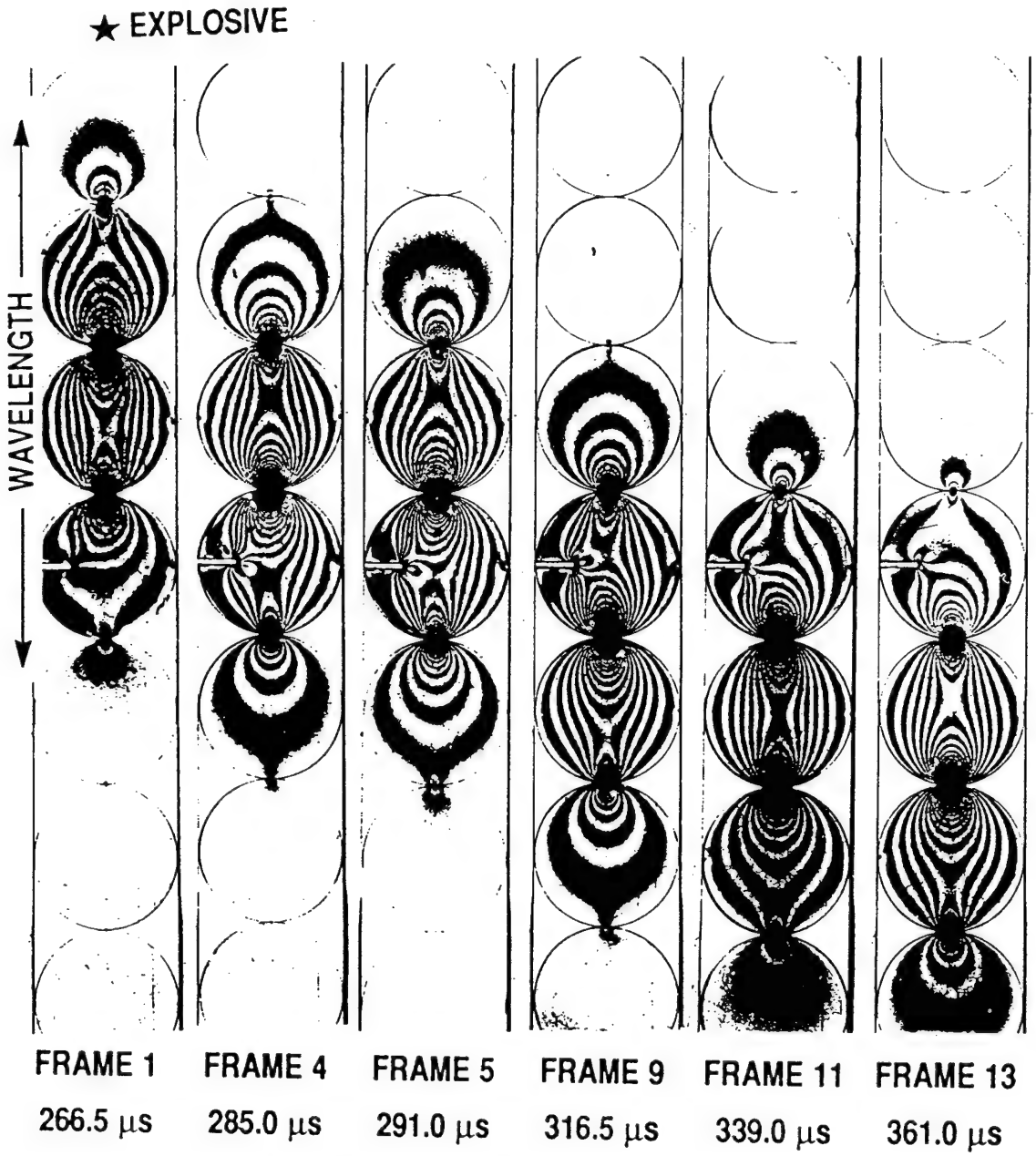

Figure 1.6. Typical isochromatic fringes obtained for a single chain assembly containing a 25% cracked disk.

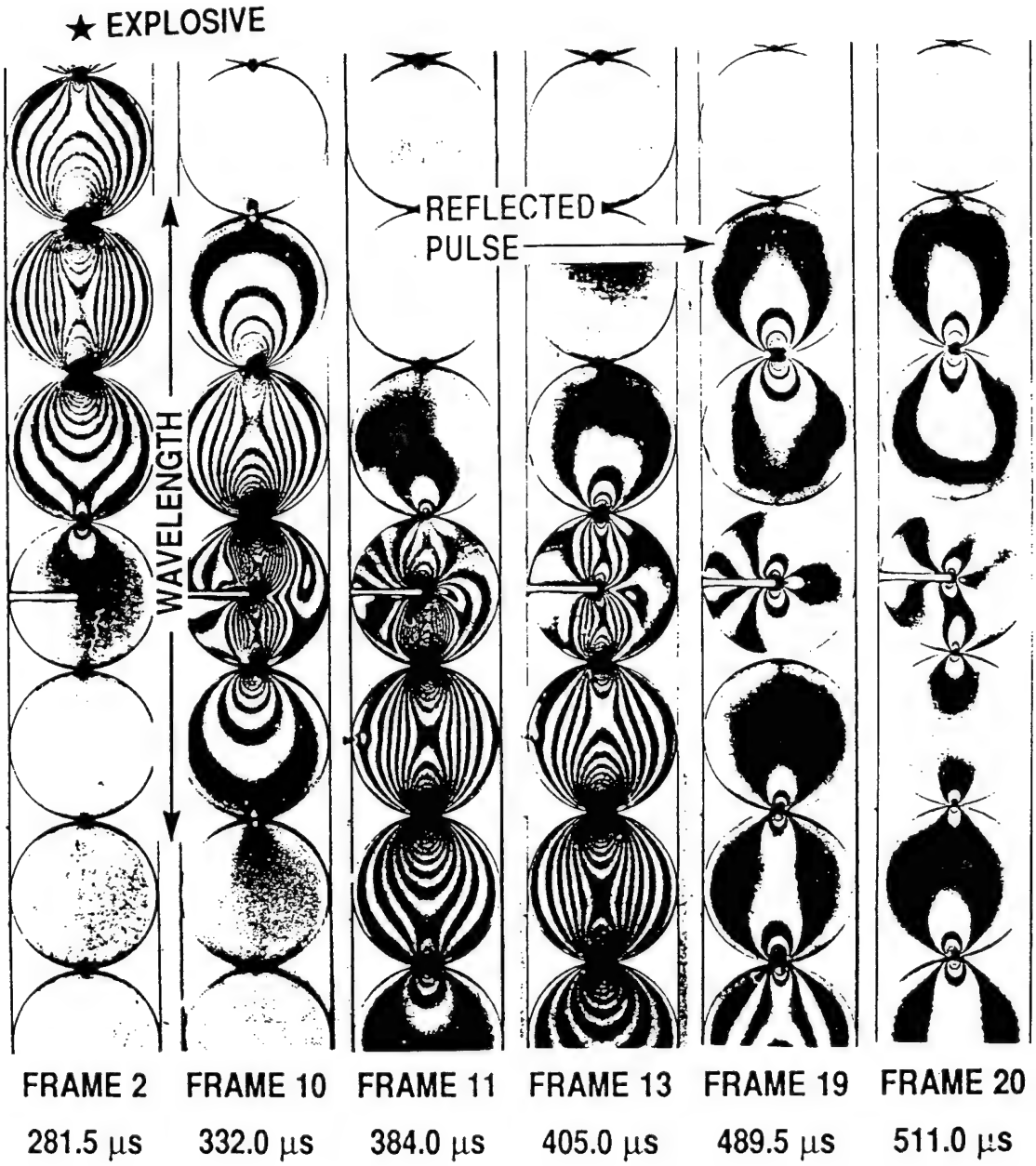

Figure 1.7. Typical isochromatic fringes obtained for a single chain assembly containing a 50% cracked disk.

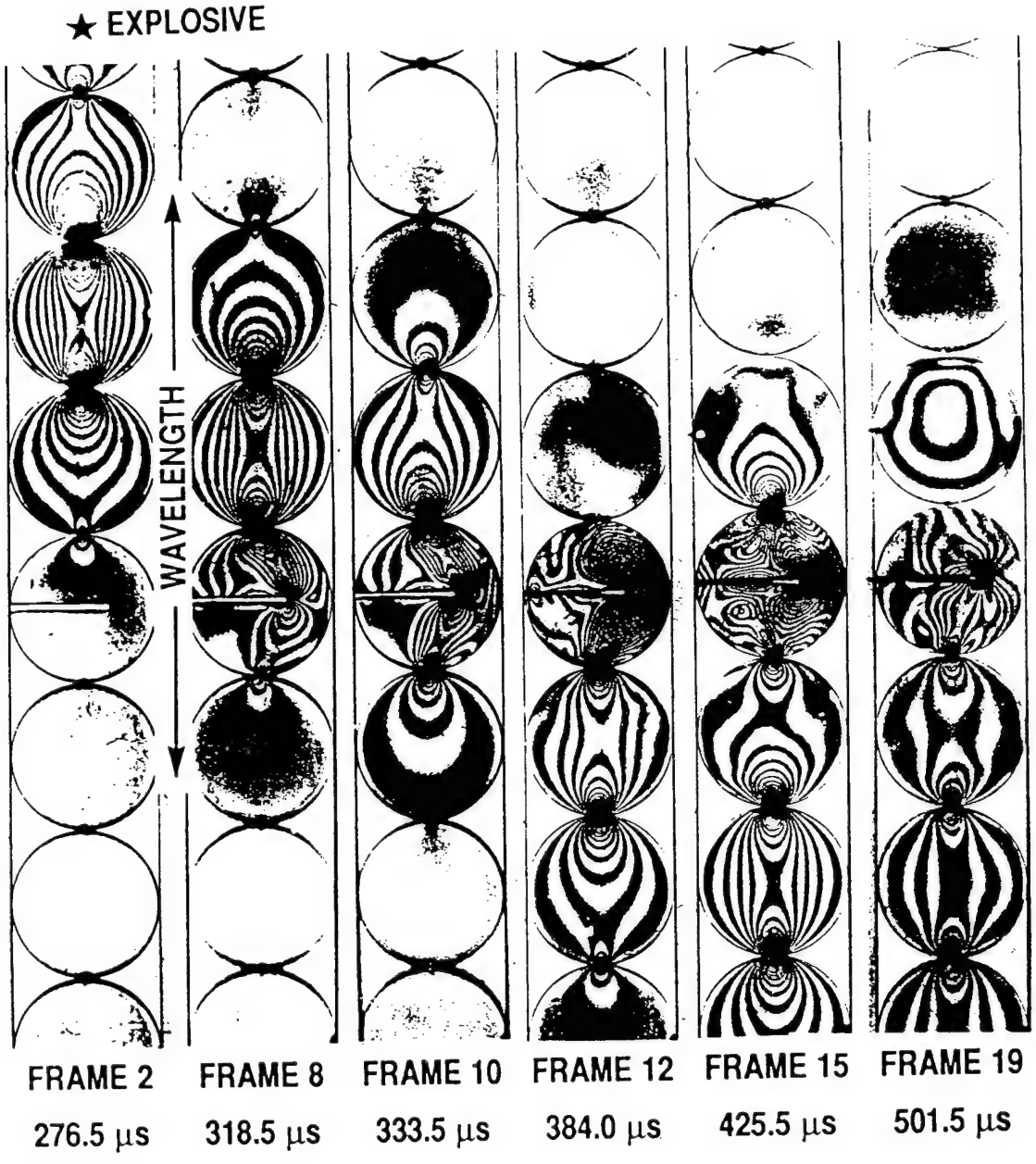

Figure 1.8. Typical isochromatic fringes obtained for a single chain assembly containing a 75% cracked disk.

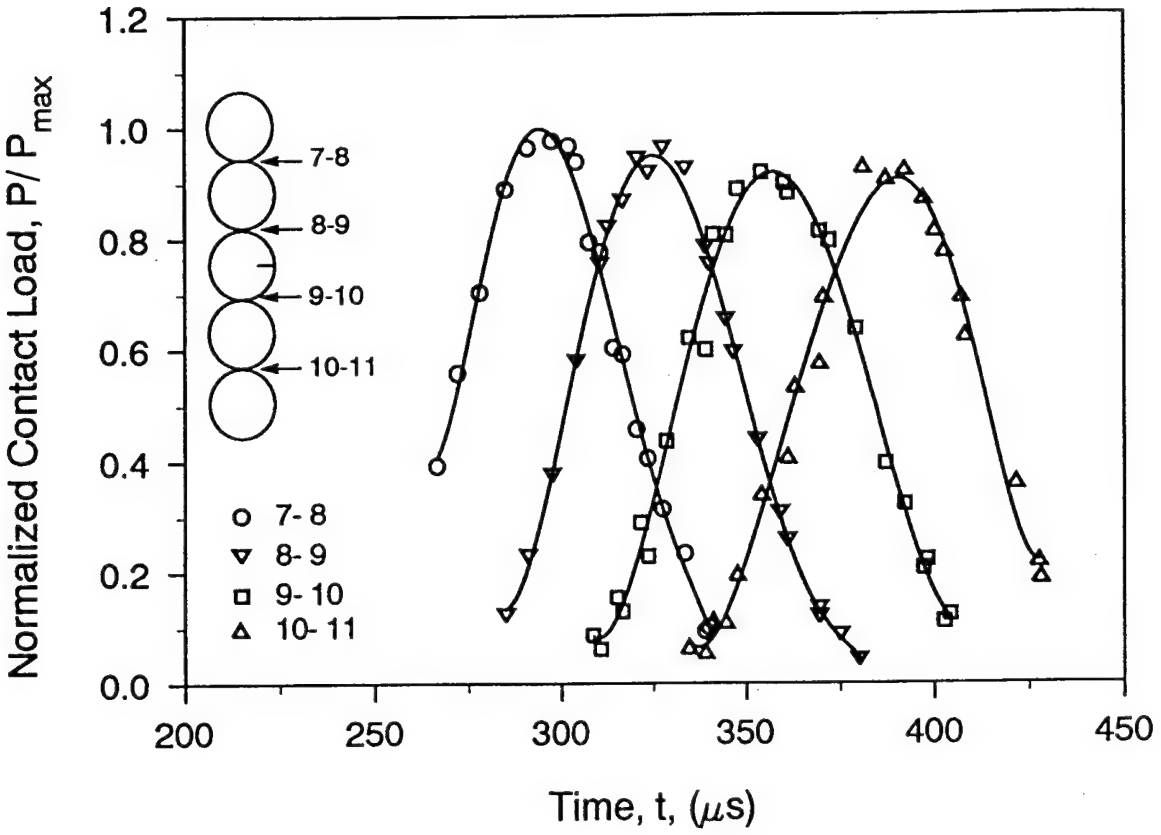

Figure 1.9. Variation of normal contact loads as a function of time for a single chain assembly containing a 25% cracked disk.

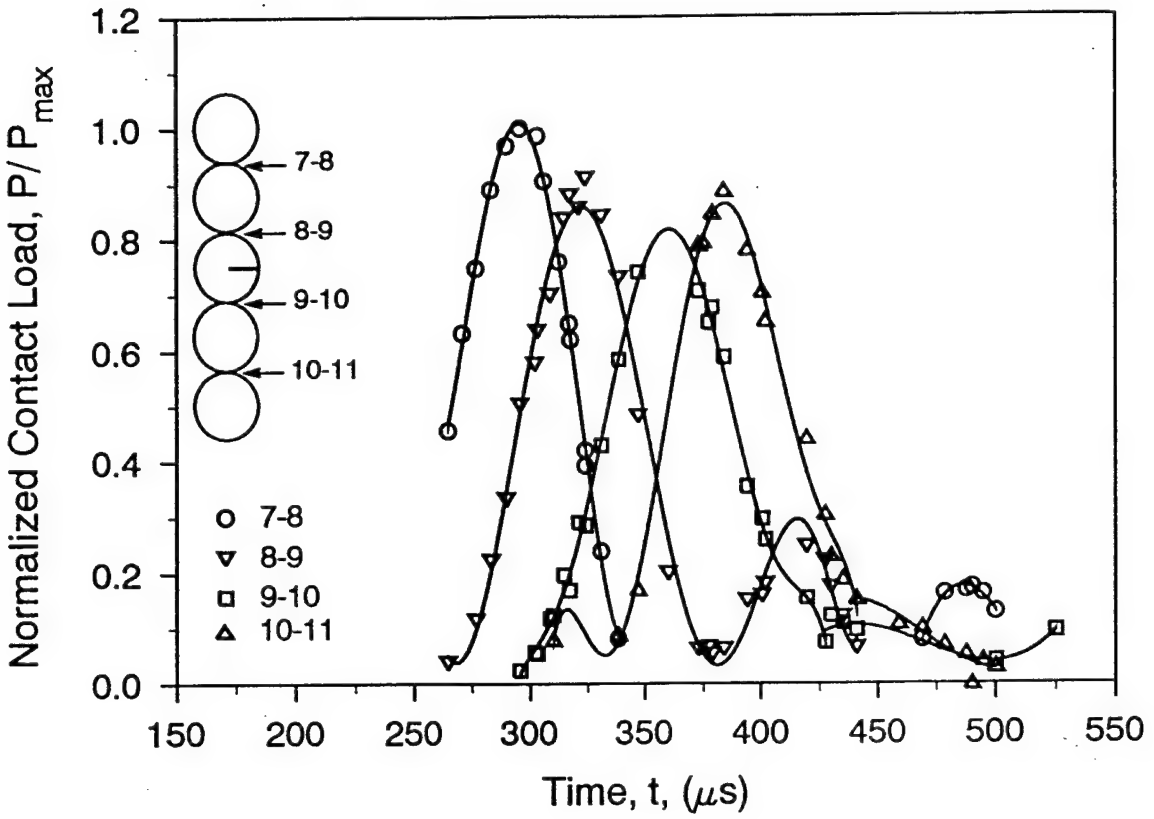

Figure 1.10. Variation of normal contact loads as a function of time for a single chain assembly containing a 50% cracked disk.

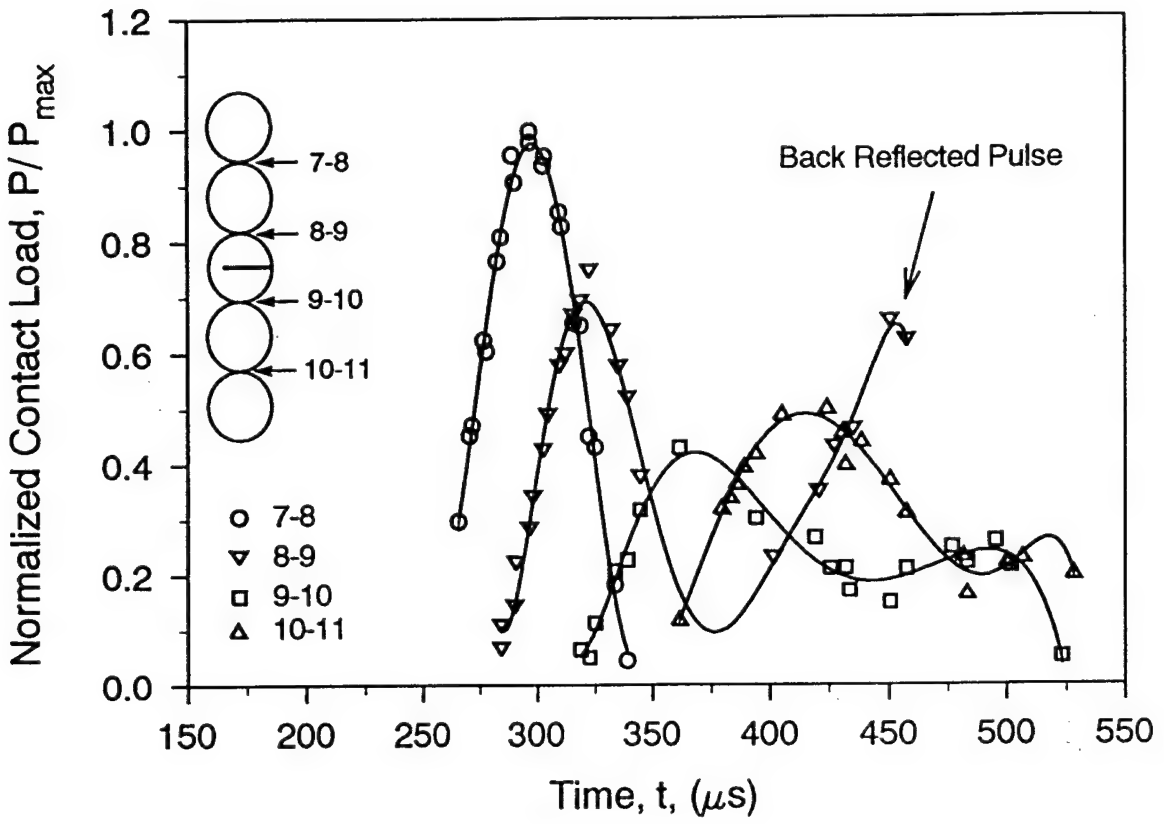

Figure 1.11. Variation of normal contact loads as a function of time for a single chain assembly containing a 75% cracked disk.

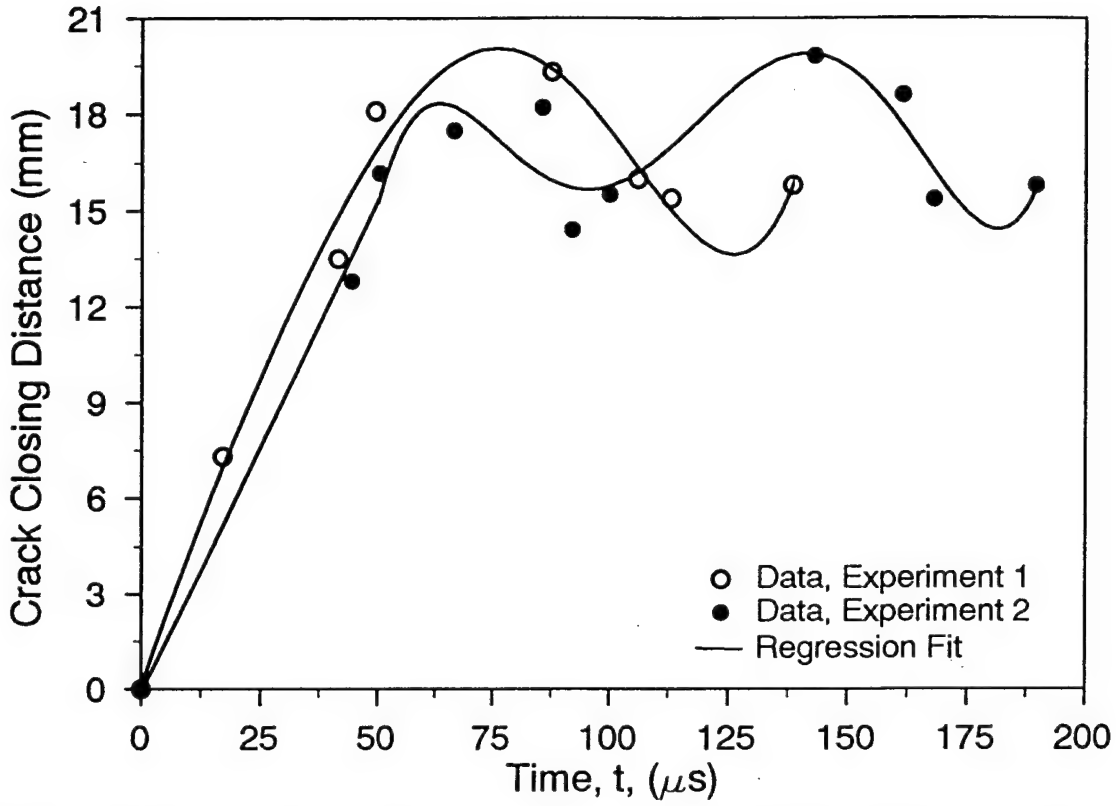

Figure 1.12. Crack closing distance as a function of time, for dynamic loading of a disk with a 75% disk-diameter crack.

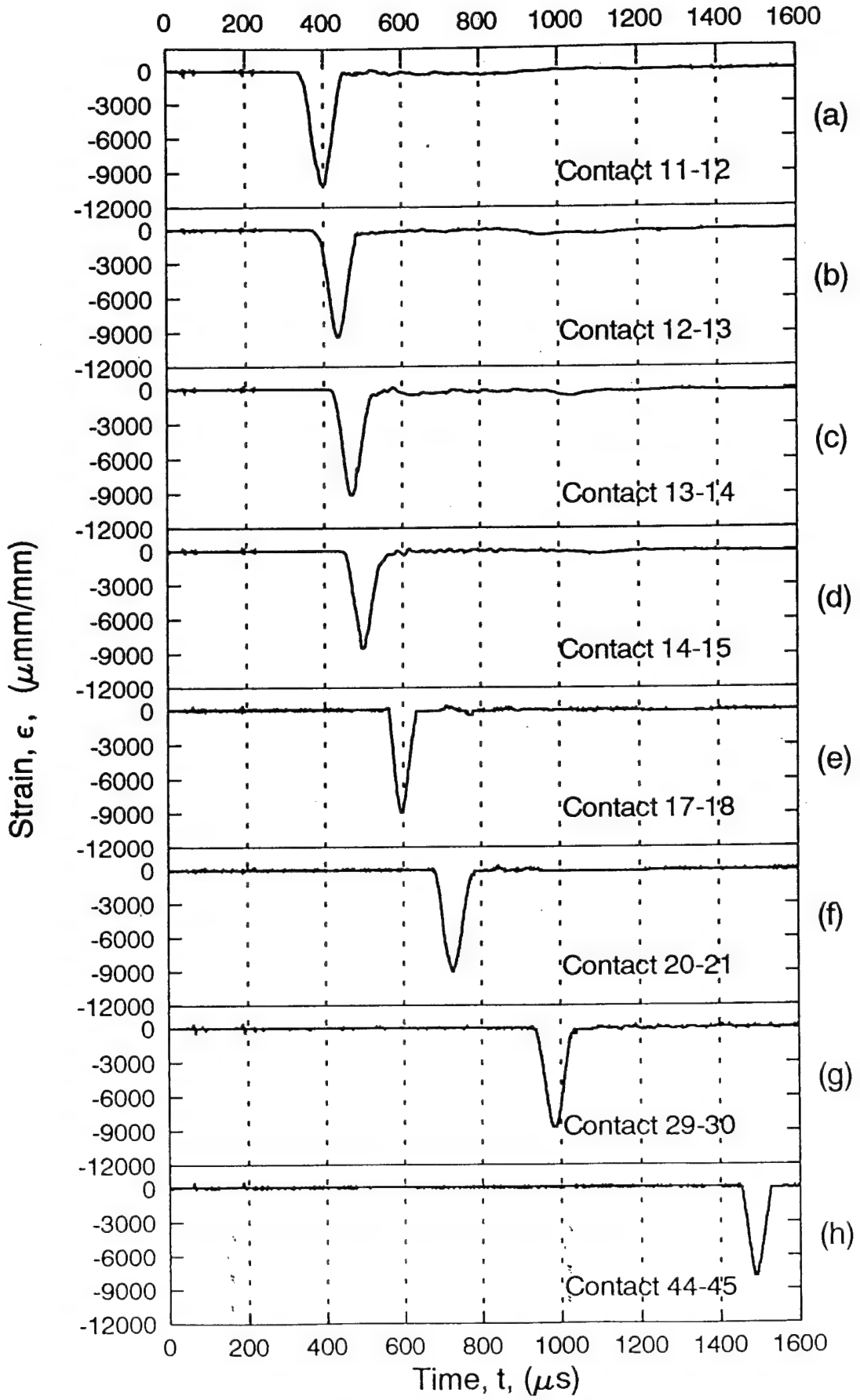

Figure 1.13. Strain gage data for a single chain assembly containing a 25% cracked disk.

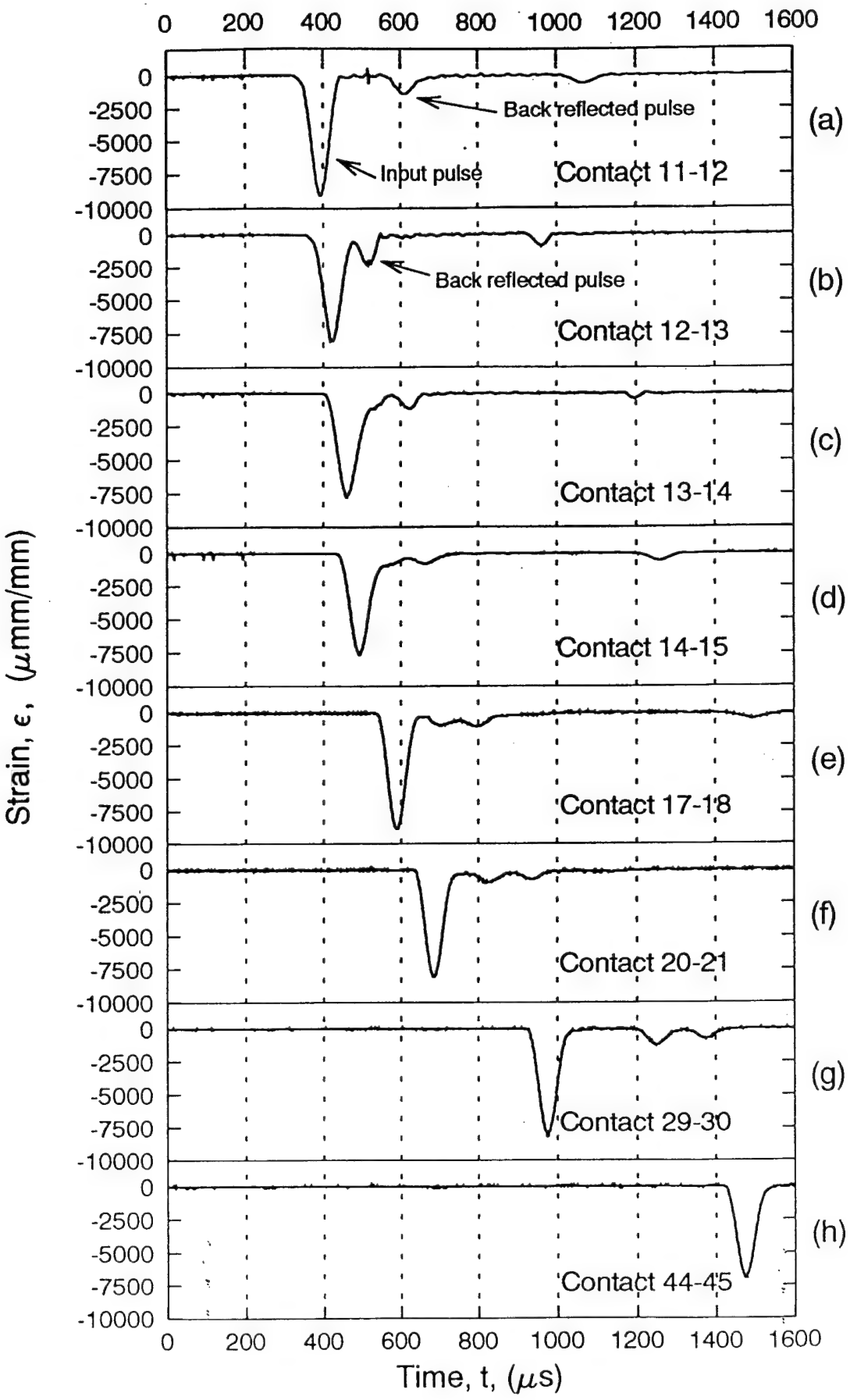

Figure 1.14. Strain gage data for a single chain assembly containing a 50% cracked disk.

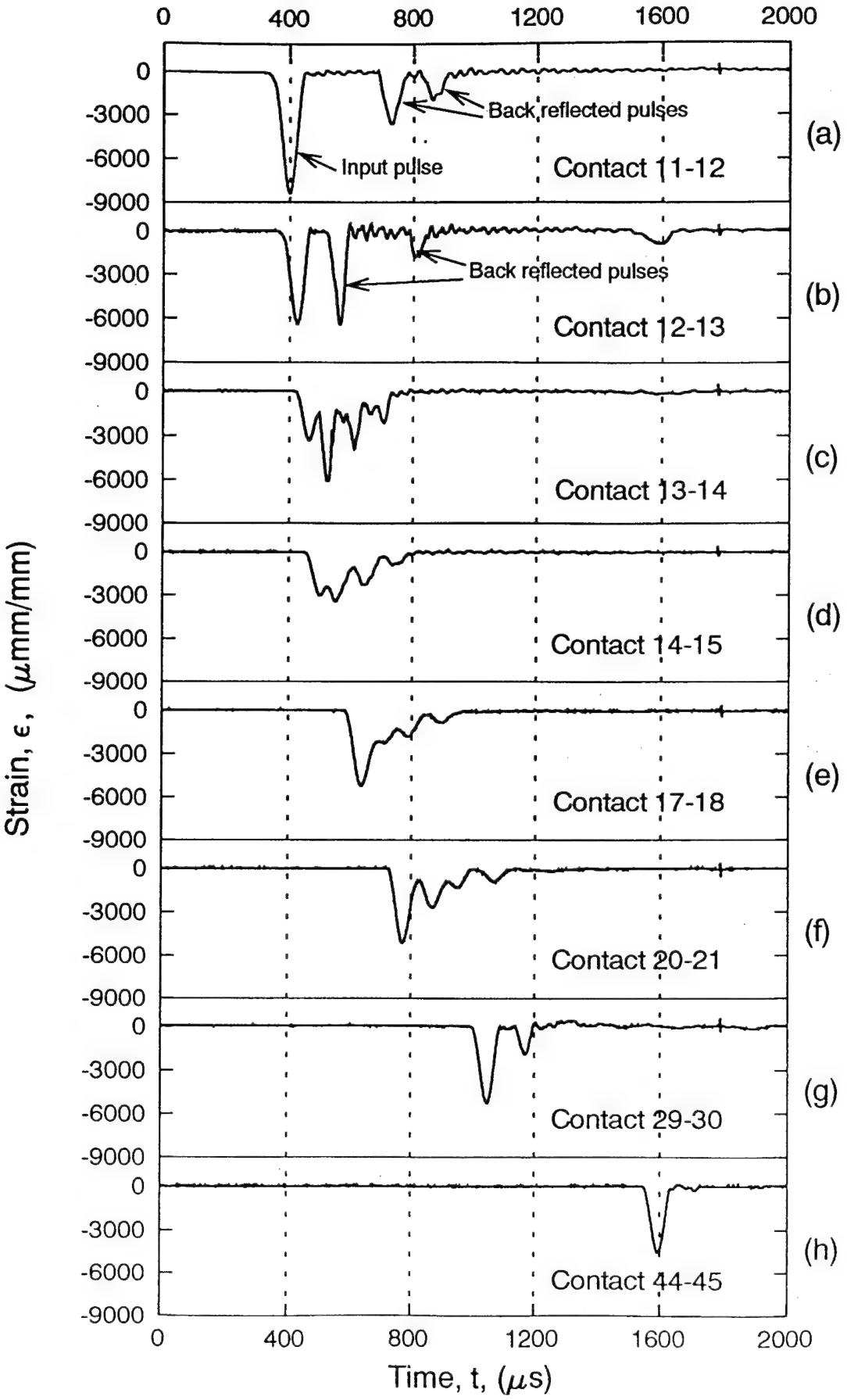

Figure 1.15. Strain gage data for a single chain assembly containing a 75% cracked disk.

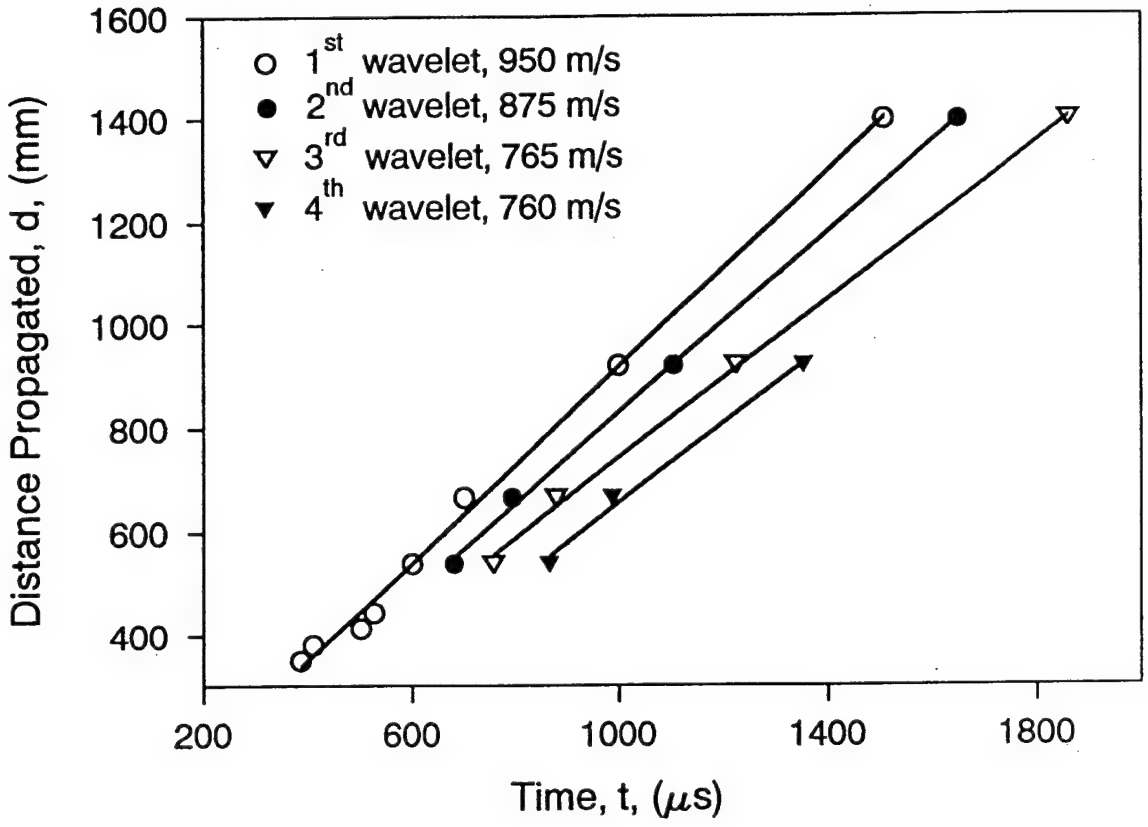

Figure 1.16. Distance propagated as a function of time by the various wavelets

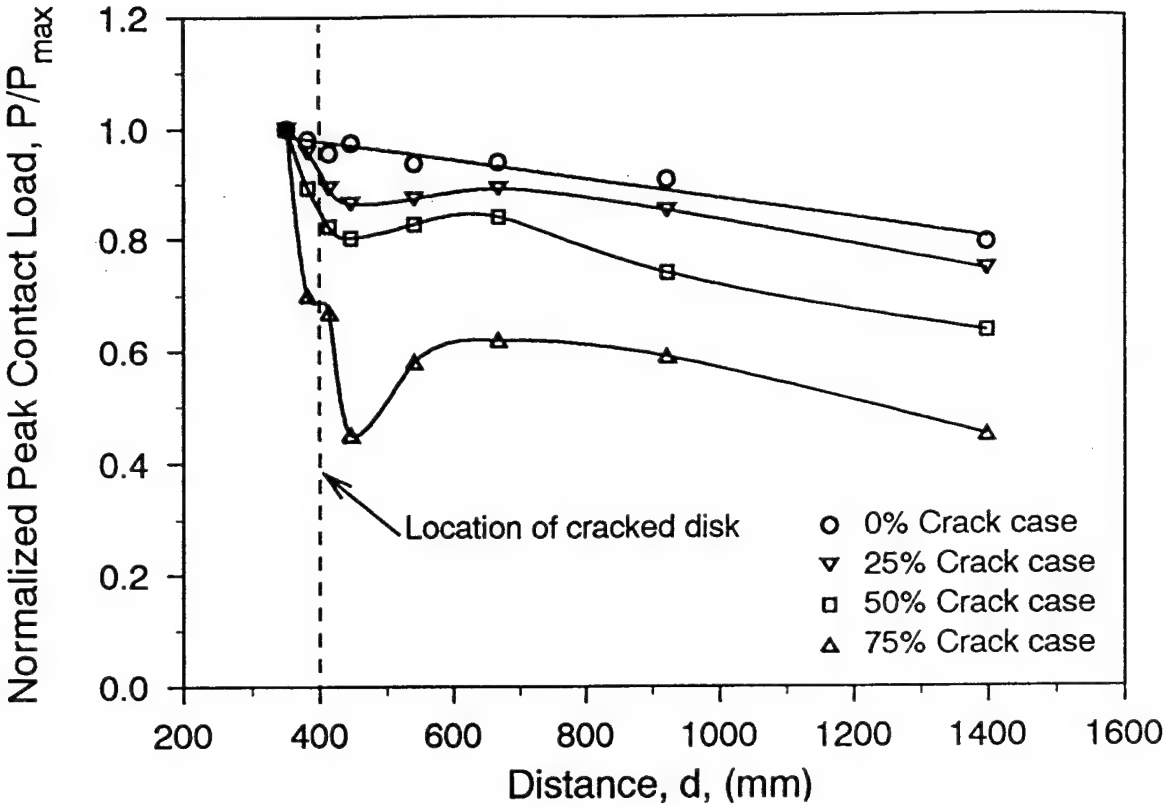

Figure 1.17. Load attenuation as a function of distance propagated for explosive loading of single chain assemblies containing disks with various crack lengths.

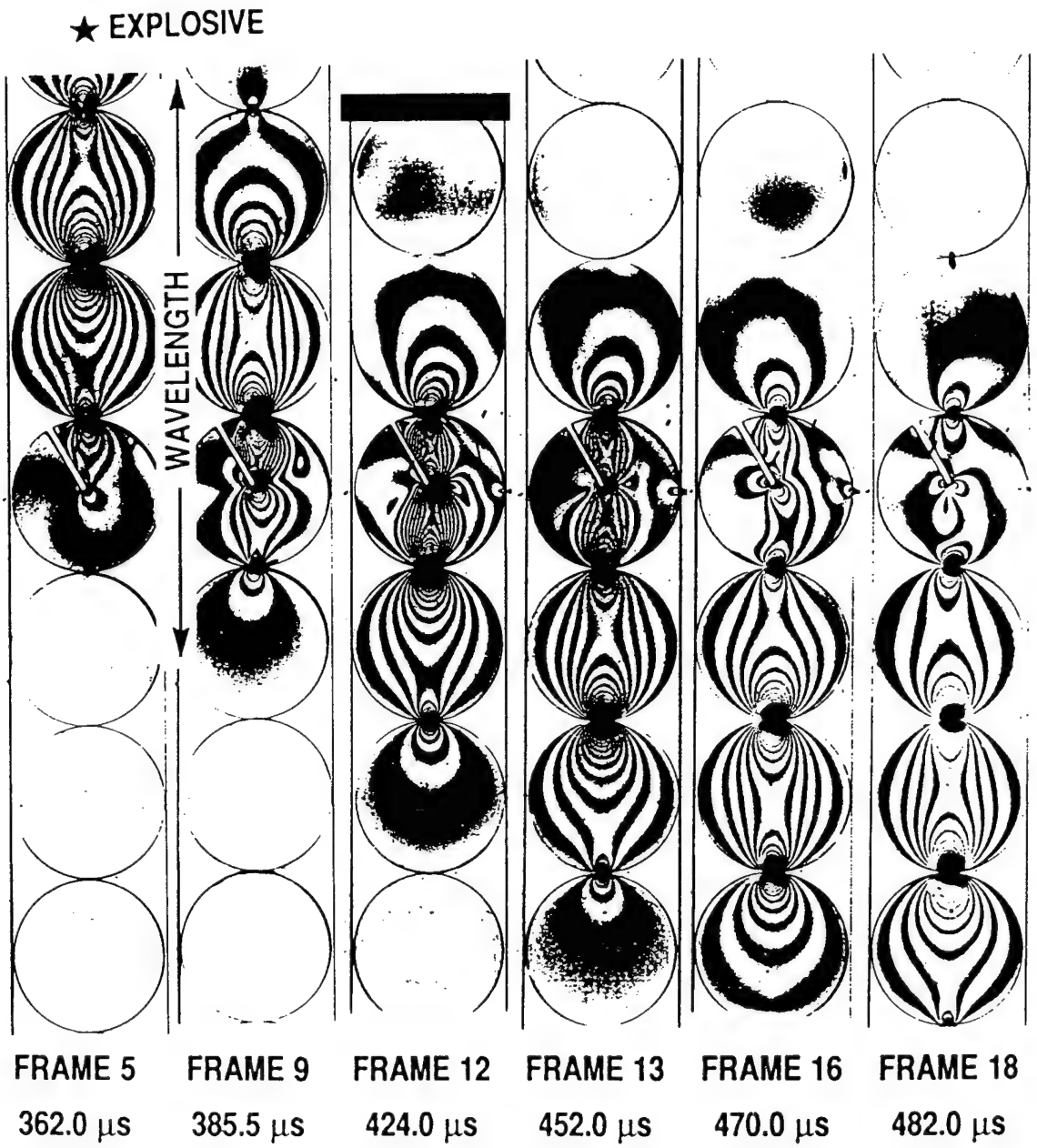

Figure 1.18. Typical isochromatic fringes obtained for a single chain assembly containing a 50% cracked disk oriented at +60'.

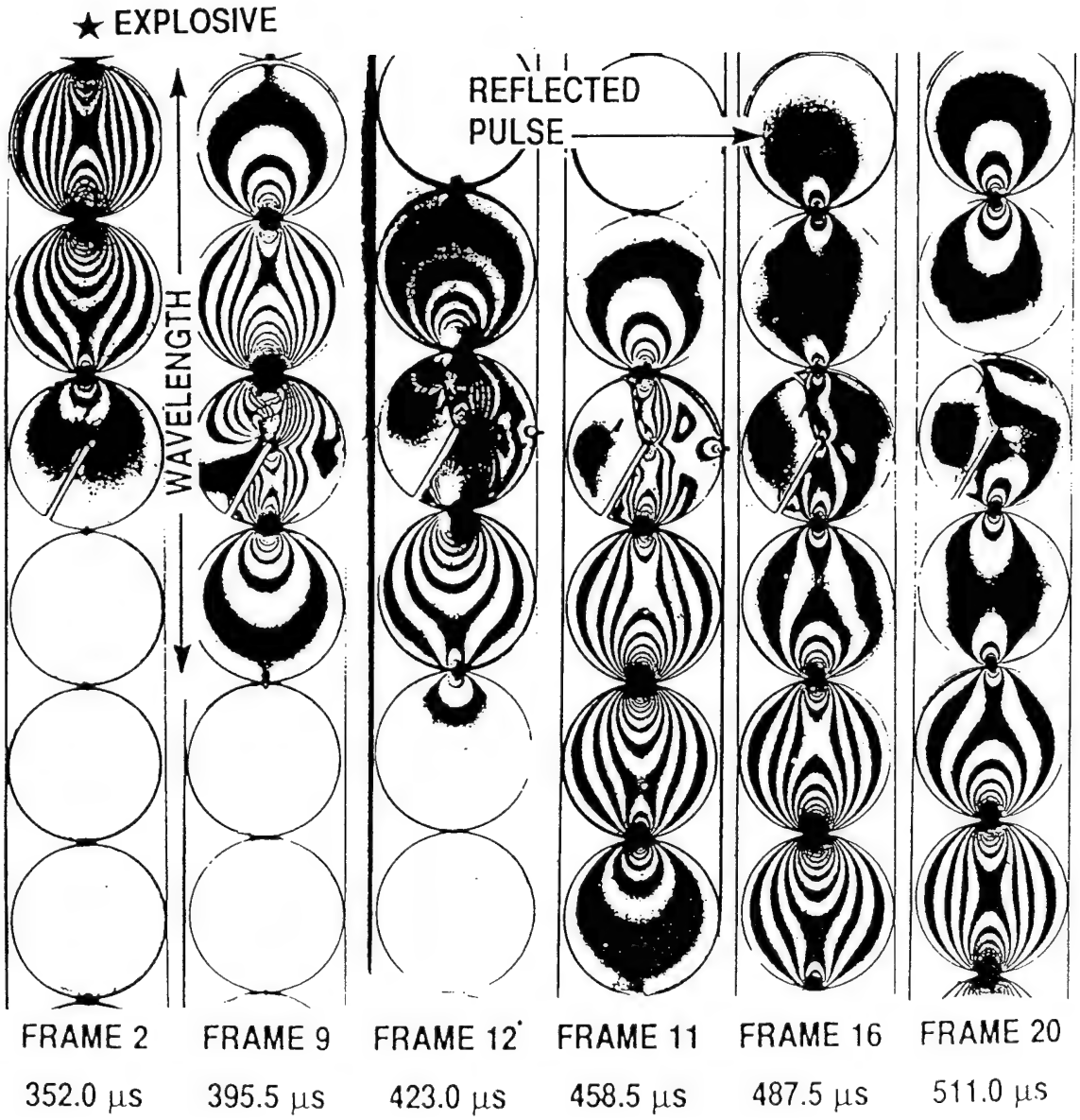

Figure 1.19. Typical isochromatic fringes obtained for a single chain assembly containing a 50% cracked disk oriented at -60°.

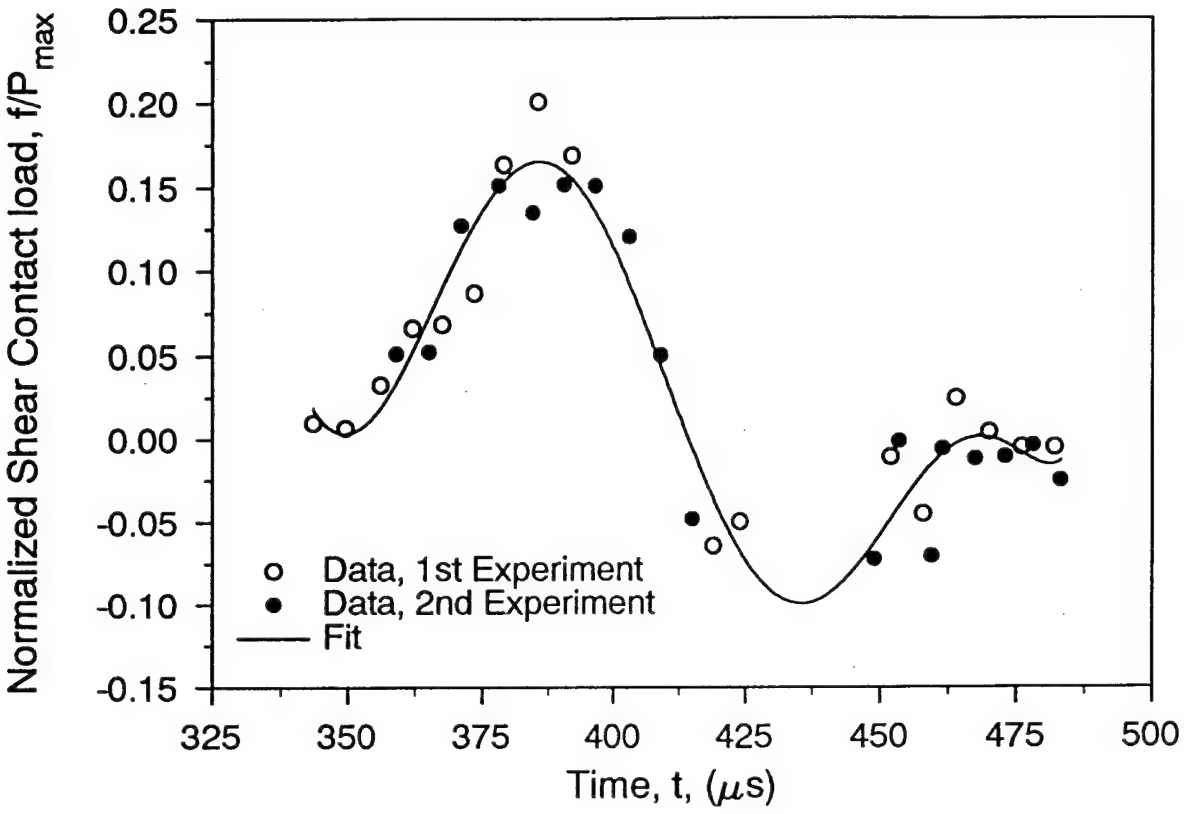

Figure 1.20. Variation of shear load at contact preceding the cracked disk for explosive loading of a single chain assembly contain a 50% cracked disk oriented at +60'.

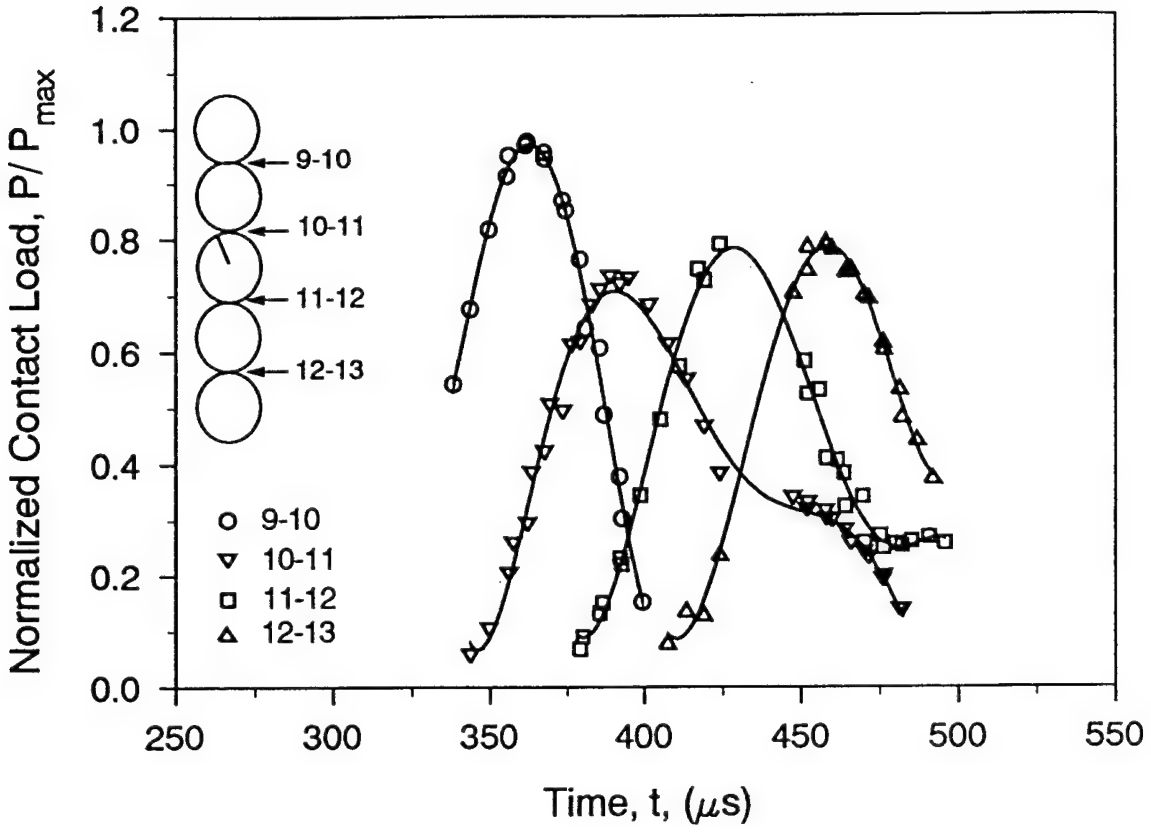

Figure 1.21. Variation of normal contact loads as a function of time for a single chain assembly containing a 50% cracked disk oriented at +60'.

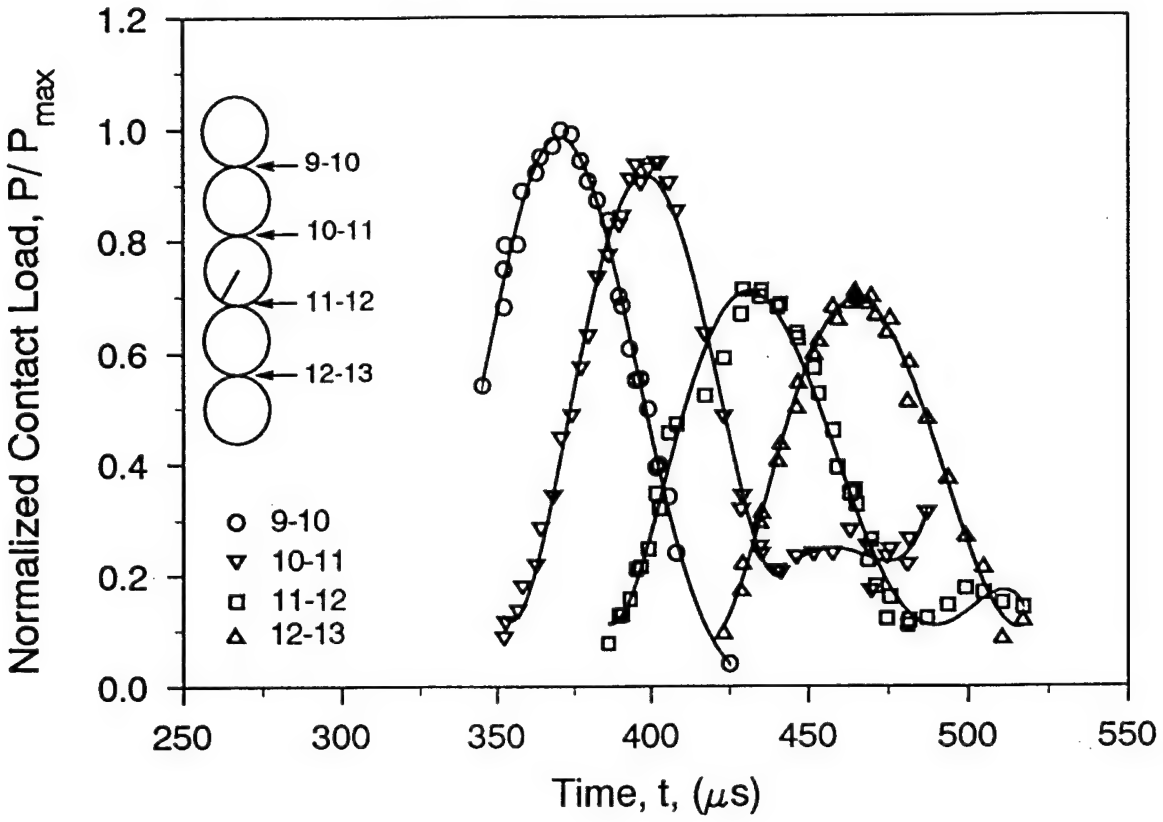

Figure 1.22. Variation of normal contact loads as a function of time for a single chain assembly containing a 50% cracked disk oriented at -60'.

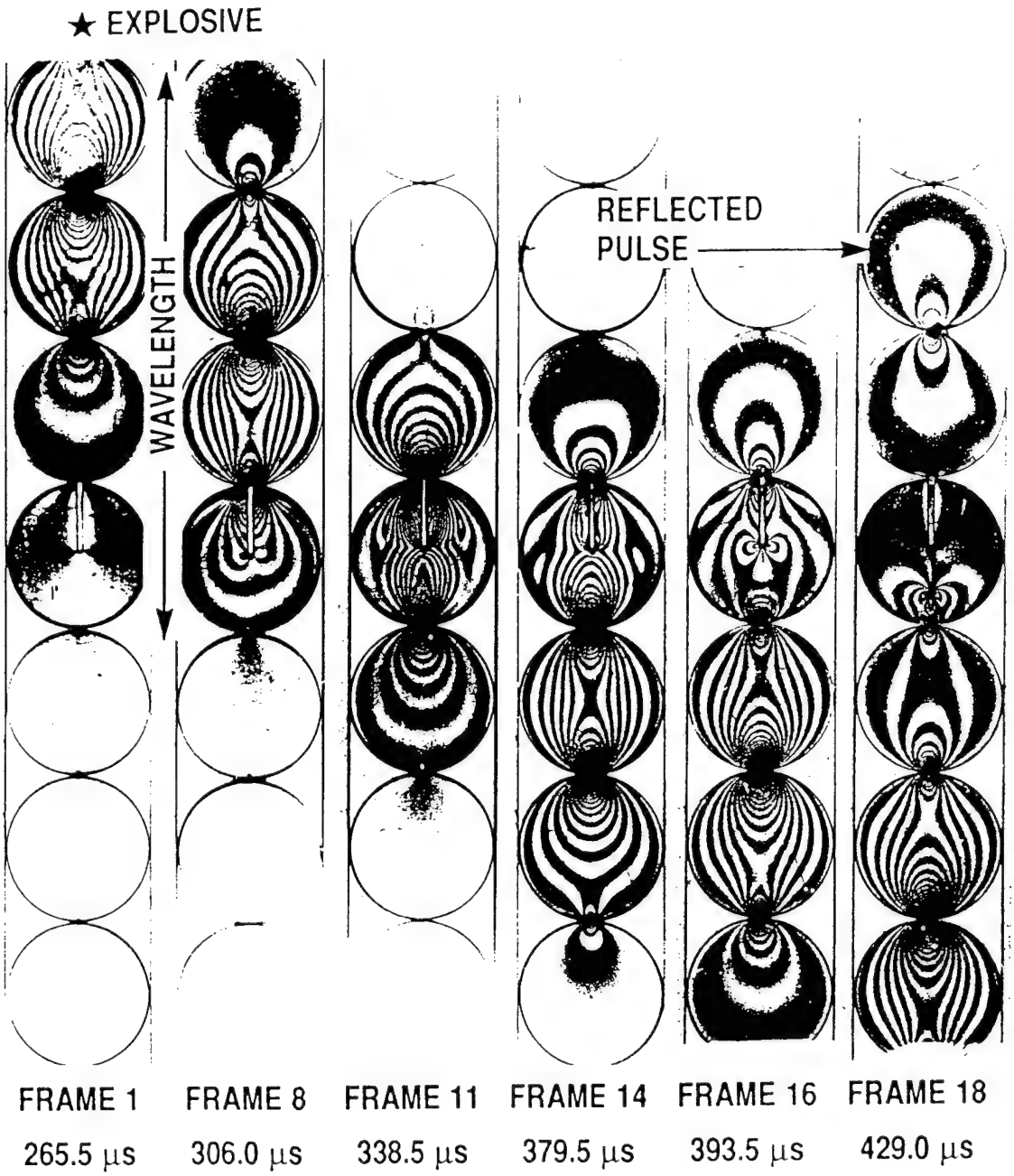

Figure 1.23. Typical isochromatic fringes obtained for a single chain assembly containing a 50% cracked disk oriented at +90'.

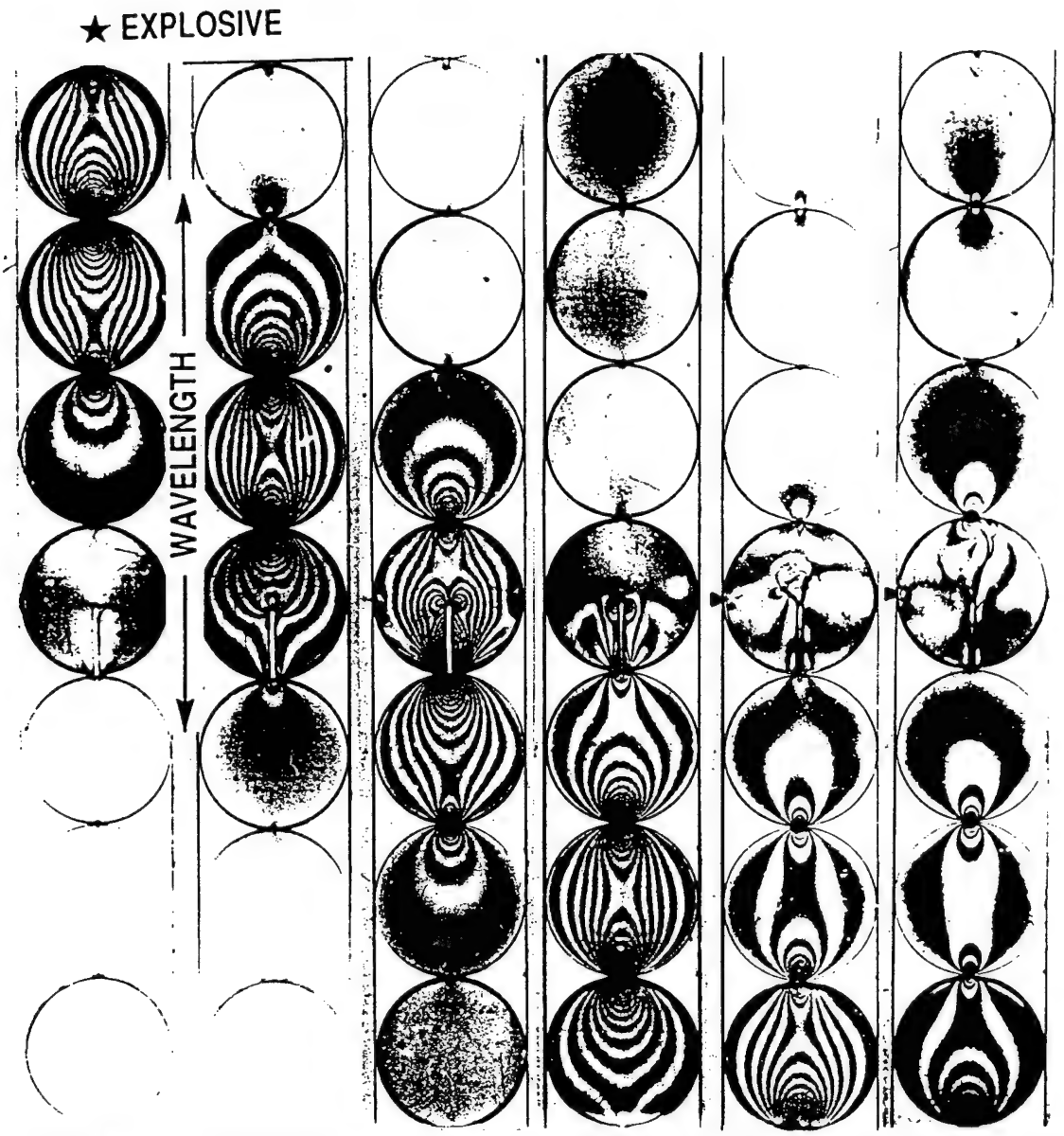

Figure 1 24. Typical isochromatic fringes obtained for a single chain assembly containing a 50% cracked disk oriented at -90'.

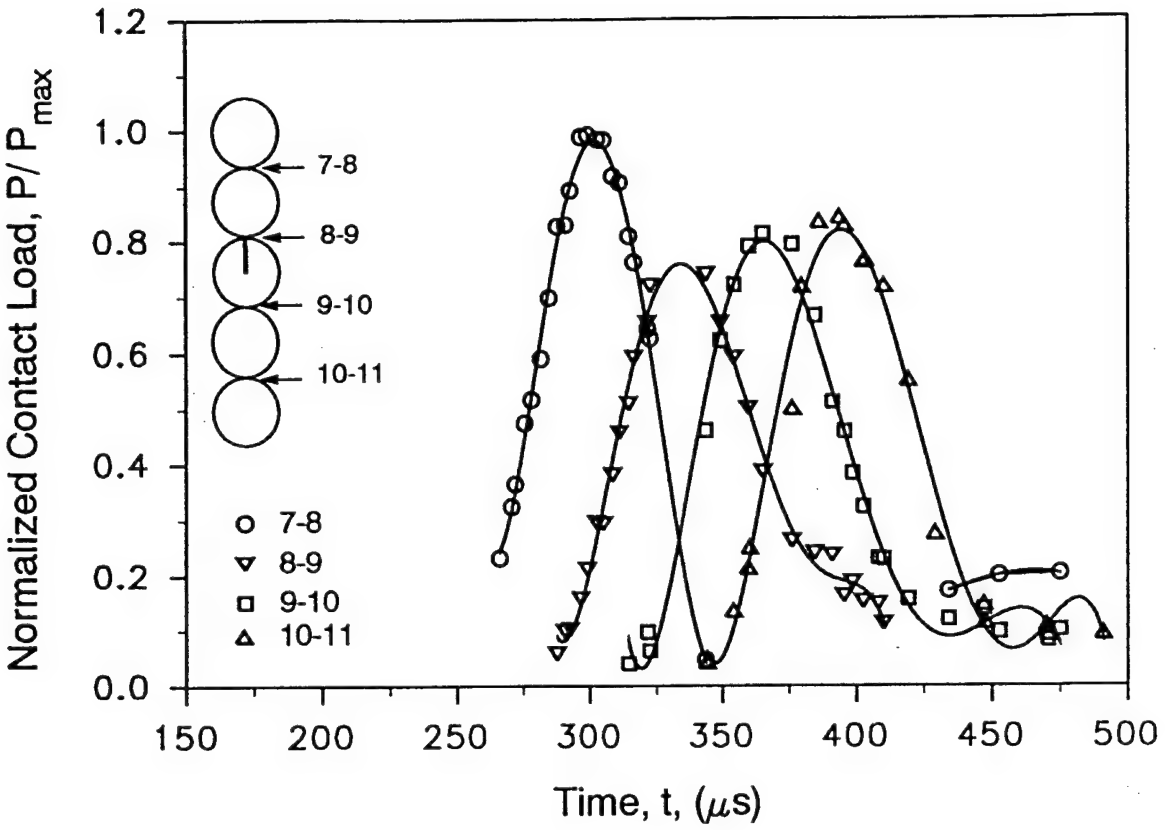

Figure 1.25. Variation of normal contact loads as a function of time for a single chain assembly containing a 50% cracked disk oriented at +90'.

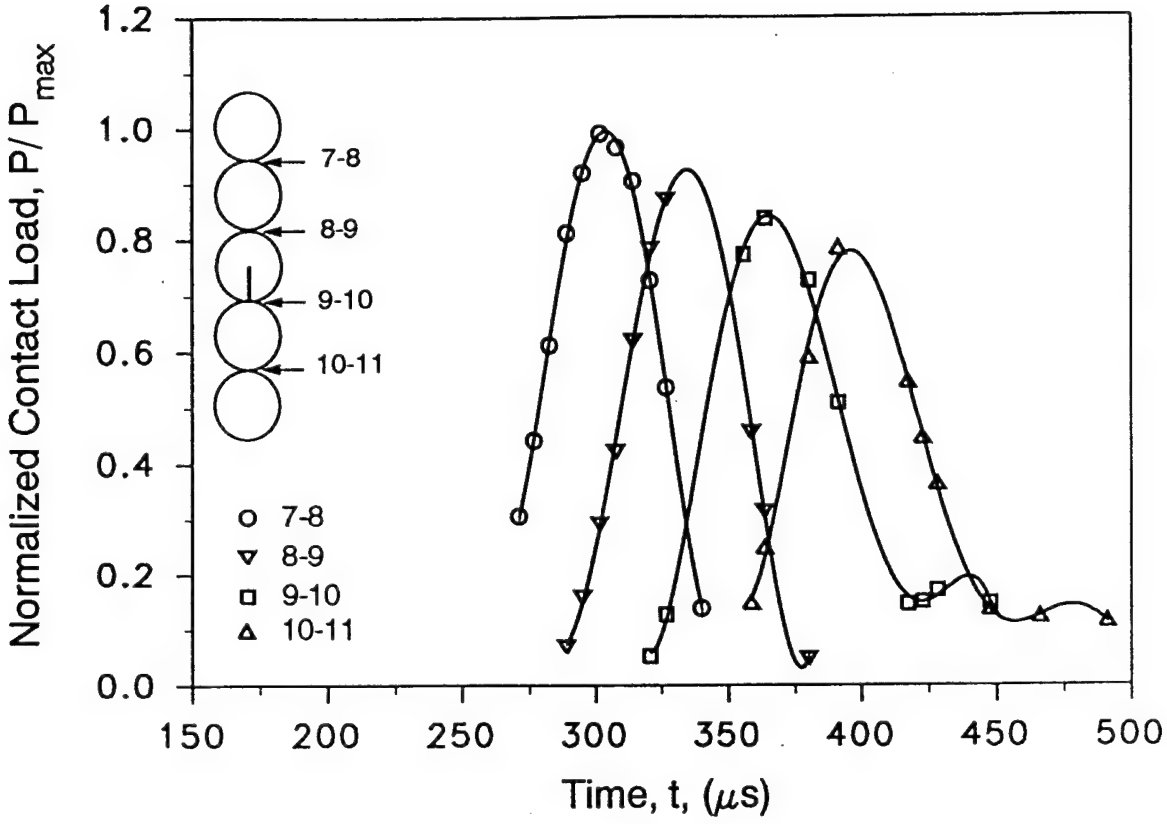

Figure 1.26. Variation of normal contact loads as a function of time for a single chain assembly containing a 50% cracked disk oriented at -900.

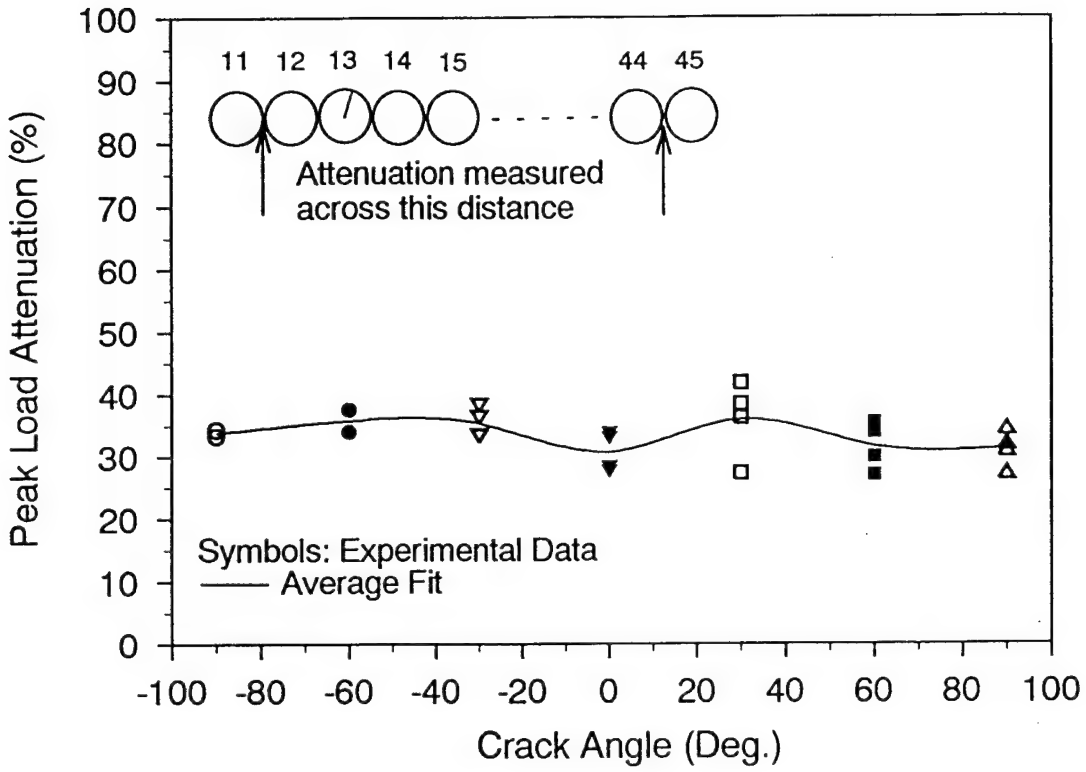

Figure 1.27. Overall peak contact load attenuation as a function of crack orientation.

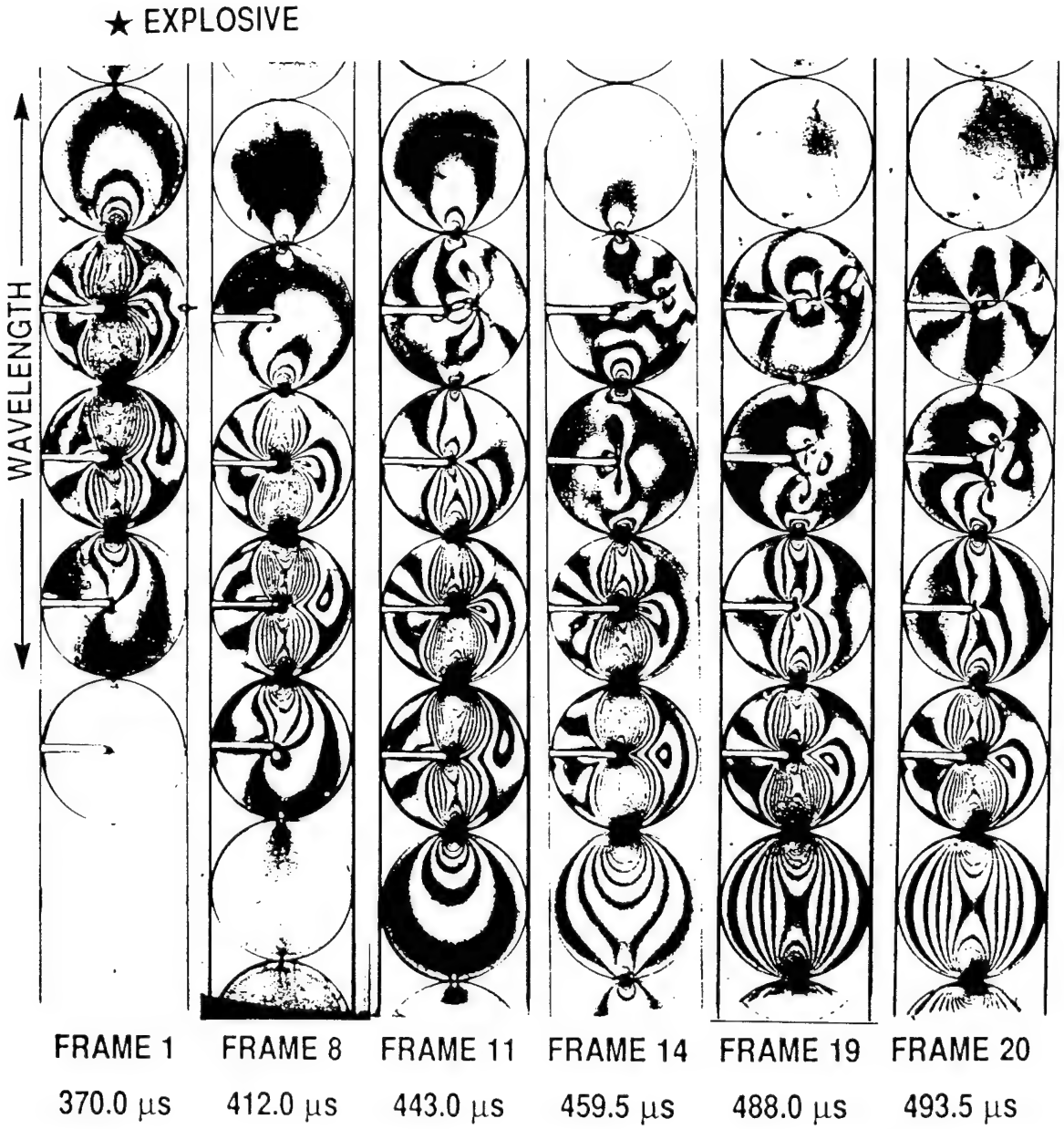

Figure 1.28. Typical isochromatic fringes obtained for a single chain assembly containing multiple cracked disks with aligned cracks.

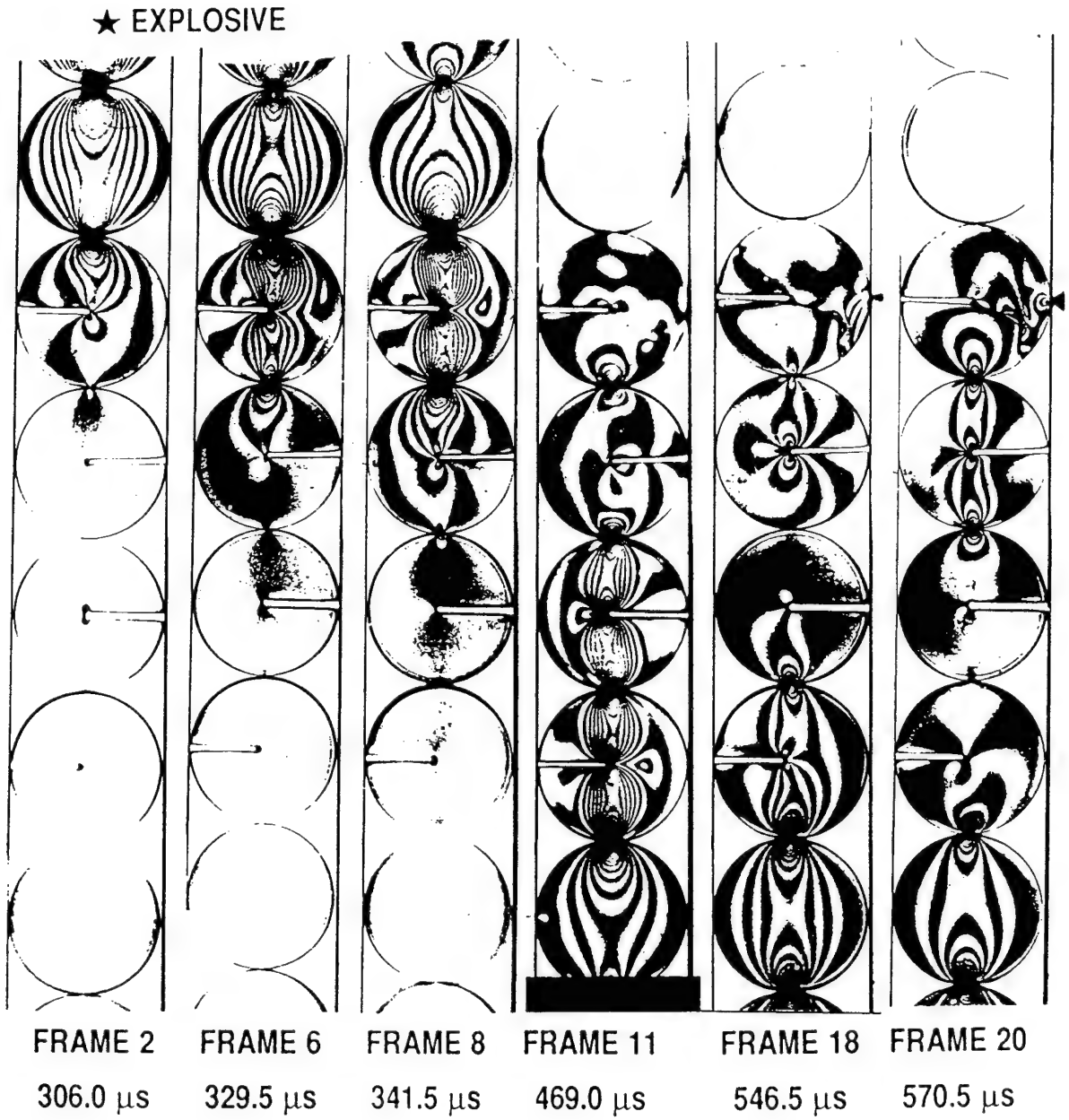

Figure 1.29. Typical isochromatic fringes obtained for a single chain assembly containing multiple cracked disks with staggered cracks.

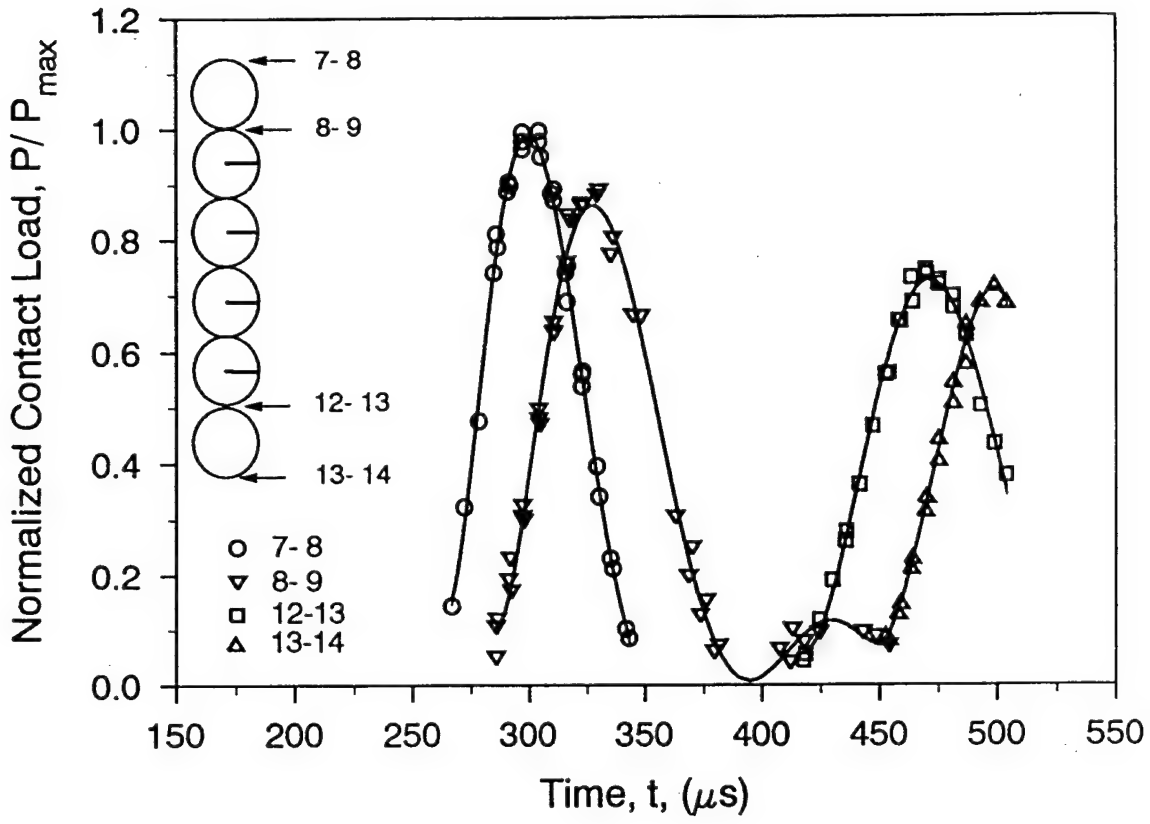

Figure 1.30. Variation of normal contact loads as a function of time for a single chain assembly containing multiple cracked disks with aligned cracks.

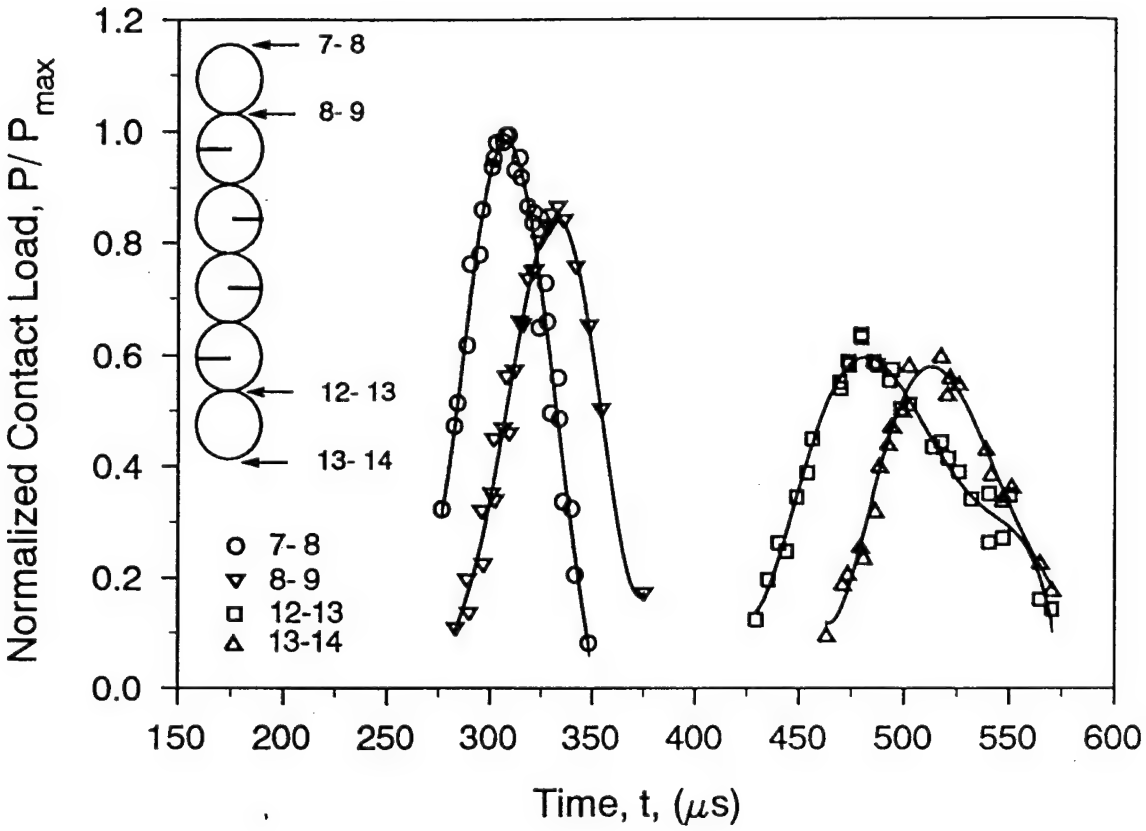

Figure 1.31. Variation of normal contact loads as a function of time for a single chain assembly containing multiple cracked disks with staggered cracks.

CHAPTER 2

EXPLOSIVELY GENERATED PULSE PROPAGATION THROUGH PARTICLES CONTAINING NATURAL CRACKS

ABSTRACT

An experimental investigation is conducted to study dynamic load transfer through particulate assemblies containing a damaged particle. The assembly is simulated by a one-dimensional array of circular disks, and the damage itself is modeled by a natural, zero-width crack. This assembly is explosively loaded and the dynamic load transfer process is observed using dynamic photoelasticity and strain gages, as the stress wave pulse propagates down the assembly. Attention is focussed on the influence of damage size and orientation on the wave velocity, wave dispersion and peak contact load attenuation of the stress wave pulse. Damage growth occurring from the interaction of the stress wave pulse with the closed natural crack tip is also studied. The results demonstrate that the inclusion of a damaged particle greatly influences the load transfer process, both locally and in the far field. The degree to which the damaged particle modifies the load transfer process is more dependent upon the orientation of the natural crack than upon the size of the crack. Moreover, damage growth within the damaged particles is also a strong function of the orientation of the natural crack.

2.1 INTRODUCTION

This paper presents the results of an experimental investigation conducted to study dynamic load transfer through particulate assemblies containing a damaged particle. The assembly was simulated by a one-dimensional array of circular disks, and the damage by a natural crack. This assembly was explosively loaded and the resulting dynamic load transfer was observed using dynamic photoelasticity and strain gages. The two techniques were employed in separate experiments to obtain the stress and strain fields at various contact locations, as the explosively generated stress wave propagated through the particulate assembly. The evaluation of these transient stress and strain fields elucidated the various mechanisms that govern dynamic load transfer through damaged particulate assemblies and hence through damaged granular media.

The motivation for this study arises from the need to understand dynamic load transfer through granular media. This information is important to several areas of technology such as soil mechanics, seismology, compaction of powders, etc. The response of a granular medium to rapid

loading represents a fairly complex problem and has been of interest to many researchers. Typically, researchers have employed both numerical and experimental techniques to investigate dynamic load transfer through granular media simulated by particulate assemblies (Subhash *et al.* 1991, Rothenburg and Bathurst, 1992 and Shukla *et al.* 1993a). Recently, Shukla *et al.* (1993b) have employed dynamic photoelasticity to evaluate the dynamic response of undamaged particulate media using assemblies of circular and elliptical particles subjected to explosive loading. Researchers (Walton, 1987, Trent, 1989, Ting and Corkum, 1992, and Sadd *et al.*, 1993) have also used a variety of numerical techniques to predict the dynamic response of granular media. Most recently, Singh *et al.* (1996) have conducted an experimental investigation to study dynamic load transfer through particulate assemblies containing notched particles. They demonstrated that the size and orientation of the notch greatly influences the load transfer process. The current study focuses on the effect of closed sharp cracks on dynamic load transfer in particulate assemblies subjected to explosive loading. The effects of crack size and orientation on the load transfer process are examined in detail. Finally, a comparison is drawn with the case of open notched flaws.

2.2 EXPERIMENTAL PROCEDURE AND ANALYSIS

A series of experiments was conducted on a one-dimensional assembly (or, single chain) of circular disks which were dynamically loaded by detonating an explosive at one end of the assembly. The assembly included a damaged particle containing a closed natural crack as the flaw. Both the size and orientation of the crack were systematically varied and the dynamic load transfer process was observed using two different experimental techniques. These techniques include, dynamic photoelasticity in conjunction with high-speed photography and electrical resistance strain gages. These two techniques were selected because of the complementary nature of information supplied by them, which when coupled together provides a complete assessment of the dynamic event. Dynamic photoelasticity is a full field experimental technique and provides complete qualitative and quantitative information about the load transfer process. However, limitations in the field of view of the high speed camera (0.032 m^2) restricts the number of disks that can be observed and analyzed in a given experiment. Thus, electrical resistance strain gages are employed to provide point-wise information over the entire particulate assembly.

The circular disks used to simulate granular media were machined from Homalite-100, a brittle, transparent polyester. This material exhibits stress induced birefringence and is ideally suited

for photoelastic studies. The flaw in the damaged disks was fabricated by initially machining a small starter notch. The disk was held in a vise and subjected to some compressive loading in the transverse direction. Then a sharp knife was tapped at the tip of the starter notch to initiate and propagate a closed natural crack. Controlling the pressure on the knife determined the length of the crack induced in the disk.

2.2.1 Photoelastic Approach: Local Observations

A schematic of the single chain assembly used for photoelastic experiments is shown in figure 2.1, which also shows the charge holder used to detonate the explosive. The assembly was placed in the optical bench of a multiple spark-gap Cranz-Schardin high-speed camera. This high speed camera records 20 photographic images of the dynamic event at a predetermined framing rate of up to a million frames/second. The explosive was detonated which caused a stress wave to propagate down the assembly of disks. The camera was synchronized to record photographs of the dynamic event after a predetermined time following the explosion.

Typical photographs obtained for stress wave propagation through a single chain of disks containing a damaged disk (50% diameter crack, oriented at 0°) are shown in figure 2.2. The isochromatic fringes in the photographs represent contours of constant maximum shear stress (τ_{max} = constant) and constitute the photoelastic data. As seen from figure 2.2, the stress wave front propagated down the single chain assembly. The velocity of this stress wave was determined by plotting the distance propagated by the wave front as a function of elapsed time. Figure 2.3, shows such a plot for the case of wave propagation in a single chain assembly containing a damaged disk (50% diameter crack, oriented at 0°). The average stress wave velocity was determined to be 1000 m/s which is about 45% of the longitudinal wave speed in the material.

The photoelastic data obtained in the form of isochromatic fringe patterns was coupled with appropriate field equations and analyzed to determine the contact loads as a function of time. Singh *et al.* (1996) have noted that the contact stresses in the undamaged disks follow a Hertzian distribution and thus are represented by the equations developed by Smith and Liu (1953). Accordingly, the stress field in the vicinity of the contact is given by,

$$\sigma_{zz} = -\frac{b}{\pi\Delta}\left[z\left(b\phi_1 - x\phi_2\right) + \beta z^2\phi_2\right] \qquad \textbf{(2.1)}$$

$$\sigma_{xx} = -\frac{b}{\pi\Delta}\left\{z\left(\frac{b^2 + 2z^2 + 2x^2}{b}\phi_1 - \frac{2\pi}{b} - 3x\phi_2\right) + \beta\left[(2x^2 - 2b^2 - 2z^2)\phi_2 + \frac{2\pi}{b}x + 2x\frac{(b^2 - x^2 - z)}{b}\phi_2\right]\right\} \quad \textbf{(2.2)}$$

$$\sigma_{xz} = -\frac{b}{\pi\Delta}\left\{z^2\phi_2 + \beta\left[(b^2 + 2x^2 + 2z^2)\frac{z}{b}\phi_1 - \frac{2\pi}{b}z - 3xz\phi_2\right]\right\} \quad \textbf{(2.3)}$$

where b is the half contact width and β is the friction factor such that $f = \beta P$ (refer figure 2.1). The parameter β will be the coefficient of friction if motion impends. Also, the following apply,

$$\phi_1 = \frac{\pi(M + N)}{MN\sqrt{2MN + 2x^2 + 2z^2 - 2b^2}}, \qquad \phi_2 = \frac{\pi(M - N)}{MN\sqrt{2MN + 2x^2 + 2z^2 - 2b^2}}$$

$$M = \sqrt{(b + x)^2 + z^2}, \qquad N = \sqrt{(b - x)^2 + z^2} \quad \textbf{(2.4)}$$

$$\Delta = 2R\left(\frac{1 - \nu^2}{E}\right)$$

The experimentally obtained isochromatic fringes represent contours of constant maximum shear stress and are governed by the stress-optic law,

$$\tau_{max} = \frac{\sigma_1 - \sigma_2}{2} = Nf_\sigma\frac{Nf_\sigma}{2h} \quad \textbf{(2.5)}$$

where, N is the fringe order, f_σ is the material fringe constant, and h is the specimen thickness. Digitized data from the isochromatic fringe patterns was analyzed using the stress field equations and the stress-optic law in conjunction with the multi-point nonlinear numerical technique developed by Shukla and Nigam (1985). This technique uses an over-deterministic least squares scheme to compute the half contact width b, and the friction factor β, from the experimental data. Once these two parameters were known the contact stresses were computed and numerically integrated over the

contact length to obtain normal and tangential contact loads. For the case of a single chain assembly of disks, the tangential loads approach zero and are therefore negligible. The normal loads were then used to generate plots of contact loads as a function of time. Figure 2.4 illustrates the variation of normal contact loads as a function of time for dynamic load transfer through a single chain assembly of disks containing a damage disk with a 50% natural crack at 0° orientation. Finally, wave velocity and attenuation of the peak contact load was determined from the variation of the contact loads as a function of time.

The wavelength of the stress wave pulse was determined directly from the isochromatic fringe patterns. As seen in figure 2.2, the wavelength of the stress wave pulse was observed to be approximately four disk diameters. Shukla et al. (1993b) have shown that such a wavelength is characteristic for stress wave propagation in single chain assemblies of undamaged circular disks.

2.2.2 Strain Gage Approach: Far Field Observations

Strain gages (MicroMeasurements: EA-13-031DE-120) were employed to provide point-wise information near the contact points over the entire particulate assembly. This complements photoelastic experiments by providing global (or far-field) information about the dynamic load transfer process. As shown in figure 2.5, a total of eight strain gages were employed to monitor the dynamic strain field at various contact locations in the single chain assembly. Four of these strain gages were mounted at contact locations around the damaged disk. The remaining strain gages were positioned at various contacts further down the single chain assembly. Strain gage data was collected and stored using Ectron amplifiers and a LeCroy digital data acquisition system, which provided the appropriate frequency response required for these experiments.

Strain gage data obtained from these experiments was in the form of strains varying as a function of time at various contact locations. Figure 2.6 shows typical strain profiles obtained for stress wave propagation down a single chain assembly of disks subjected to explosive loading. The wave velocity and wavelength of the stress wave pulse was determined directly from the arrival and departure time of the stress wave at various contact locations. Moreover, the dynamic strain gage data was also analyzed to determine the normal contact loads at various locations. For the case of plane stress,

$$\epsilon_{zz} = \frac{1}{E}\left(\sigma_{zz} - \nu\sigma_{xx}\right) \qquad \textbf{(2.6)}$$

Using the stress field equations (2.1) and (2.2), the strain along the z-axis (x=0) is given as (Xu and Shukla, 1993),

$$\epsilon_{zz} = -\frac{1}{E}\left[\frac{(1-\nu)b^2 - 2\nu z^2}{\Delta\sqrt{b^2+z^2}} + \frac{2\nu z}{\Delta}\right] \tag{2.7}$$

The half contact width ,b, was determined from (2-7) given the strain, ϵ_{zz}, and the strain gage location, z. Then, the normal contact load was determined as, (Smith and Liu, 1953),

$$w = \frac{b^2\pi}{2\Delta} \tag{2.8}$$

Figure 2.7 plots the variation of normal contact loads for dynamic load transfer through a single chain assembly containing a damaged disk with a 50% natural crack at 0° orientation. As for the photoelastic case, attenuation of the peak contact load was determined from the variation of the normal contact loads.

2.3 RESULTS AND DISCUSSION

Various experiments were conducted to study the effect of crack size and orientation on dynamic load transfer through single chain assemblies containing a damaged disk. In the first series of experiments the crack length was varied from 0 to 75% of the disk diameter, while maintaining the crack orientation fixed at 0° from the tangent plane of inter-disk contact. In the next series of experiments the crack orientation was varied from +90° to −90° while the crack length was kept fixed at 50% of the disk diameter. In both the series of experiments data from dynamic photoelasticity and strain gages were analyzed to monitor the load transfer process. Specifically, the experiments were analyzed to determine peak contact load attenuation, wave velocity, wave dispersion, and damage growth associated with stress wave propagation through the assembly.

2.3.1 General Observations

Dynamic isochromatic fringe patterns obtained for the 50% disk diameter crack oriented at 0° are shown in figure 2.2. They clearly show that the stress field in the damaged disk was distorted

as compared to the undamaged disks. This distortion was due to the presence of the natural crack. It should be noted that dynamic load transfer through granular media occurs through multiple reflections of stress waves at various free surfaces and through contact mechanisms. The net result of these reflections is a group wave that propagates through the assembly of particles. The inclusion of a crack within a given disk creates an additional surface for reflection and scattering of stress waves. Tensile stress waves impinging on the crack surface suffer scattering and reflection, while compressive stress waves close the natural crack and are transmitted. Moreover, the transmittance (or scattering) of shear stress waves is governed by the friction between the two crack surfaces and the sign of the normal component of load, i.e. tensile or compressive. Thus, stresses are only partially transmitted across the crack surface. This results in the discontinuity in the fringe contours across the crack surfaces, as seen in figure 2.2. Scattering of the stress waves at the crack surface can also result in the reflection of energy back up the chain in the form of a back reflected pulse. Additionally, a portion of the stress wave is momentarily trapped in the damaged disk due to the increased multiple reflections. This "trapping" results in an elongation of the stress wave pulse (as seen in frame 19 in figure 2.2) and in local changes in the contact loads.

An additional effect due to the presence of a crack is diffraction of stress waves at the tip of the natural crack. These diffractions result in crack tip loading, which could be sufficient to cause damage growth. Such damage growth would dissipate energy in the formation of new surfaces and also cause a change in the microstructural fabric of the particulate assembly. However, in the 0° orientation experiments no such crack growth was observed.

2.3.2 Effect of Crack Length

Two different crack lengths were used in this study, namely, 50%, and 75% of the disk diameter. These experiments were compared with the undamaged case which served as the baseline.

Typical isochromatic fringe patterns obtained for the 50% and 75% disk diameter crack cases are shown in figures 2.2 and 2.8, respectively. As discussed earlier the presence of a crack distorted the stress field within the damaged disk. However, the extent of distortion was greater for the 75% case, as seen by comparing the isochromatic fringes in frame 9 of figure 2.8 with those in frame 11 of figure 2.2.

The isochromatic fringes were analyzed to determine the normal contact loads. The variation of the normal contact load as a function of time, for the 50% crack case, is plotted in figure 2.4. The

peak contact load suffered a 10% attenuation across the four contact locations (between the 11th and the 15th disks). This was higher than the 3% attenuation observed earlier for wave propagation through a single chain of undamaged disks. Similar results were obtained for the case of a 75% crack disk (figure 2.9), and are ascribable to two mechanisms. The primary mechanism is due to the elongation of the stress wave pulse resulting from the "trapping" phenomenon discussed earlier. Elongation of the stress wave pulse results in the spreading of energy over a greater envelop and thus a drop in the peak contact load. The second and less significant mechanism is a result of energy dissipation by the frictional forces between the crack faces. Apart from increased attenuation and pulse elongation, the inclusion of a 50% (or 75%) cracked disk oriented at 0° does not significantly alter the load transfer mechanism through the damaged disk. This is apparent from the fact that the contact load profiles preceding the damaged disk are similar in shape to those after the damaged disk.

Strain gage experiments offered added insight into the effects of including a 50% (or 75%) cracked disk oriented at 0° in the single chain assembly. Typical strain versus time plots, for the case of a 50% cracked disk, are shown in figure 2.6. The stress wave pulse elongated by 25% from a duration of 110μs to 140μs as it propagated through the damaged disk. Once again, similar results were obtained for the case of a 75% cracked disk. As the stress wave propagated further down the chain, the duration of the pulse reverted back to the input pulse duration, 110μs.

Figure 2.10 plots the peak contact load attenuation as a function of distance propagated by the stress wave pulse for the different cases of undamaged and 50% and 75% cracked disks at 0° orientation. The peak contact load was normalized with respect to the maximum peak contact load, while the propagation distance was normalized with respect to the disk diameter. The normalizations were made to ease comparison between various cases. The figure shows a distinct difference between the cracked cases (50% and 75%) as compared to the undamaged case. For the cracked cases the peak contact load decreased locally right after the stress wave pulse propagated through the damaged disk. This drop was primarily due to the local elongation of the stress wave pulse. With further propagation the peak contact load increased as the elongated pulse regrouped into a pulse with the same duration as the input stress wave pulse. However, overall attenuation for the damaged cases (50% and 75%) was greater than that for the undamaged case. As shown in figure 2.10, the peak contact load attenuation increased from 20%, for the undamaged case, to 28% for the 75% cracked case for 1m distance of travel by the stress wave pulse (between the 11th and the 45th disks).

The wave velocity of the stress wave pulse was not affected by the presence of a damaged

disk in the single chain assembly. The average velocity for both the damaged and undamaged cases was determined to be 1000 m/s. Also, back reflected pulses were absent and no energy was returned up the single chain assembly due to the presence of a damaged disk.

2.3.3 Effect of Crack Orientation

In this series of experiments the orientation of the crack in the damaged disk was systematically varied from +90° to −90° in increments of 30°, while the length of the crack was kept constant at 50% of the disk diameter. The 50% crack case oriented at 0°, discussed in the previous section, served as the baseline case for this series of experiments. The ±90° cases represented special situations in which the open end of the crack was at one of the contacts.

Typical isochromatic fringe patterns obtained for dynamic load transfer through a single chain assembly containing a damaged disk with 50% crack oriented at +30° are shown in figure 2.11. A comparison of figures 2.2 and 2.11 demonstrates that the crack oriented at +30° influenced the load transfer process to a much greater degree that the crack oriented at 0°. The primary distinction was crack tip loading and subsequent crack growth for +30° orientation case. As shown in frames 1 and 4 in figure 2.11, the isochromatic fringes surrounding the crack tip correspond to a predominantly mode-II loading of the crack tip. This shear loading of the crack caused the crack tip to initiate and subsequently grow. Shear loading dominated crack tip initiation causing the crack to kink sharply and grow towards the contact following the damaged disk, parallel to the direction of stress wave propagation. Once the crack had started to grow the crack tip loading was predominantly mode-I in nature, as demonstrated in frame 9 of figure 2.11. Thereafter, the crack did not curve or kink and kept growing towards the contact following the damaged disk. The average crack tip velocity was determined to be ≈ 250 m/s which represents a typical value for dynamic crack propagation in Homalite-100. Post-mortem analysis of the fracture surface revealed a smooth surface, which corresponds well with the observed crack speed for this material. Crack growth was initiated early in the process of interaction of the stress wave pulse and the damaged disk. In fact, the crack had propagated through the entire disk even before the trailing edge of the stress wave pulse had left the damaged disk.

Crack growth resulted in a fragmentation of the damaged disk and hence in a rearrangement of the microstructure of the single chain assembly. As a result of disk fragmentation a portion of the damaged disk broke free and no longer contributed to the load transfer path. Moreover,

fragmentation also resulted in the redirection of the energy in the form of side loads. The side loads, as shown in frames 9, 12 and 19 in figure 2.11, resulted in energy transfer to the side supporting walls and hence in an energy loss from the stress wave pulse propagating down the single chain assembly. The rearrangement of microstructure would also play an important role in the load transfer process if the single chain assembly was subjected to another explosive loading.

Stress wave propagation through a single chain assembly containing a 50% cracked disk oriented at -30, +60°, or -60° also exhibited similar phenomenon as the +30° orientation case. As before, the stress wave loaded the crack tip and caused crack initiation and subsequent growth. The crack kinked sharply upon initiation and then grew parallel to the direction of stress wave propagation, either in the direction of the preceding contact or the following depending on orientation of the original crack. For the +30° and +60° orientations the crack propagated towards the following contact. Whereas for the -30° and -60° orientations the crack propagated towards the preceding contact. The direction of kinking and crack propagation was a function of the nature of shear loading at the crack tip, which in turn depended on the orientation of the pre-existing crack. This relationship between kinking direction and crack orientation is discussed in greater detail in the following sub-section. For all the ±30° and ±60° orientations crack growth was initiated early in the process of interaction of the stress wave pulse and the average crack tip velocity was ≈ 250 m/s.

The isochromatic fringes were analyzed to determine the variation of normal contact loads as a function of time. Figure 2.12 shows the plot for the +30° orientation case. Similar contact load profiles were obtained for all the ±30° and ±60 ° orientation cases. For all these cases the peak contact load suffered a 20% attenuation across the four contact locations (between the 11th and the 15th disks). This was twice the 10% attenuation observed for the case of a 50% cracked disk oriented at 0°. The increase in attenuation was primarily due to the elongation of the stress wave pulse as it propagated through the damaged disk. Additionally, some of the energy was transferred to the side supports in the form of side loads. These side loads were determined to be as high as 15% of the peak contact load. Some of the energy would be expected to be dissipated in the fracturing of the damaged disk. However, Singh *et al.* (1996) have shown that the energy dissipated in the fracture process represents a negligible fraction of the energy associated with the stress wave pulse

Strain gage data confirmed the elongation of the stress wave pulse. As shown in figure 2.13, the pulse elongated to a duration of 175 μs as compared to the input duration of 110 μs as it propagated through the damaged disk. This elongation was the primary factor contributing to the

attenuation in the peak contact load. The elongated stress wave pulse exhibited some *ringing* as it propagated further down the single chain assembly. This phenomenon involves the splitting of the elongated pulse into smaller wavelets and has been observed earlier (Shukla *et al.*, 1993b and Singh *et al.*, 1996). The presence of a back reflected pulse was also observed using strain gages. This pulse represented energy that was reflected back up the pulse due to multiple reflections occurring off the crack surface in the damaged disk. The pulse elongated to a duration of 175μs for all the ±30° and ±60 ° orientation cases.

The ±90° cases represented special orientations of the damage in the cracked disk. The open end of the crack formed one of the contact points and the crack itself was oriented along the direction of propagation of the stress wave. Typical isochromatic fringes obtained for stress wave propagation in a single chain assembly of disks containing a 50% cracked disk oriented at −90° are shown in figure 2.14. The propagating stress wave interacted with the natural crack resulting in crack tip loading. However, unlike the ±30° and ±60° cases the crack tip was loaded predominantly in mode-I as shown in frame 6 of figure 2.14. Such loading of the crack tip occurred because the crack was oriented parallel to the direction of propagation of the stress wave. Loading of the crack tip resulted in crack initiation and subsequent growth. The crack initiated under predominantly mode-I conditions and extended parallel to the direction of stress wave propagation. Crack kinking did not occur in this case due to the absence of any shear loading on the crack tip. This is explained in greater detail in the following sub-section. The average crack tip velocity was determined to be ≈ 320 m/s which was 28% greater than that observed for the ±30° and ±60° cases. Experiments conducted with the +90° case also resulted in crack initiation under mode-I conditions with no kinking. Moreover, the crack tip velocity was observed to be the same as the −90° case. Crack growth for the ±90° did not involve kinking and thus less energy was required to initiate and extend the crack. This resulted in the greater average crack tip velocities observed for these cases.

Crack growth resulted in a fragmentation of the damaged disk and hence in a rearrangement of the microstructure of the single chain assembly. However, both the disk fragments served as load bearing members in the single chain, as shown in frame 15 in figure 2.14. This facilitated the load transfer process through the fragmented disk and also reduced the transference of energy to the side supports. Thus, disk fragmentation did not affect the load transfer process as drastically as for the ±30° and ±60° cases.

Contact load profiles were also obtained for the ±90° crack orientation cases from an analysis

of the isochromatic fringe patterns. Figure 2.15 shows the variation of the normal contact load for stress wave propagation through a single chain assembly containing a damaged disk with a natural crack oriented at −90°. For both the ±90° orientation cases the peak contact load attenuation was determined to be 8% across four contact points. This attenuation was much lower than that observed for the other crack orientation experiments, and even lower than that observed for a 50% crack oriented at 0°. This was due to the more direct transmission of the stress wave pulse through the damaged disk as the crack surface was parallel to the direction of stress wave propagation.

Strain gage experiments were also conducted on long single chain assemblies containing 50% cracked disks oriented at ±90°. These experiments demonstrated that there was no appreciable elongation of the stress wave pulse as it propagated through the damaged disk. This lack of pulse elongation was also a factor contributing to the lower peak contact load attenuation observed for these two special crack orientations.

2.3.4 Damage Growth in Naturally Cracked Particles

Crack initiation and subsequent growth was observed for all the ±30°, ±60° and ±90° orientation cases. Post-failure photographs of the damaged disks are shown in figure 2.16. As shown, the crack grew parallel to the direction of the stress wave propagation, either in the direction of the preceding contact or the following depending on orientation of the original crack. For the ±30° and ±60° orientation cases, crack initiation was also associated with sharp kinking. Kinking was not observed for the ±90° orientation cases.

Consider stress wave propagation through a damaged disk. Since, the wavelength of the loading pulse was four times greater than the diameter of the disk we can consider the disk to be subjected to dynamic loads at the two contact points, as shown in figure 2.17. This dynamic axial compression of the cracked disk loads the crack either in shear or in tension depending on the relative orientation of the natural crack. Thus, the ±30° and ±60° orientation cases were loaded predominantly in shear accompanied by crack face sliding, as shown in figure 2.17(a), while, the ±90° orientation cases were loaded in pure tension, as shown in figure 2.17(b). It was also apparent that no crack tip loading would occur if the crack was perpendicular to the longitudinal axis of the disk. This explained the absence of crack tip loading for the 50% (and 75%) crack oriented at 0°.

Quasi-static experiments by Brace & Bombolakis (1963) and by Hoek and Bieniawski (1965) on glass plates containing cracks oriented at certain angles with respect to the direction of axial

compression showed that the relative sliding of the faces of the pre-crack produced, at the tip of these pre-cracks, small tension cracks which kinked at sharp angles from the sliding plane. More recently, Nemat-Nasser & Horii (1982) and Horii & Nemat-Nasser (1985) analytically and experimentally investigated the axial compression of plates containing flaws oriented at an angle with respect to the compression direction. They showed that, under axial compression, tension cracks nucleated at the tips of the sliding pre-existing crack and extended along the maximum compressive stress direction.

The crack kinking observed in the ±30° and ±60° orientations was a result of a tensile crack being nucleated at the tip of the sliding pre-existing crack. In accordance with the analytical work of Nemat-Nasser and Horii (1982), this tensile crack grew parallel to the direction of axial compression. The direction of kinking was governed by the relative sliding of the crack faces. Thus, the -30° and -60° cracks kinked upward, as shown in figure 2.17(c), while the +30° and +60° cracks kinked downward, as shown in figure 2.17(d). The ±90° cracks were not subjected to crack face sliding and thus no kinking was observed.

Crack initiation (and subsequent growth) would occur if the axial compression sufficiently loaded the crack tip. This loading would primarily depend upon the relative orientation of the natural crack. Thus, the probability of crack initiation (and subsequent growth) can be expressed as,

$$P_{initiation} = H\left(|\,\theta\,| - \theta_C\right), \tag{2.9}$$

where H(•) denotes the Heaviside step function, θ is the orientation of the natural crack, and θ_C is the critical angle of initiation. From experimental observations,

$$0° < \theta_C \leq 30°, \textit{ for the case of natural cracks.} \tag{2.10}$$

2.3.5 Natural Cracks versus Open Notches

Singh *et al.* (1996) have investigated dynamic load transfer through particulate assemblies containing damaged particles where the damage was simulated by open notched flaws. The results of the current study indicate several similarities and differences that exist between the cases of natural cracks and open notches. The open notch served as a greater barrier to stress wave propagation through the damaged disk than the closed natural crack. All the stress waves impinging on the open notch suffered scattering and reflection, unlike the case of the closed crack. Thus, the open notch resulted in more reflections of the stress wave within the damaged disk as compared to the natural crack. This caused a greater elongation of the stress wave pulse as it propagated through the

damaged disk. For example, the pulse elongated to a duration of 330μs as it propagated through a damaged disk containing a 75% disk diameter open notch oriented at 0°, as compared to only 140μs when the damage was in the form of a natural crack. This increased pulse elongation resulted in greater local attenuation of the peak contact load, produced ringing and dissipation of secondary wavelets and thus lead to greater overall attenuation of the peak contact load. The open notch also resulted in more energy being sent back up the chain in the form of a back reflected pulse.

Analogous to the 0° orientation cases, the angled cases also showed significant differences when the damage was simulated by an open notch, or by a natural crack. The notch resulted in greater elongation and attenuation of the stress wave pulse. Also, there were significant differences between the notched case and the natural crack case with regards to the crack initiation and propagation behavior. All the natural cracks oriented at angles other than 0° initiated early on in the stress wave - crack interaction process. Whereas, for the open notch cases, crack initiation and growth occurred only for the −60° and ±90° orientations and that too only after most of the stress wave-pulse had already propagated through the damaged disk. For both types of flaws crack initiation occurred due to tensile reflections that impinge upon the crack tip. For the natural crack the crack tip was sharp and initiated easily. However, for the open notch the tip was blunt. Thus, initiation occurred only after most of the stress wave pulse had propagated through the damaged disk and the tensile reflections could dominate over the compressive stress wave pulse. The open notch oriented at +60° did not initiate and extend (unlike the open notch oriented at −60°). This was due to the grazing incidence that the stress wave impinged at upon the +60° notch. The notch was loaded only from one side and the tensile stresses at the tip were not sufficient to warrant initiation and extension. This grazing incidence of the stress wave at +60° notch caused shear waves to be reflected off towards the preceding contact. This resulted in a time dependent shear loading at the contact preceding the damaged disk. The shear load was oscillatory in nature and of a magnitude up to 20% of the peak normal contact load. Such shear loading was not observed in the case of a natural crack oriented at +60°.

2.4 CLOSURE

The results have shown that the presence of damaged disks significantly influenced dynamic load transfer through a one-dimensional particulate assembly. The effects of varying crack length and crack orientation on the load transfer process are summarized as follows :

(1). The stress field in the damaged disk was distorted as compared to the undamaged disks due to the presence of a flaw in the form of a closed natural crack. The crack reflected and scattered the tensile and (some) shear stress waves within the damaged disk. Scattering of the stress waves by the crack caused an elongation of the stress wave pulse as it propagated through the damaged disk, and also reflected energy back up the chain in the form of a back reflected pulse. These two mechanisms contributed to a *local* attenuation in the peak contact load. The elongated stress wave pulse exhibited ringing and broke into separate wavelets. The secondary wavelets dissipated with further propagation contributing to increased *overall* attenuation.

(2). Results of varying the crack length from no-damage to 50% of the disk diameter (oriented at 0°) showed that the pulse was elongated from 110μs to 140μs as it propagated through the damaged disk. However, no appreciable change was noted as the crack length was further increased to 75% of the disk diameter. For the ±30° and ±60° orientations the pulse elongated from 110μs to 170μs as it propagated through the damaged disk. However, no appreciable pulse elongation was observed for the ±90° orientation cases as the crack surfaces were oriented parallel to the direction of stress wave propagation and thus offered little resistance to the propagating stress wave.

(3). Stress wave diffraction at the tip of the natural crack loaded the crack tip and in certain cases resulted in crack initiation and damage growth. Crack extension was observed for all cracks oriented at angles other than 0°. For the ±30° and ±60° cases the crack was loaded predominantly in shear accompanied by crack face sliding. This sliding resulted in a kinked tensile crack to be nucleated at the tip of the pre-existing crack. After initiation the crack grew parallel to the direction of stress wave propagation without further kinking. For the ±90° the crack was initiated under mode-I and kinking did not occur. Crack growth resulted in a fragmentation of the damaged disk and in a rearrangement of the microstructure of the single chain assembly. For the ±30° and ±60° cases a portion of the damaged disk broke free and no longer contributed to the load transfer path. Moreover, fragmentation also resulted in the redistribution of the energy in the form of side loads. For the ±90° cases both the fragments still acted as load bearing members and the side loads were minimized.

(4). The average wave velocity of the stress wave pulse was not affected due to the presence of a damaged disk. The group wave velocity was determined to be ≈1000 m/s for all the various

assemblies studied.

(5). Damage in the form of a closed natural crack served as less of a barrier to the propagating stress wave as compared to an open notch. Thus, the closed natural crack resulted in less elongation of the stress wave pulse as it propagated through the damaged disk and thus in smaller local and far field attenuations.

(6). Closed natural cracks were more conducive to crack initiation and subsequent growth than the open notches. Thus, all the $\pm 30°$, $\pm 60°$ and $\pm 90°$ orientation cases exhibited crack growth for the case of natural cracks, whereas only the $-60°$ and $\pm 90°$ cases exhibited crack growth for the case of open notches. This difference was basically due to the presence of a sharp crack tip in the former cases, as compared to a blunt notch tip in the latter.

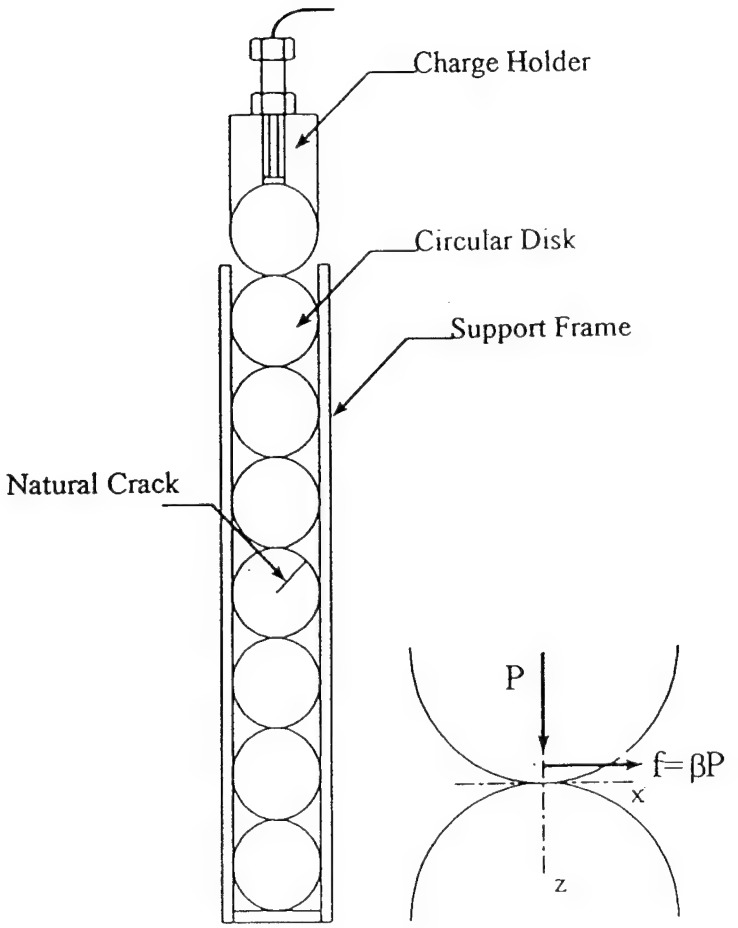

Figure 2.1. Schematic of a single chain setup of Homalite-100 disks containing a damaged particle for dynamic photoelastic experiments.

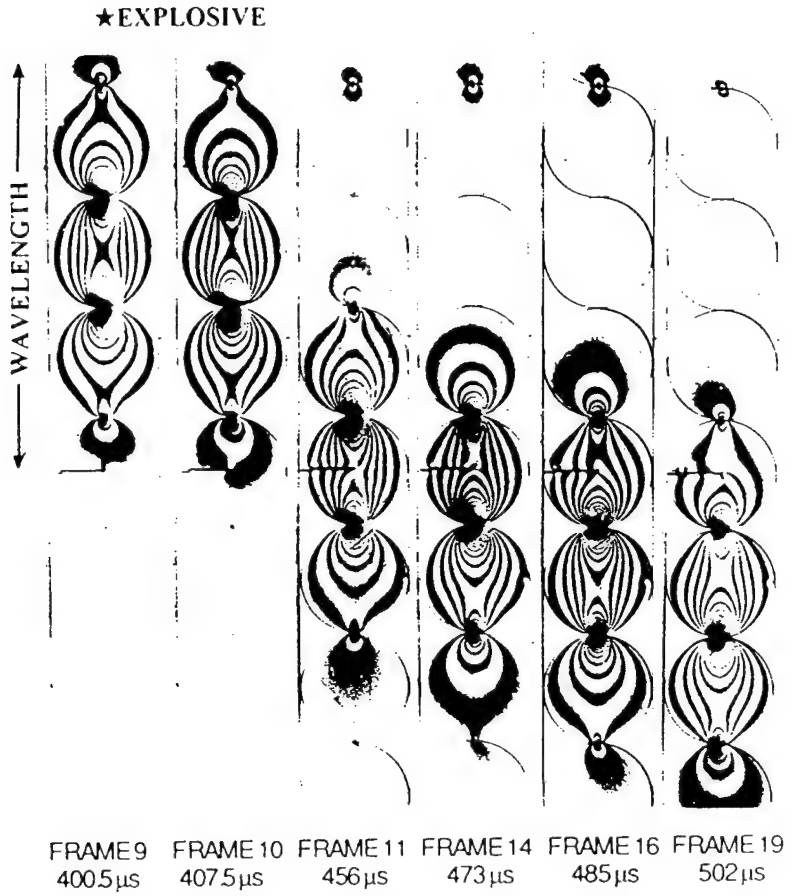

Figure 2.2. Typical isochromatic fringe patterns obtained for dynamic load transfer through a single chain assembly containing a damaged particle with a 50% natural crack at 0° orientation.

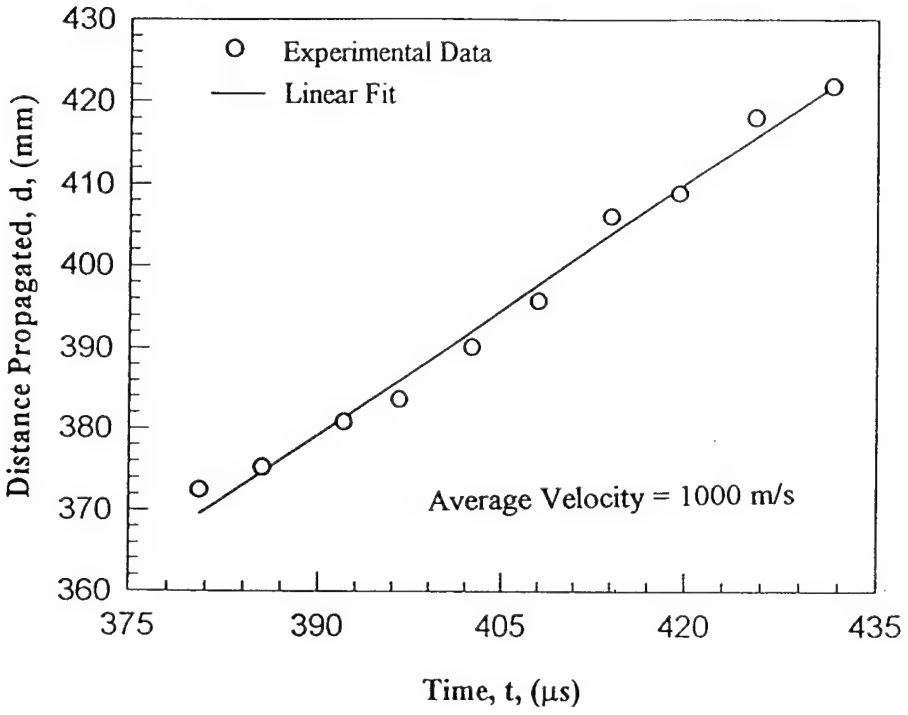

Figure 2.3. Distance propagated by the stress wave as a function of time through a single chain assembly containing a damaged particle with a 50% natural crack at 0° orientation.

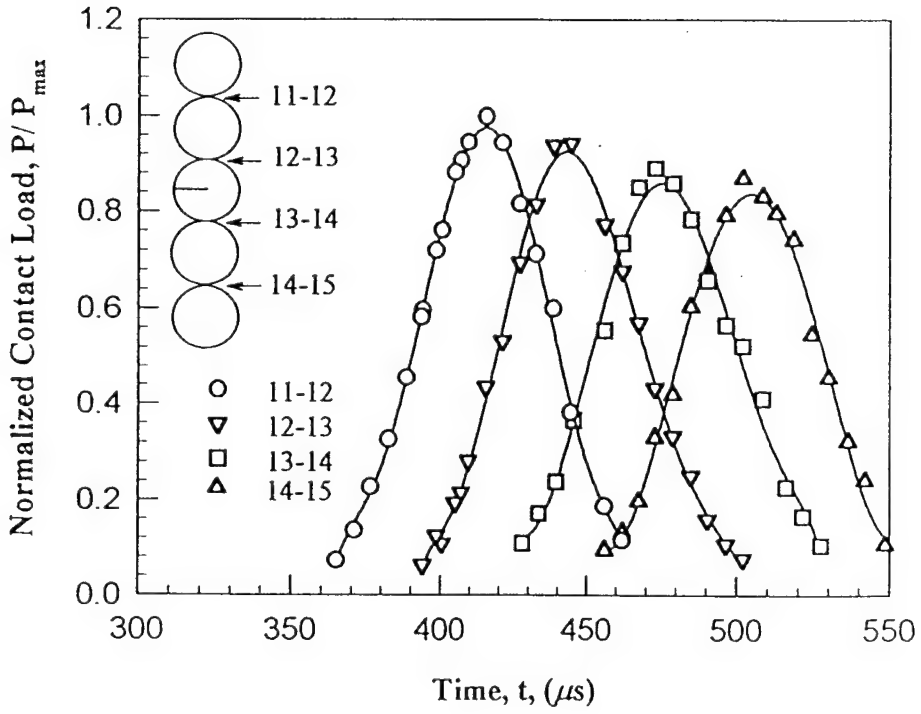

Figure 2.4. Variation of normal contact loads for dynamic load transfer through a single chain assembly containing a damaged particle with a 50% natural crack at 0° orientation.

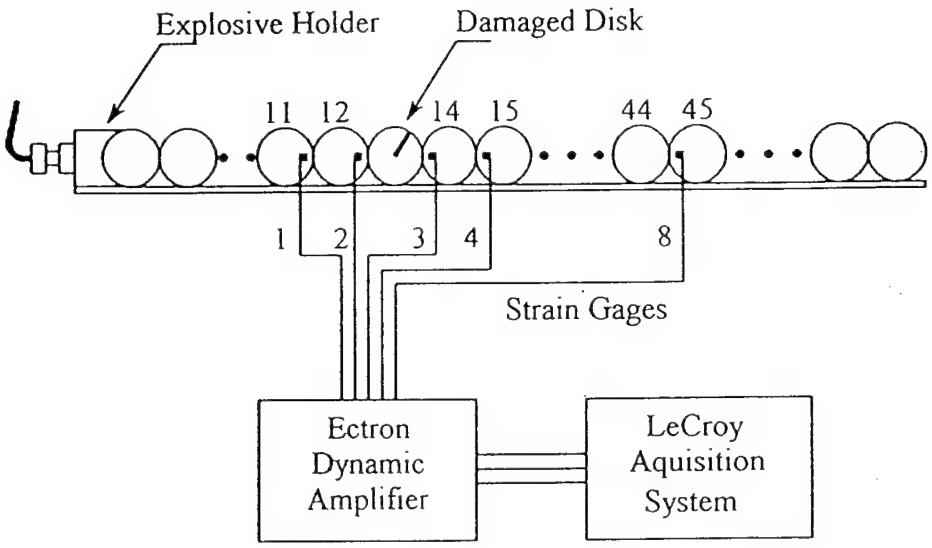

Figure 2.5. Schematic of a single chain setup of Homalite-100 disks containing a damaged particle for strain gage experiments.

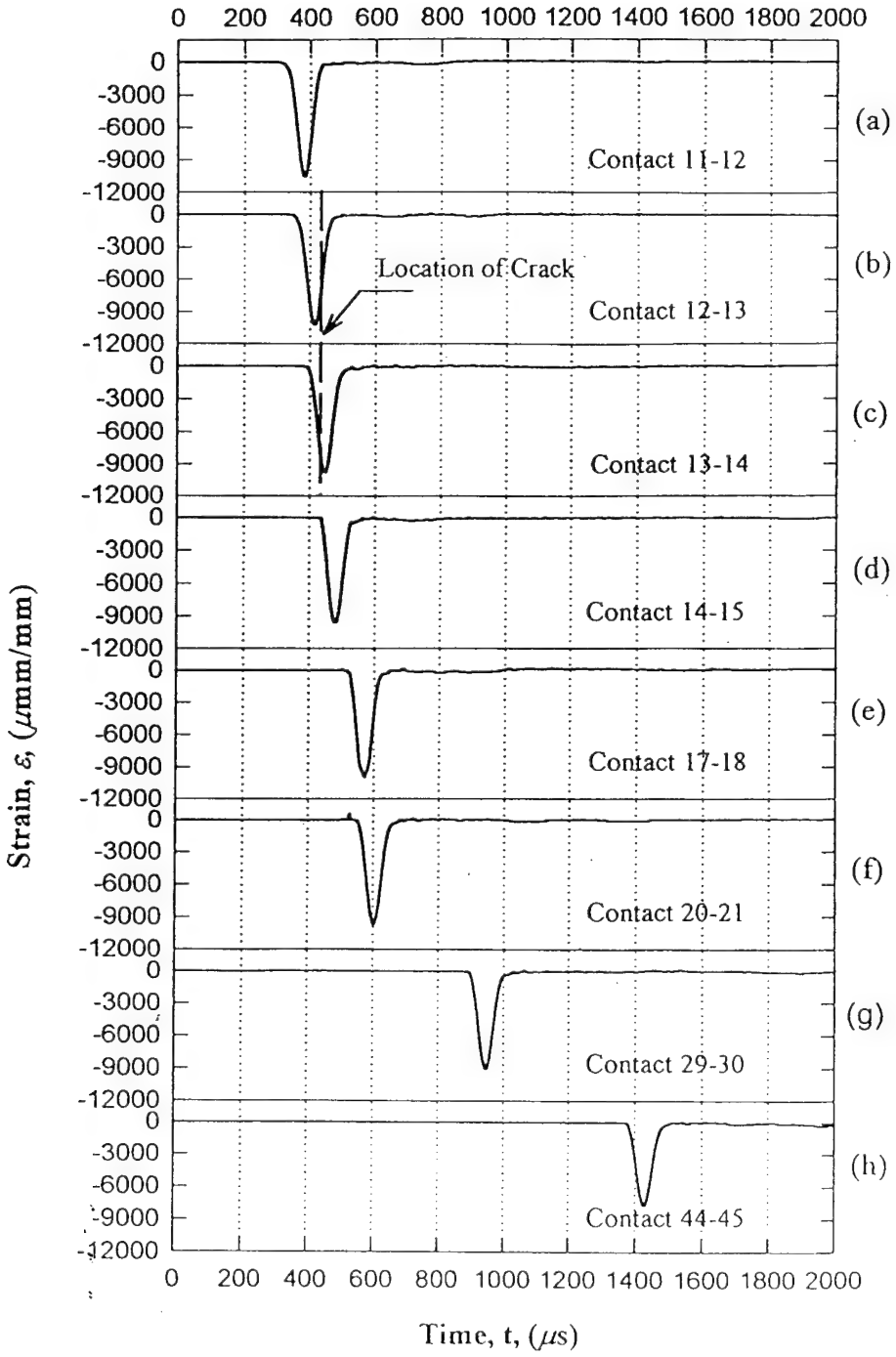

Figure 2.6. Strain gage data for dynamic load transfer through a single chain assembly containing a damaged particle with a 50% natural crack.

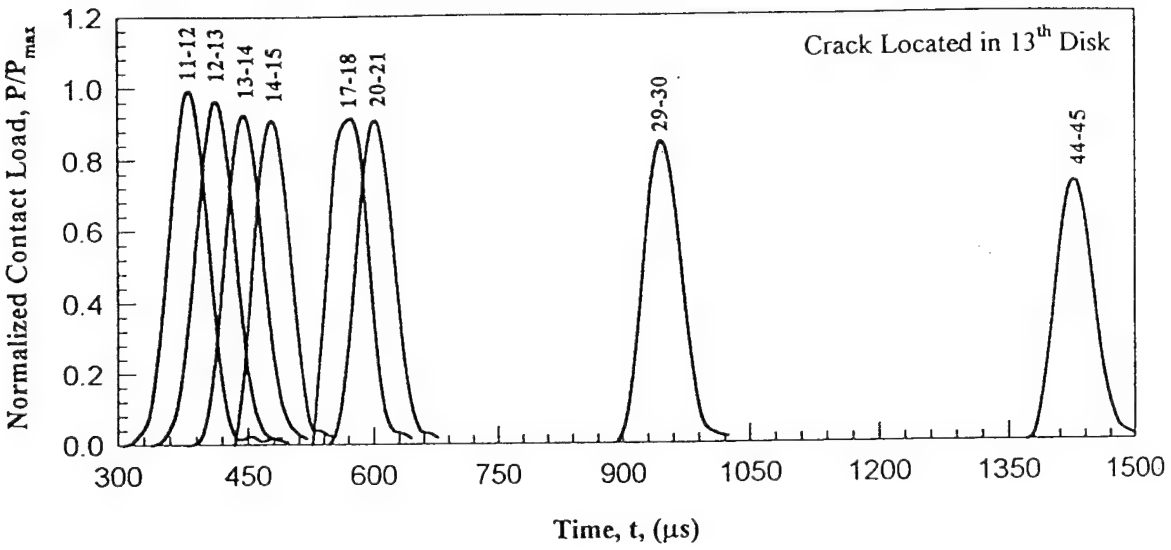

Figure 2.7. Variation of normal contact loads for dynamic load transfer through a single chain assembly containing a damaged particle with a 50% natural crack oriented at 0° (strain gage data).

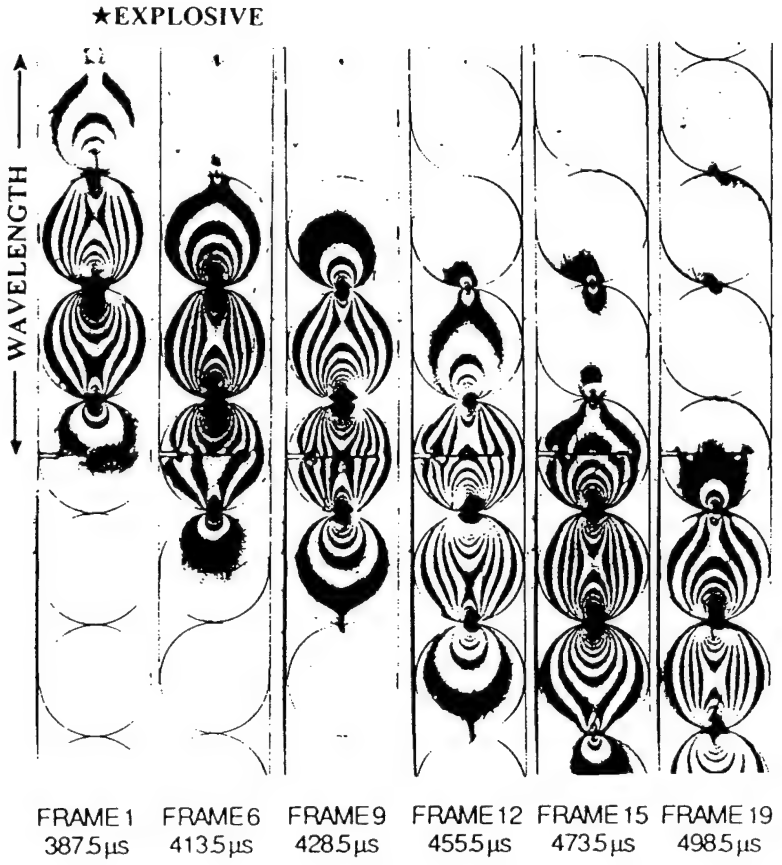

Figure 2.8. Typical isochromatic fringe patterns obtained for dynamic load transfer through a single chain assembly containing a damaged particle with a 75% natural crack oriented at 0°.

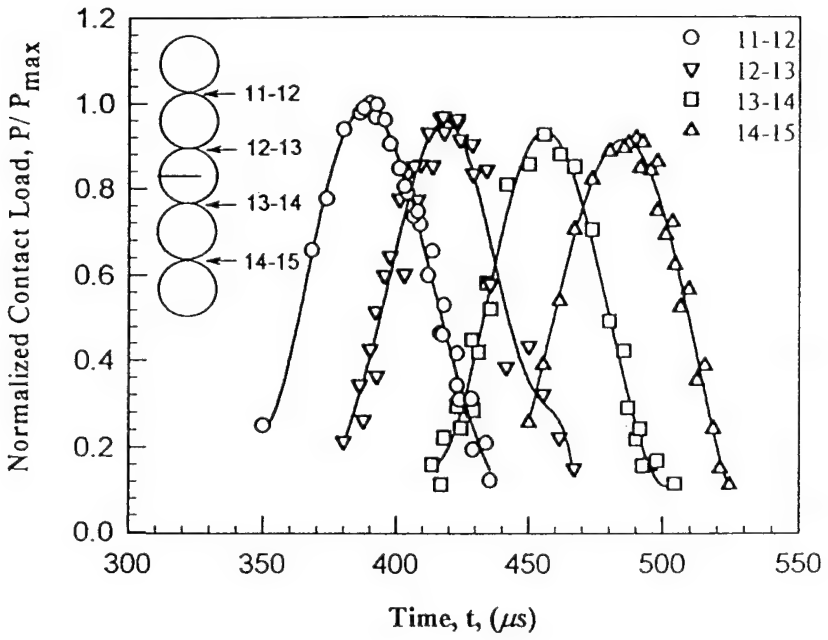

Figure 2.9. Variation of normal contact loads for dynamic load transfer through a single chain assembly containing a damaged particle with a 75% natural crack oriented at 0°.

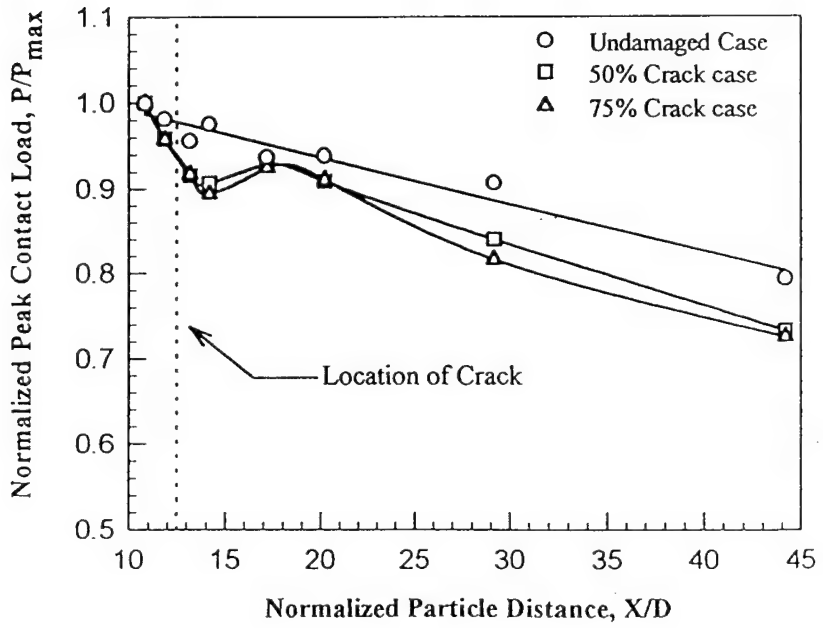

Figure 2.10. Normalized peak contact load attenuation as a function of normalized distance propagated for the case of undamaged and 50% and 75% cracked disks oriented at 0° (strain gage data).

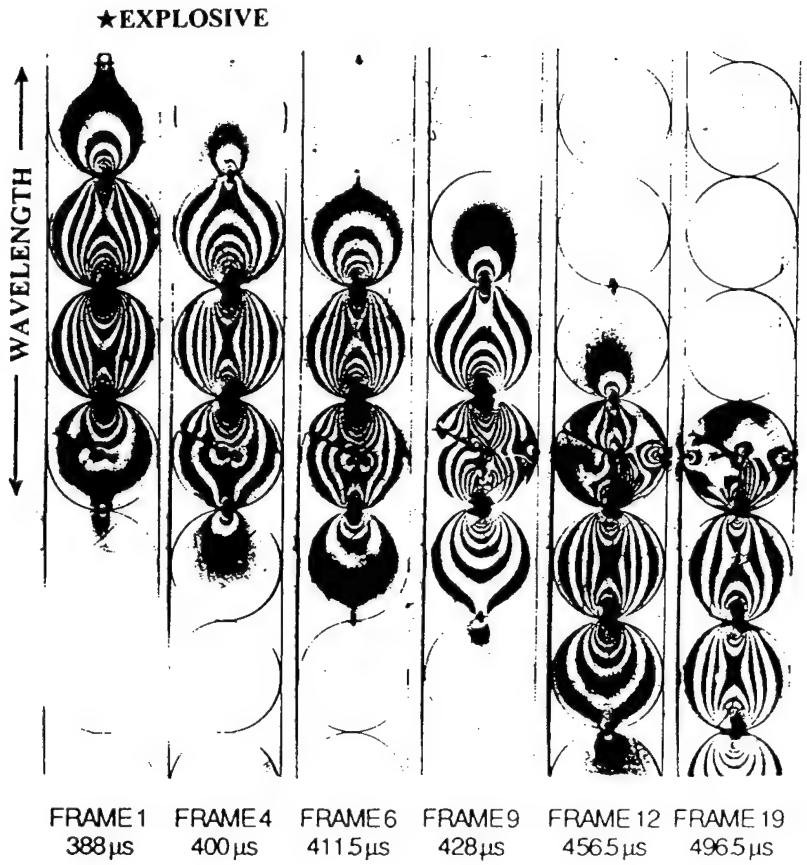

Figure 2.11. Typical isochromatic fringe patterns obtained for dynamic load transfer through a single chain assembly containing a damaged particle with a 50% natural crack at +30° orientation.

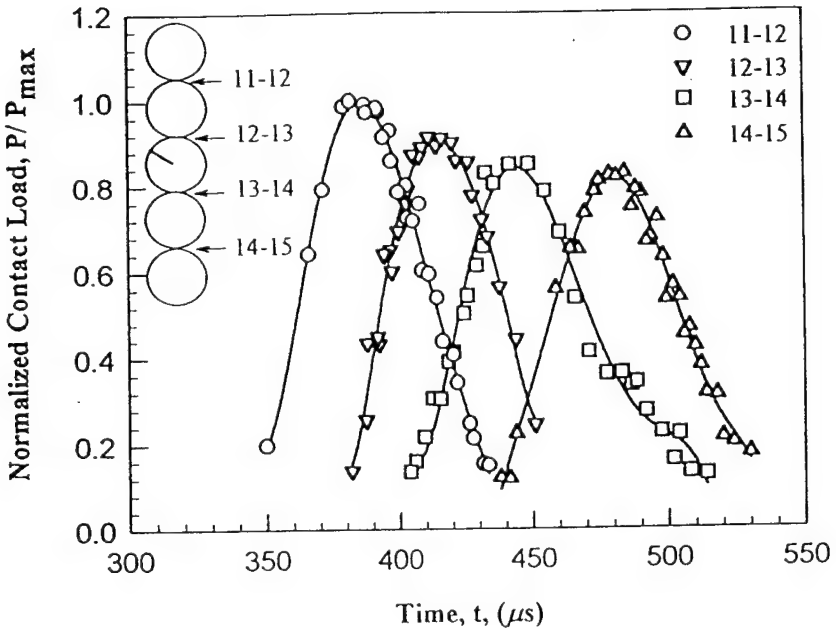

Figure 2.12. Variation of normal contact loads for dynamic load transfer through a single chain assembly containing a damaged particle with a 50% natural crack oriented at +30°.

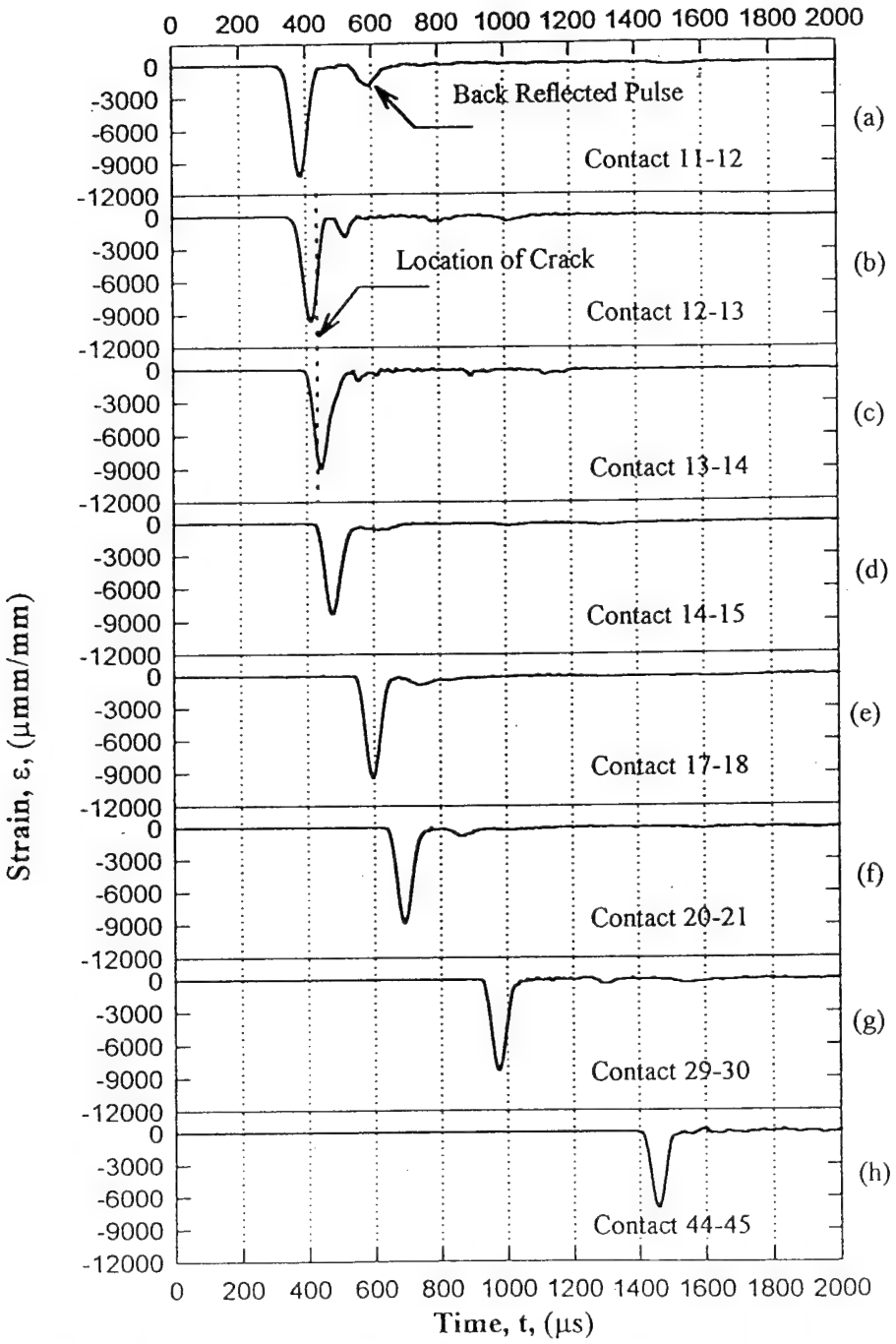

Figure 2.13. Strain gage data for dynamic load transfer through a single chain assembly containing a damaged particle with a 50% natural crack oriented at +30°.

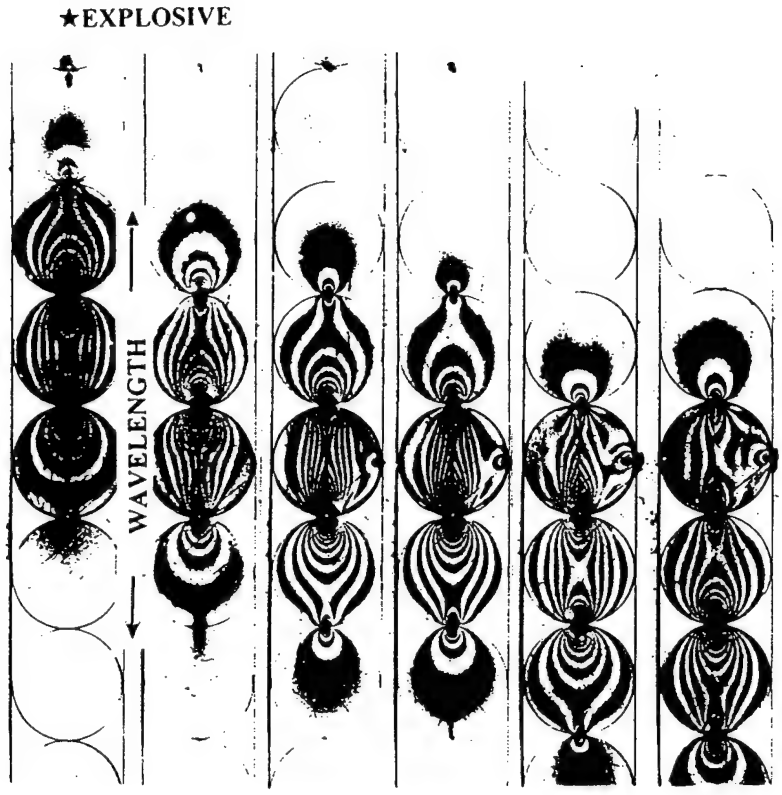

Figure 2.14. Typical isochromatic fringe patterns obtained for dynamic load transfer through a single chain assembly containing a damaged particle with a 50% natural crack oriented at -90°.

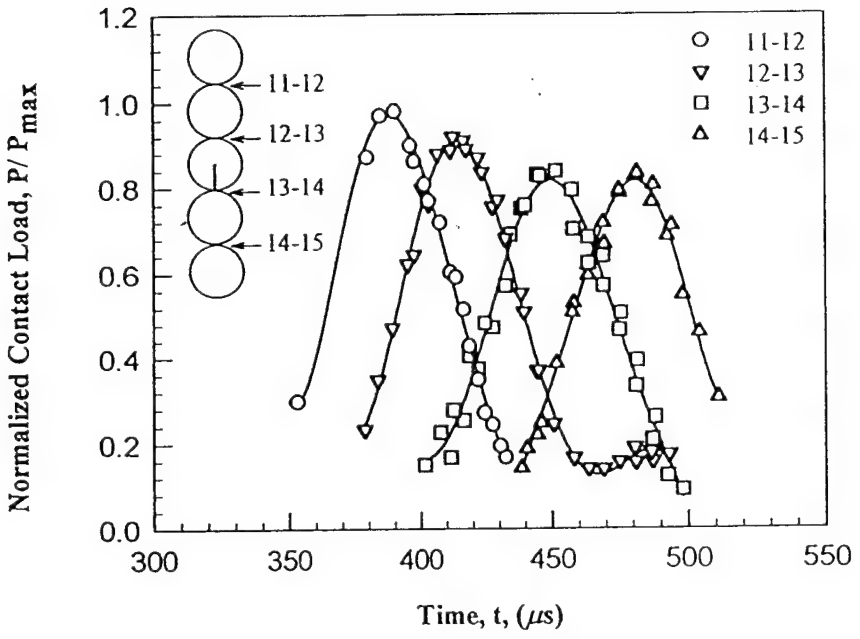

Figure 2.15. Variation of normal contact loads for dynamic load transfer through a single chain assembly containing a damaged particle with a 50% natural crack oriented at -90°.

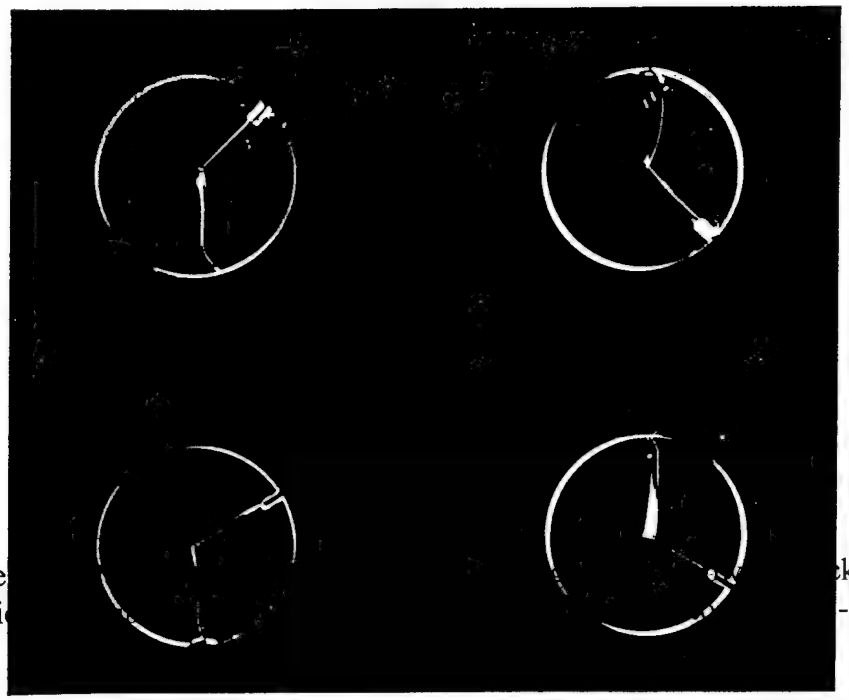

Figure ck
initiati -30°,
+60°,

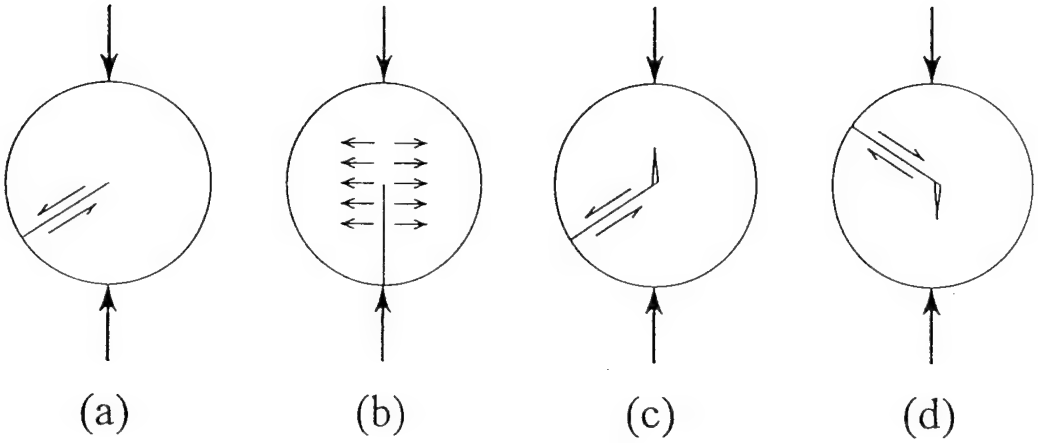

Figure 2.17. Damage growth of crack subjected to dynamic loading by the propagating stress wave. (a) Shear loading of ±30° and ±60° cracks; (b) Tensile loading of ±90° cracks; (c) Upward kinking in -30° and -60° cracks; and (d) Downward Kinking in +30° and +60° cracks.

CHAPTER 3

STRESS WAVE PROPAGATION THOUGH PARTICULATE MEDIA

ABSTRACT

This chapter provides the results of an experimental study, which was conducted using strain gage techniques to study near and far field effects of repeated loading of cracked particles and the effect of stress wave interaction with multiple spaced particles containing flaws on the dynamic load transfer process. In the context of this study, "repeated loading" refers to loading of previously fractured notched open cracks. The study also focuses on the interaction of multiple spaced particles containing single flaws which are separated by relatively long distances within the single chain assembly. Experimental data is analyzed to obtain the wave velocity, wave dispersion, damage growth, and peak contact load attenuation, during the dynamic load transfer process. The results show that repeated loading of fractured particulate media effects the pulse duration and peak contact load attenuation locally. Interaction of the stress wave with multiple spaced particles containing flaws results in rapid dissipation of the stress wave pulse and separation of the pulse into wavelets.

3.1 INTRODUCTION

In the study of stress wave propagation in damaged particulate media, cases of repeated loading of cracked particles and/or stress wave interaction with multiple spaced particles containing flaws need to be considered. Scattering and diffraction effects would lead to a modification of the stress wave pulse, which may cause a change in the velocity and attenuation of the pulse. Rearrangement of the media and/or fracture of particles may result in greater attenuation and possibly further restructuring of the media. As a result, a study is conducted to investigate the effect of repeated dynamic loading on fractured particulate systems. A series of experiments is conducted using the single chain assembly of disks and the setup is shown in figure 3.1(a). Assemblies containing one or more fractured disks within the single chain assembly are then subjected to a stress wave pulse. Strain gage methods are employed for near and far-field observation and analysis of the stress wave pulse.

In addition, a study is conducted to investigate the effect of stress wave interaction with multiple spaced particles containing flaws on the dynamic load transfer process in a single chain assembly of particles. A series of experiments is conducted using the single chain assembly of disks

and setup shown in figure 3.2. As shown in this setup, additional cracked disk(s) are placed further down the single chain assembly to allow for repeated interaction of the affected stress wave pulse. Results obtained from these experiments are then used to provide insight on the nature of the stress wave pulse after encountering a second section of flawed disks in a single chain assembly.

Previous results obtained using notched open crack flaws indicate that the stress wave pulse is affected both locally in terms of wave elongation, wave dispersion and attenuation and in the far field in terms of attenuation and separation into primary and secondary wavelets (i.e. ringing phenomenon). As the pulse travels down the single chain assembly and encounters a precracked disk, under certain conditions, damage growth occurs. Previous experimental results using notched open flaws have shown that the affected stress wave pulse traveling down the single chain assembly eventually begins to resemble the input pulse with a lower amplitude. Reintroduction of this pulse to another set of flawed particles down the single chain assembly provide other features which are discussed in this section.

3.2 EXPERIMENTAL PROCEDURE

A series of experiments was conducted on single chain assemblies of circular disks containing one or more flawed particulates which were loaded by detonating a small amount of explosive material (lead azide) on one end of the assembly. A sketch of such an assembly, including the specially designed explosive charge holder, is provided in figure 3.2. This assembly was kept simple by the use of circular disks arranged in a one dimensional chain in order to fix as many variables as possible and simplify the physics involved. An explosive charge of 15 mg was detonated in the charge holder.

Circular disks used to simulate particulate media were machined from Homalite-100, a brittle transparent polyester, which is birefringent has been used in previous photoelastic studies. Particle damage was introduced by fabricating notched open cracks in these disks using a band-saw.

3.2.1 Strain Gage Approach and Analysis

Electrical resistance strain gages are employed to study the near and far-field aspect of the stress wave pulse. In particular, stress wave pulse elongation and/or separation into primary and secondary wavelets (i.e., ringing phenomenon) and overall stress wave pulse peak contact load attenuation were investigated.

Electrical resistance strain gages (MicroMeasurements: EA-13-031DE-120) were also

employed to study stress wave propagation and attenuation at prescribed locations along the entire chain assembly. As shown in figure 3.2, eight separate strain gages were placed at various locations to monitor the strains resulting from the stress wave pulse propagating through the assembly. The first four strain gages were positioned at contact locations around the cracked disk for both series of experiments. The remaining strain gages were located at various contacts further down the single chain assembly as shown in figure3.2. The analysis procedure for the strain gage experiments is discussed in detail in Shukla and Yi (1993).

3.3 RESULTS AND DISCUSSIONS

A sequential experimental inquest of the factors influencing stress wave propagation in flawed particulates was conducted. In the repeated loading experiments the crack length was fixed while the crack orientation with respect to the incoming stress wave pulse was varied. Assemblies were initially loaded and fractured and then reloaded to observe additional effects. In experiments dealing with stress wave interaction of multiple spaced particles containing flaws, two different assemblies were studied; one assembly contained two disks with single 75% percent disk diameter cracks, each placed at a distance apart, and the second assembly contained two sets of four disks containing 50% disk diameter cracks and these sets were also placed at a distance apart.

Results from these experiments were analyzed to determine peak load attenuation at prescribed contact locations, wave dispersion and any additional damage associated with wave propagation through the flawed particulates. Results are discussed in detail and compared with previous experimental results of notched open type flaws.

3.3.1 Effect of Repeated loading

These sets of experiments were conducted on single chain assemblies containing a single disk with a simulated notched open crack. The crack length in all the experiments was maintained constant at 50% of the disk diameter. A total of three different chain assemblies was selected to investigate the dynamic load transfer process. These included crack orientations -60^0, -90^0 and $+90^0$ as measured from the tangent plane of contact (the zero degree plane is the plane normal to the incoming stress wave pulse). Selection of these assemblies was based on previous experimental results, in which damage growth occurred after being subjected to dynamic loading. After each experiment, fractured disks were placed back in the assembly with the same crack orientations and reloaded with the same

loading conditions.

Typical strain gage data, obtained for a single chain assembly containing no precracked disks, shown in figure 3.1(b), indicates that the stress wave pulse propagates through the assembly with negligible attenuation. However, when a damaged particulate is introduced in the assembly, it influences stress wave propagation through the medium. Several experiments were conducted initially on assemblies containing damaged particulates with crack lengths and orientations as described earlier. After each experiment the fractured disk was then placed in the assembly in the same location with the crack oriented in the same direction prior to reloading. Results from strain gage experiments, for the -60^0 crack case is provided in figure 3.3. These results indicate that the crack influences the stress wave pulse propagating through the assembly resulting in an increase in both wavelength and peak load attenuation. As the pulse propagated through the cracked disk, the duration of the pulse increased from 115 μs to 170 μs, as shown in figure 3.3 b, c and d. This represents a 48 percent increase from the input pulse and is consistent with previous results obtained for this assembly. As a result, the peak load attenuation increased from 2 percent for the no crack case to 28 percent for the -60^0 case.

Repeated loading of the fractured disk resulted in a further increase in wavelength and peak load attenuation for the same crack orientation, with no further damage. As shown in figure 3.4 b, c and d, the stress wave pulse duration prior to and immediately following the precracked disk was slightly longer than the initial loading case. For instance, the duration of the loading pulse passing through the fractured disk was slightly greater, (from 110 μs to 180 μs) than that observed in the initial loading case. This represents a 64 percent increase in wave length as compared to the input pulse. This is due to the increased multiple reflections resulting from an increase in free surface area of the crack.

A comparison of peak contact load attenuation between the initial loading and repeat loading -60^0 cases, is provided in figure 3.5. As shown, reloading of the fractured disk resulted in a greater increase in the peak contact load attenuation through the fractured disk. The peak contact load attenuation for the initial loading case was 28 percent versus 37 percent for the reloaded case. The difference in attenuation is attributed to the increased surface area present in the fractured specimen. As the stress wave pulse propagates through the fractured specimen, more reflections occur, because of the greater surface area present. This results in greater elongation of the stress wave pulse and therefore an increase in the attenuation of the stress wave pulse. Overall peak contact load attenuation

increased slightly from 37 percent for the initial -60^0 loading case to 40 percent for the repeat loading case.

Strain gage experiments were also conducted for the -90^0 and $+90^0$ notched open crack orientations. The cracks in these assemblies were oriented such that one of the contacts occurred at the open end of the crack resulting in a two-point contact. With these orientations energy transfer at the two point contact location occurred via two separate paths. Also, with these orientations the crack surfaces were aligned in the direction of the stress wave pulse resulting in minimal direct reflections off the crack surfaces. As the stress wave pulse propagated through the precracked disk, crack propagation occurred. In both cases the crack propagated straight along the crack axis to the next contact point. Figures 3.6 and 3.7 provide the results of both crack orientations, respectively, for the initial loading case. The pulse duration for both of these assemblies was consistent with the -60^0 case discussed earlier.

Repeat loading of each of these assemblies, containing the fractured disk, was conducted using the same strain gage set up shown in figure 3.2. Strain gage results for the -90^0 and $+90^0$ cases, are provided in figures 3.8 and 3.9 respectively. A comparison between these results and the results from the corresponding initial loading case indicates that changes to the wavelength were minimal for both orientations. Also, the peak contact load attenuation in each case was slightly greater for the repeat loading of fractured disk's series, as shown in figures 3.10 and 3.11. Peak contact load attenuation across four contact points, prior to and after the precracked or fractured disk, indicate an increase from 24 percent to 27 percent for the -90^0 case and from 22 percent to 27 percent for the $+90^0$ case. However, in comparison this increase is smaller than the increase observed in repeat loading of the -60^0 case. This is indicative of the two point contact present at the contact locations in both 90^0 cases. In the initial loading case the transfer of energy occurred via two separate paths at the contact location as stated earlier. As the stress wave propagated through the precracked disk, crack propagation occurred along the crack axis resulting in a two point contact at the opposite end of the open crack. Upon reloading the assembly containing the fractured disk, the transmission path was again noted to be via two separate paths, occurring at both contact points. A slight increase in attenuation was observed, which is attributed to the increased surface area present in the fractured disk.

The average velocity of the stress wave pulse for all assemblies was determined to be 930 m/s, which remained constant throughout the propagation of the stress wave pulse. These results are in

agreement with the experimental results provided in Shukla and Yi (1993) for notched crack assemblies.

3.3.2 Effect of Stress Wave Interaction with Multiple Spaced Flawed Particles

A series of strain gage experiments was conducted on single chain assemblies containing particulates with notched open cracks to observe near and far-field effects of stress wave interaction of multiple spaced flawed particles on stress wave propagation through particulate media. Essentially, two different single chain assemblies were adopted for this study, one of the assemblies contained two 75% disk diameter cracks, one placed near the top of the assembly (disk 13) and the other near the end of the assembly (disk 49) and the other assembly contained two sets of multiple (four) adjacent disks with single 50% disk diameter cracks oriented in parallel to the plane of contact. In this assembly, the cracks were placed in a staggered fashion with crack opening directions of 180^0, 0^0, $0^{0'}$ and 180^0 in series. One set of four precracked disks was placed at the 13th through 16th disk location and a second set of disks was placed at the 52nd through 55th disk location as shown in figure 3.2.

Selection of these assemblies was based on previous experimental results presented in the Shukla and Yi (1993), using similar assemblies containing a single set of notched open cracks. Results indicated greater peak contact load attenuation and greater wave elongation through the precracked disk(s). For instance, in the 75% crack case, the duration of the loading pulse was almost tripled, from 120 μs to 330 μs, as the stress wave pulse passed through the precracked disk. Also, the peak contact load attenuation for these assemblies averaged between 35 percent and 55 percent, depending on the assembly. However, in all of these assemblies the elongated wavelength at distances approaching one meter from the cracked disk eventually resembled the input pulse with a lower amplitude. As a result, a series of experiments was conducted to study the effect of reintroducing the affected stress wave pulse with an identical disturbance (flaw) at this location.

Strain gage experiments were conducted using the setup shown in figure 3.2. Typical strain gage data obtained for a single chain assembly containing two disks with single 75 percent notched open cracks, one located at disk location #13 and another at disk location #49, is shown in figure 3.12. The strain pulses shown in frames a through d resemble those of the notched crack series in which a single precracked disk was placed in the assembly. The same features observed in previous experiments, such as strong back reflected pulses, jaggedness of the pulse profile after passing through the precracked disk, wave elongation and peak contact load attenuation were also observed

in this series of experiments. As the pulse continued to propagate through the assembly, it began to resemble the input pulse. When the pulse interacted with another disk containing a single 75% crack, the pulse then separated into more wavelets each with much lower amplitude, as shown in frame f of figure 3.12. These wavelets resembled the jaggedness shape observed during the first interaction of the pulse with the crack. The jagged shape observed was a result of increased reflections of the stress wave as it propagated through the disk containing the crack. As noted in Shukla and Yi (1993), jaggedness or perturbations in the stress wave pulse are an indication of high frequency components present in the wave profile. With dissipation of some of these high frequency components by the particulate medium, the shape of the elongated pulse peak becomes smoother, as shown in frames b, c, and d of figure 3.12. To evaluate the makeup of the wave in terms of low and high frequency components, Fast Fourier Transform analysis was conducted for this series. Results provided in figure 3.13 indicate that the pulse is high frequency dominated as it enters the pre-cracked disk (#13), as shown in frames a and b of figure 3.13. As the pulse exits the precracked disk it quickly becomes low frequency dominated, as shown in frames c and d of figure 3.13. As the pulse approaches the second precracked disk, its makeup becomes more high frequency dominated with much lower amplitude. Again, as the pulse interacts and exits the precracked disk, its makeup becomes entirely low frequency. Further travel of the pulse down the single chain assembly, approximately twenty disks, results in minimal change to the makeup of the pulse (remains in the form of several wavelets).

Recovery of the stress wave pulse, after interacting with the first crack, occurred after traveling a distance of only one disk diameter. Full recovery occurred after traveling a distance of thirty-two disk diameters, as shown in frames d and f of figure 3.12, respectively. However, as the affected pulse interacted with the second crack further down the single chain assembly, it elongated and separated into more wavelets with very little recovery even after propagating through a distance of 18 disk diameters, as shown in frame h of figure 3.12. This implies that the wave recovers much slower when the pulse consists of many lower amplitude wavelets. The energy transfer of the wavelets, at the contact point is occurring at lower strain rates, which results in greater dissipation through the material with less recovery time.

The elongation and separation of the stress wave pulse into several wavelets is a process that occurs as a result of redistribution of energy associated with a ringing phenomenon which produces oscillations within long wavelength pulses. Pulse elongation and wave separation were observed in this series of experiments. As the pulse propagated through the cracked disk, the wavelength

increased and the amplitude decreased. The elongated pulse shown in frame d of figure 3.12 had a duration of 380 μs, which represents approximately 12 disk diameters. As the pulse propagated further it separated into wavelets, each with a duration of 110 μs. However, when the pulse, in the form of several wavelets, interacted with the second crack, the duration increased to 780 μs in conjunction with a decrease in amplitude.

The inclusion of a second particle, containing a single 75% crack, down the single chain assembly resulted in extremely large far-field attenuation of the peak contact load. Normalized peak contact load attenuation was plotted for this series of experiments and provided as figure 3.14. This figure shows that the interaction of the pulse with the first cracked disk results in a large drop in peak contact load attenuation. The load drops to 57 percent and then quickly recovers to 38 percent at which point it continues to decay as it propagates through the assembly. The pulse entering the second cracked disk is now at 50 percent of the input pulse. As it passes through the cracked disk the pulse is further attenuated to approximately 70 percent of the input value. With no recovery, the pulse continues to be dissipated by the media. Overall peak contact load attenuation was 78 percent of the input pulse.

The average velocity of the stress wave pulse was determined to be 950 m/s for this series of experiments, which remained constant throughout the propagation of the pulse. Damage was not observed in this series of experiments, which is consistent with results provided in Shukla and Yi (1993) for this type of flaw within the medium.

Typical strain gage results obtained for the case of multiple (four) adjacent disks with single 50% disk diameter notched cracks is shown in figure 3.15. As the pulse interacted with the first series of disks containing cracks, pulse elongation occurred. Again the increased surface area present in the cracked disks resulted in many more reflections. As the pulse propagated through the initial arrangement of disks, the duration of the stress wave pulse increased from 110 μs to 190 μs. Moreover, the local and overall attenuation prior to interacting with the second arrangement of disks, was 37 and 47 percent respectively, as shown in figure 3.16.

As the affected stress wave pulse interacted with the second arrangement of disks similar results were observed. The pulse entering the second arrangement of disks resembled the input pulse with a much lower amplitude. The interaction of the affected pulse with the cracked disk produced a similar increase in pulse duration. As shown in frames e through g of figure 3.15, the pulse duration increased from 120 μs to 230 μs. In addition, the pulse contact load attenuation increased from 47 percent to

65 percent overall. Unlike the rapid increase and recovery in peak contact load attenuation observed through the first arrangement of disks, attenuation was more gradual when the second interaction occurred, as shown in figure 3.16. This implies that the affected pulse, which interacts with the second arrangement of disks contains less of the high frequency components resulting from the interaction with the initial arrangement.

The average wave velocity of the stress wave pulse propagating through both arrangements of multiple disks was determined to be 905 m/s, which remained constant throughout the propagation of the pulse.

In this series of experiments damage growth was also observed as the pulse propagated through the first arrangement of disks. In every experiment the first disk in the path of the stress wave pulse fractured. However, with the affected pulse containing less of the energy, damage growth was not observed when the pulse interacted with the second arrangement of cracked disks. This implies that the stress intensity at the crack tip was low enough to preclude damage growth.

3.4 SUMMARY

The presence of damaged particles in particulate media influences the stress wave propagation through the media. The effects of repeated loading of cracked particles and stress wave interaction with multiple spaced flawed particles on the dynamic load transfer process are summarized as follows;

(1). The results show that repeated loading of fractured particulate media effects the pulse duration and peak contact load attenuation locally. This is due to the increased reflections resulting from the additional free surface area and particle shape change present in the fractured particle. It also results in microstructural changes to the media.

(2). Interaction of the stress wave with multiple spaced flawed particles in particulate media results in rapid dissipation of the stress wave pulse and separation of the pulse into wavelets. As the affected stress wave pulse, which is initially composed of mainly low frequency components, interacts with an identical flawed disk(s) further down the single chain assembly it separates into many wavelets with very little recovery.

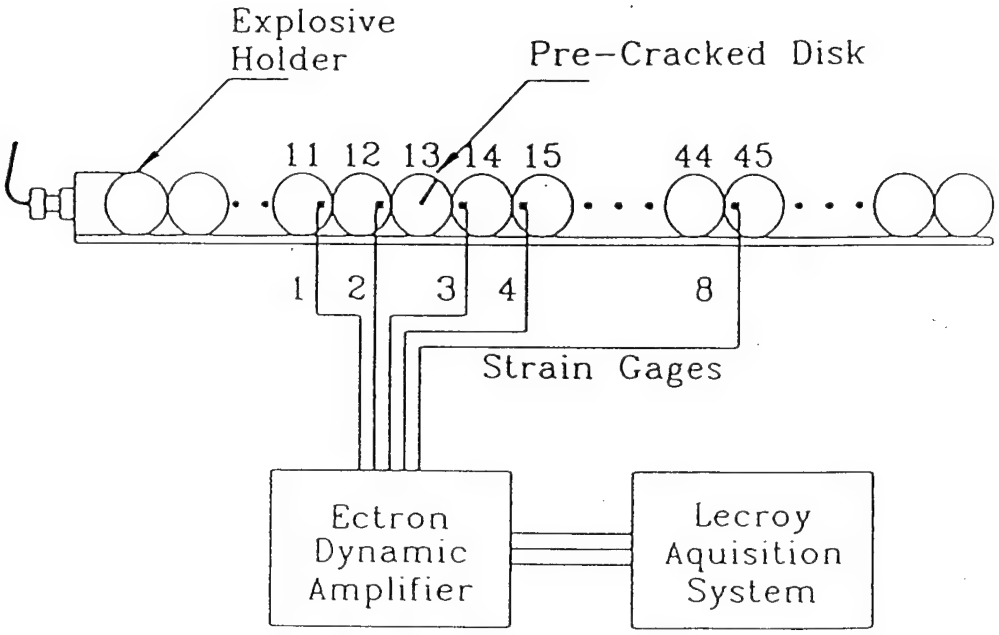

Figure 3.1. (a) Experimental setup for long chain experiments using strain gages.

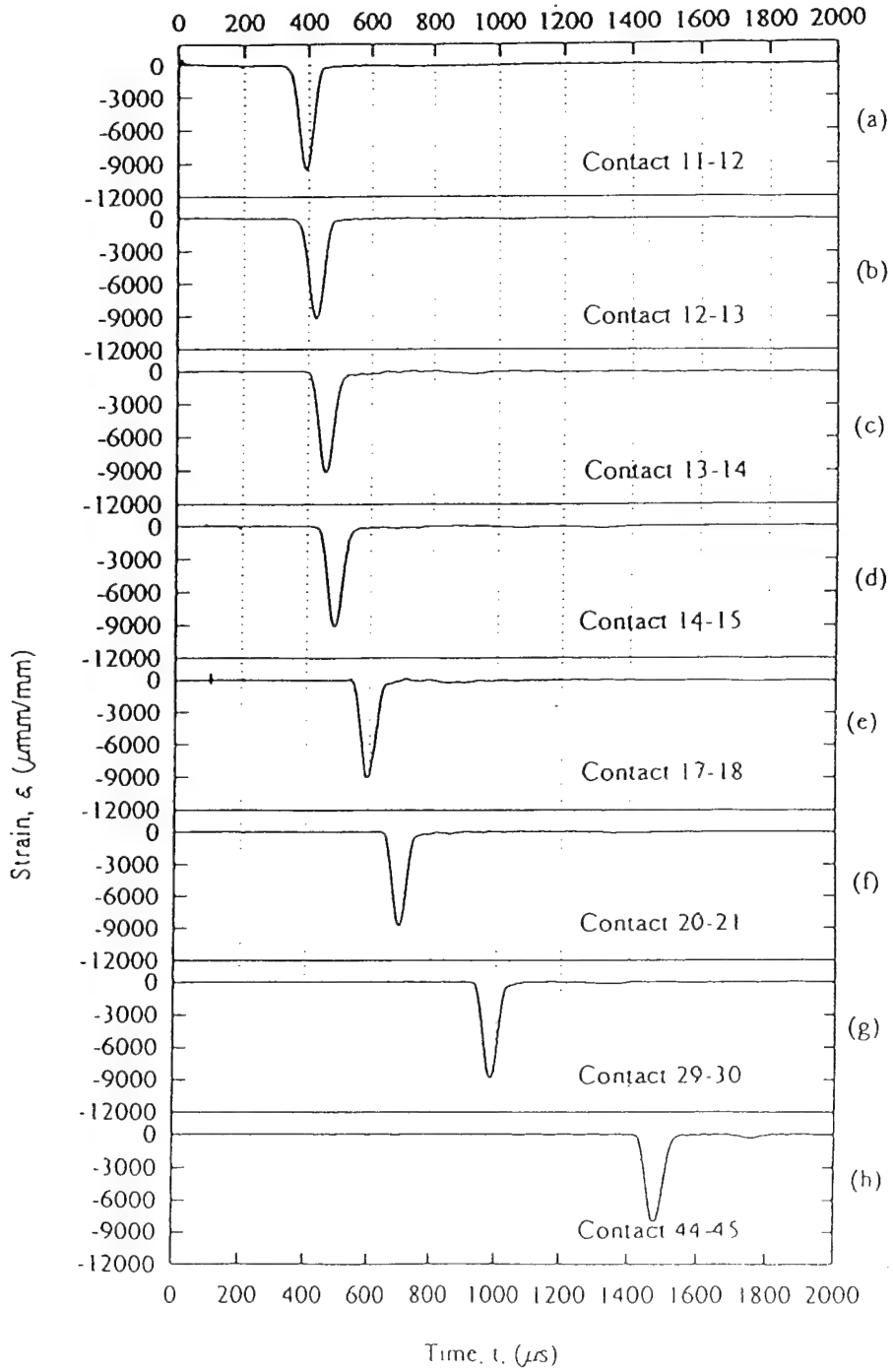

Figure 3.1. (b) Strain gage data for a single chain assembly with no cracked disks.

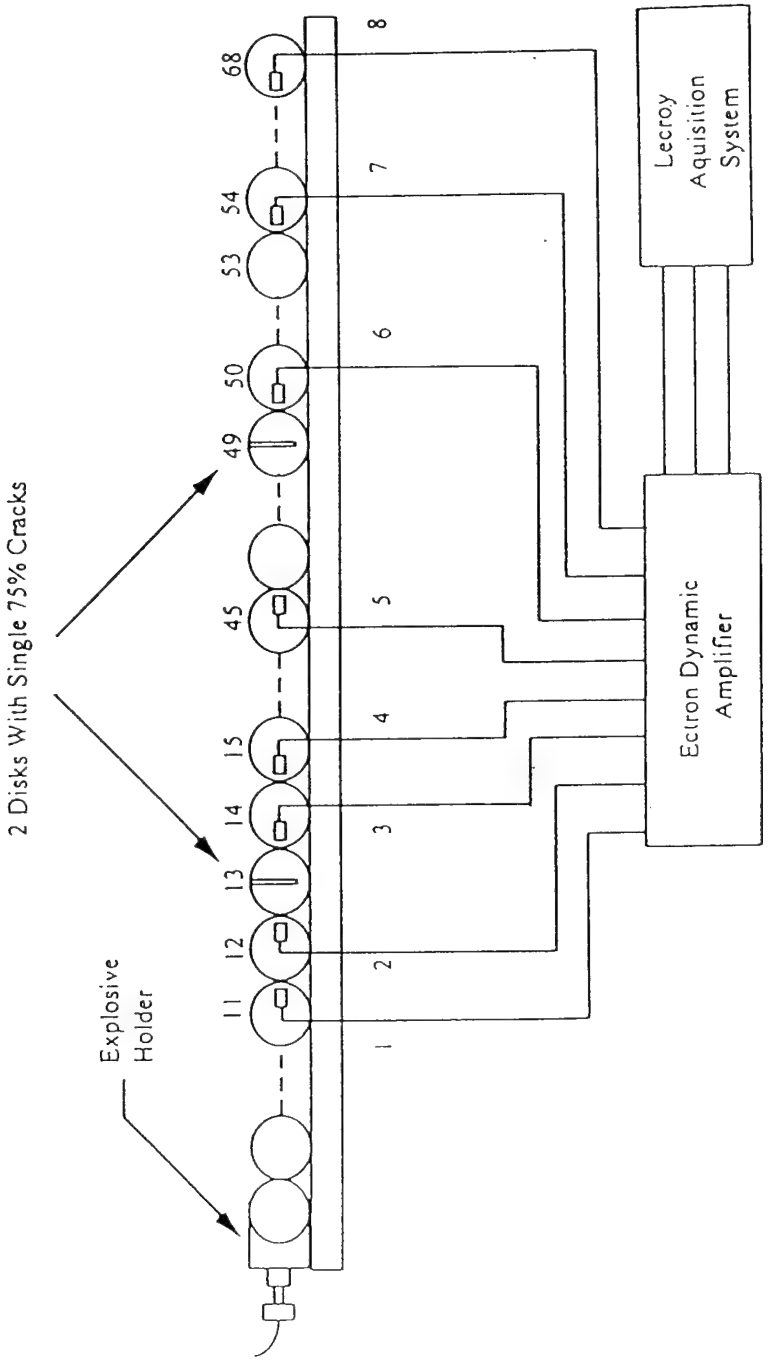

Figure 3.2. Experimental setup for stress wave interaction of multiple spaced flawed particles in long single chain assemblies.

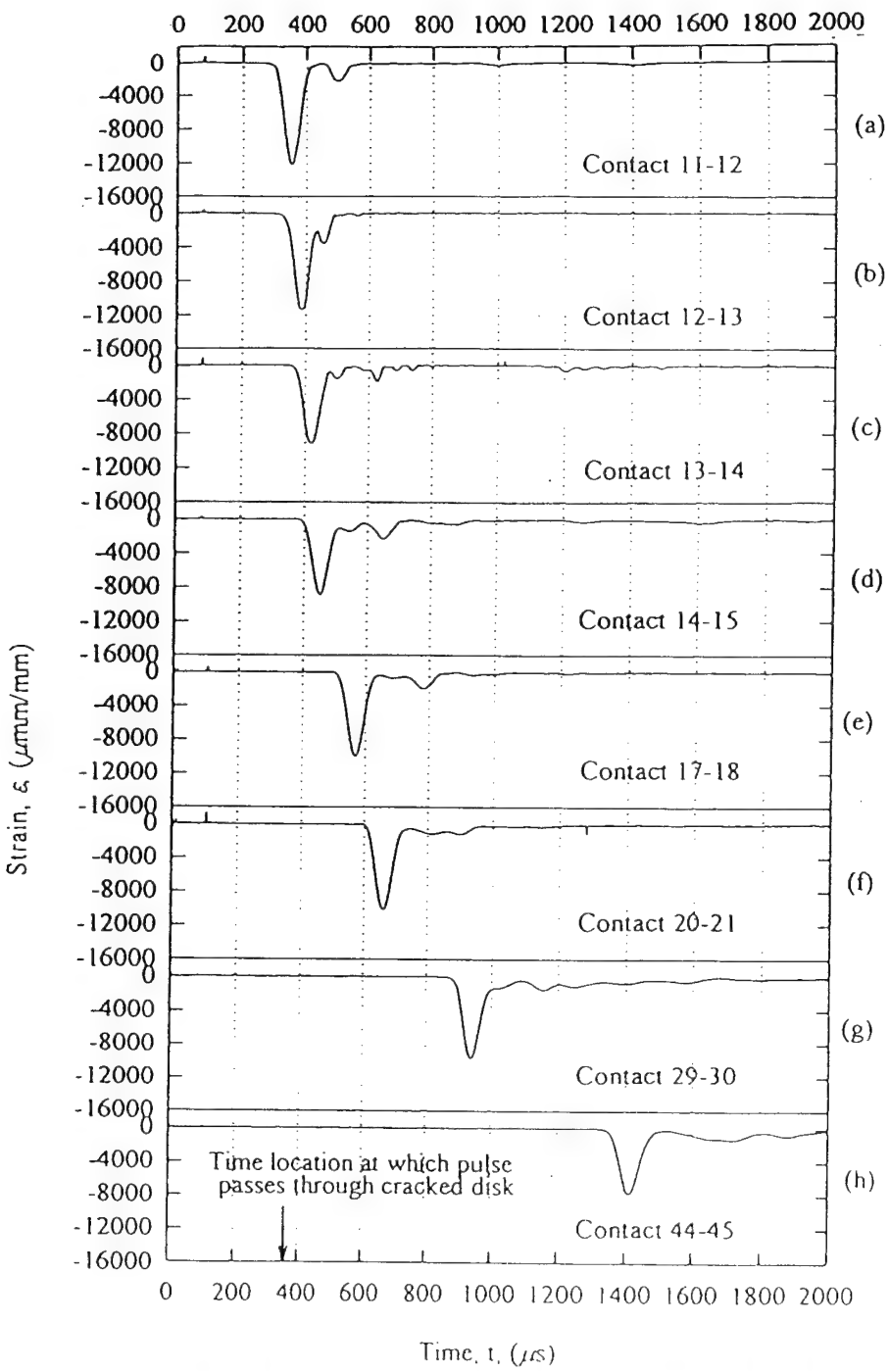

Figure 3.3. Typical strain gage data for a single chain assembly containing a disk with a single 50% disk diameter notched open crack oriented -60°.

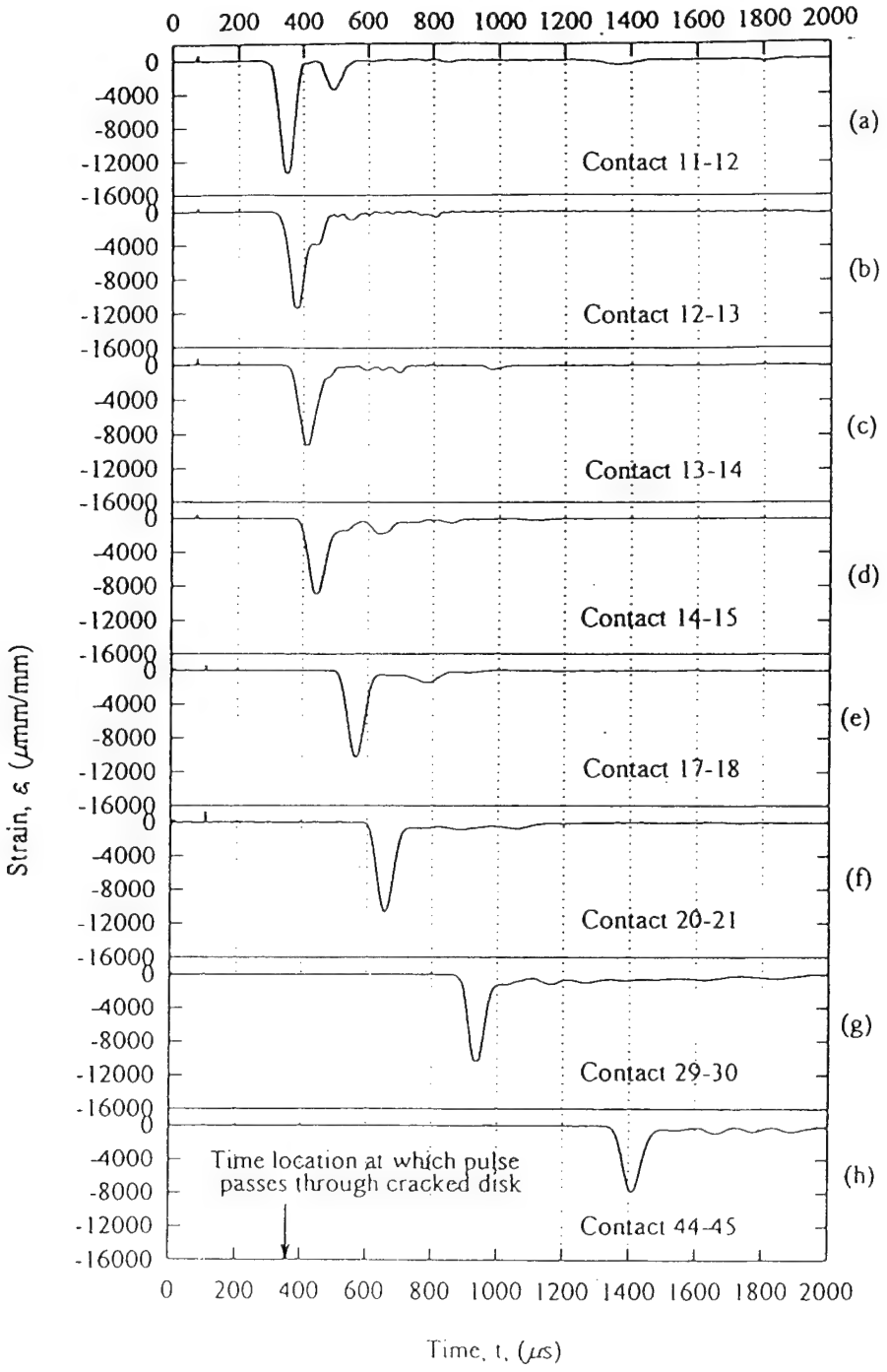

Figure 3.4. Typical strain gage data for a single chain assembly containing a previously fractured disk with a single 50% disk diameter notched open crack oriented -60°.

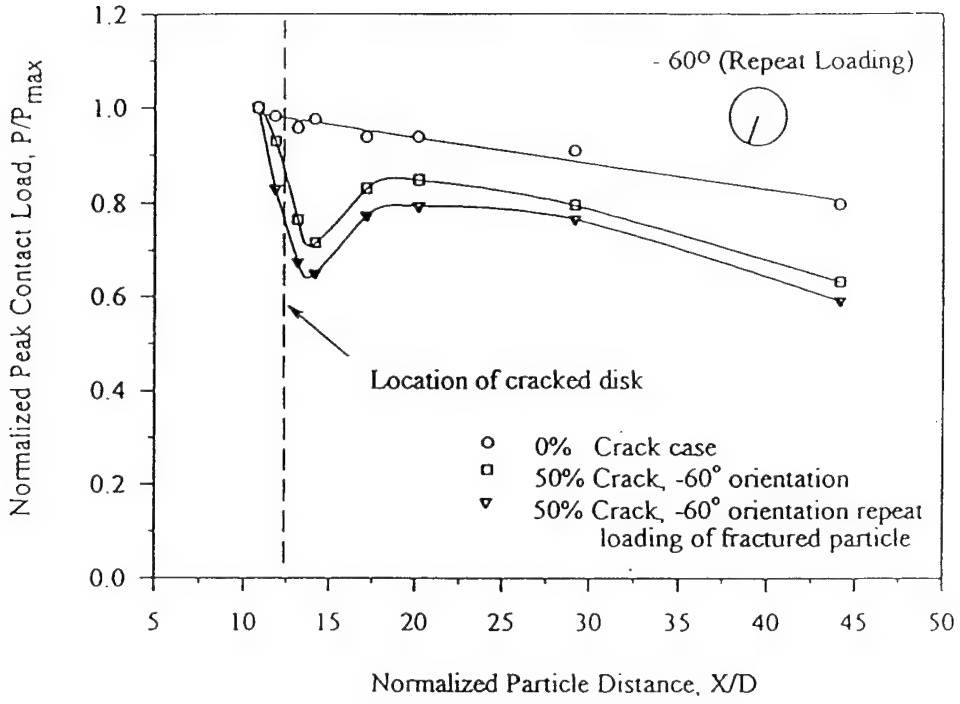

Figure 3.5. Comparison of normalized contact loads as a function of normalized particle distance for the -60° notched open crack loading and reloading of the fractured particle.

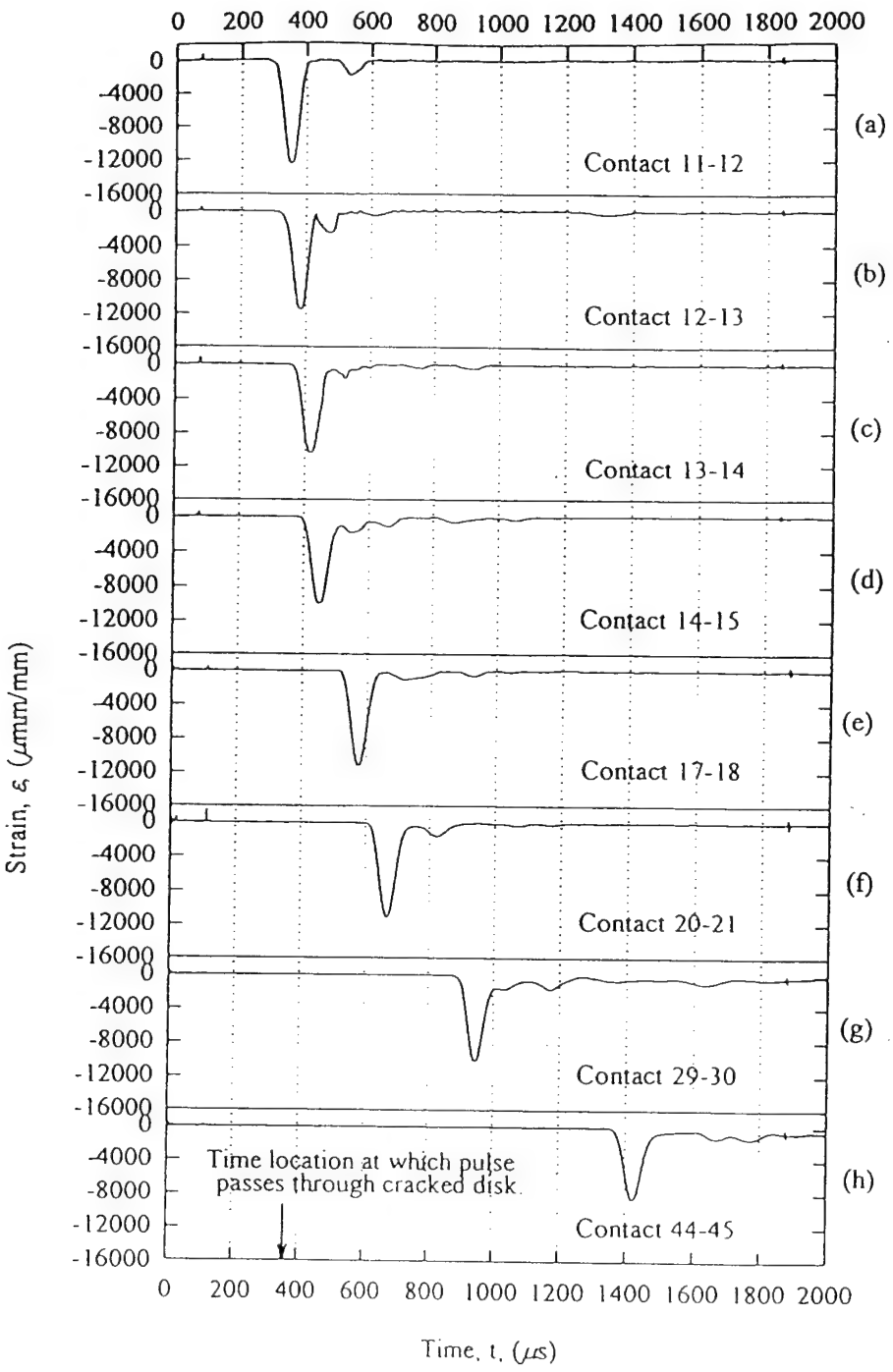

Figure 3.6. Typical strain gage data for a single chain assembly containing a disk with a single 50% disk diameter notched open crack oriented -90°.

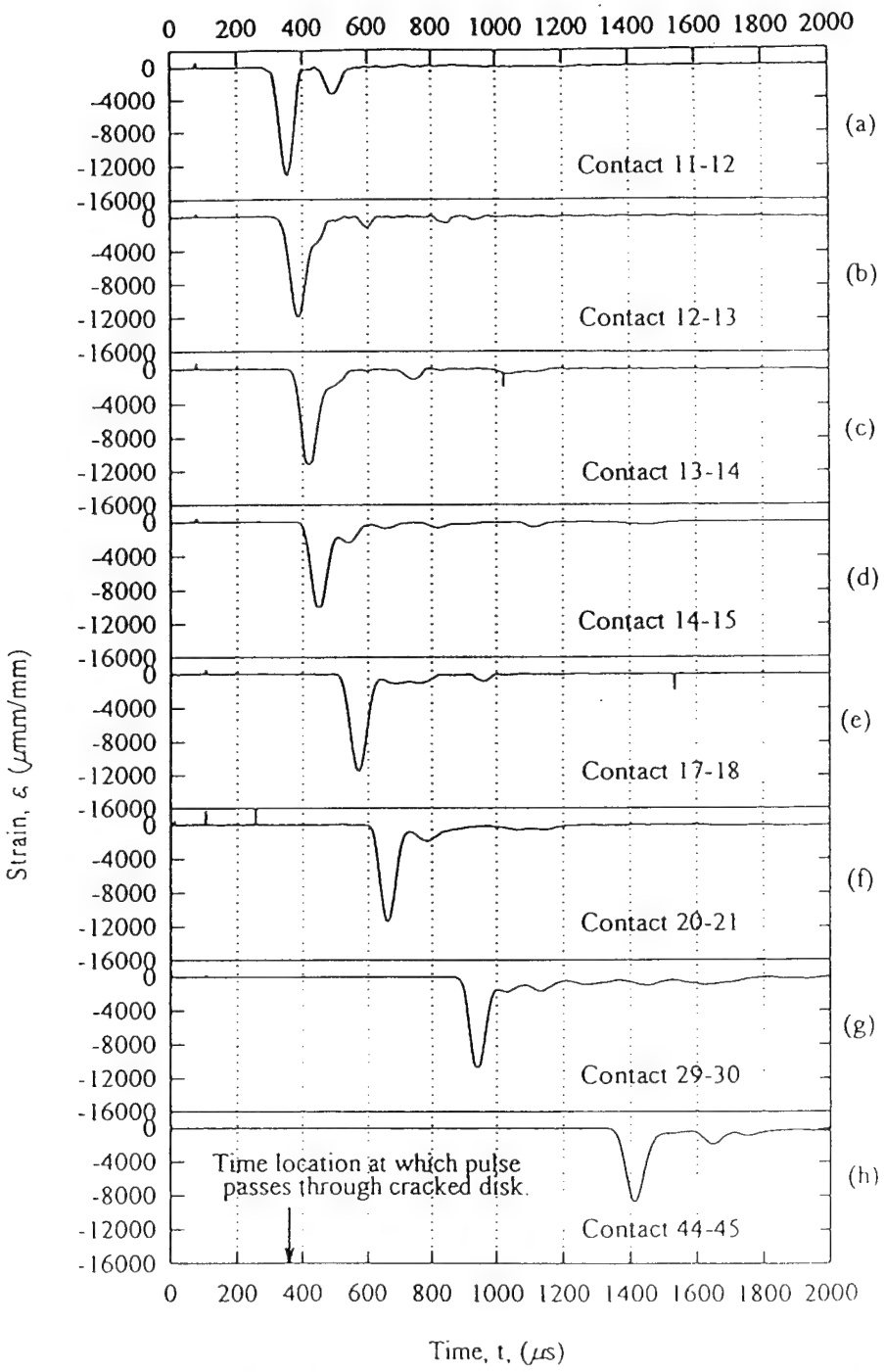

Figure 3.7. Typical strain gage data for a single chain assembly containing a disk with a single 50% disk diameter notched open crack oriented +90°.

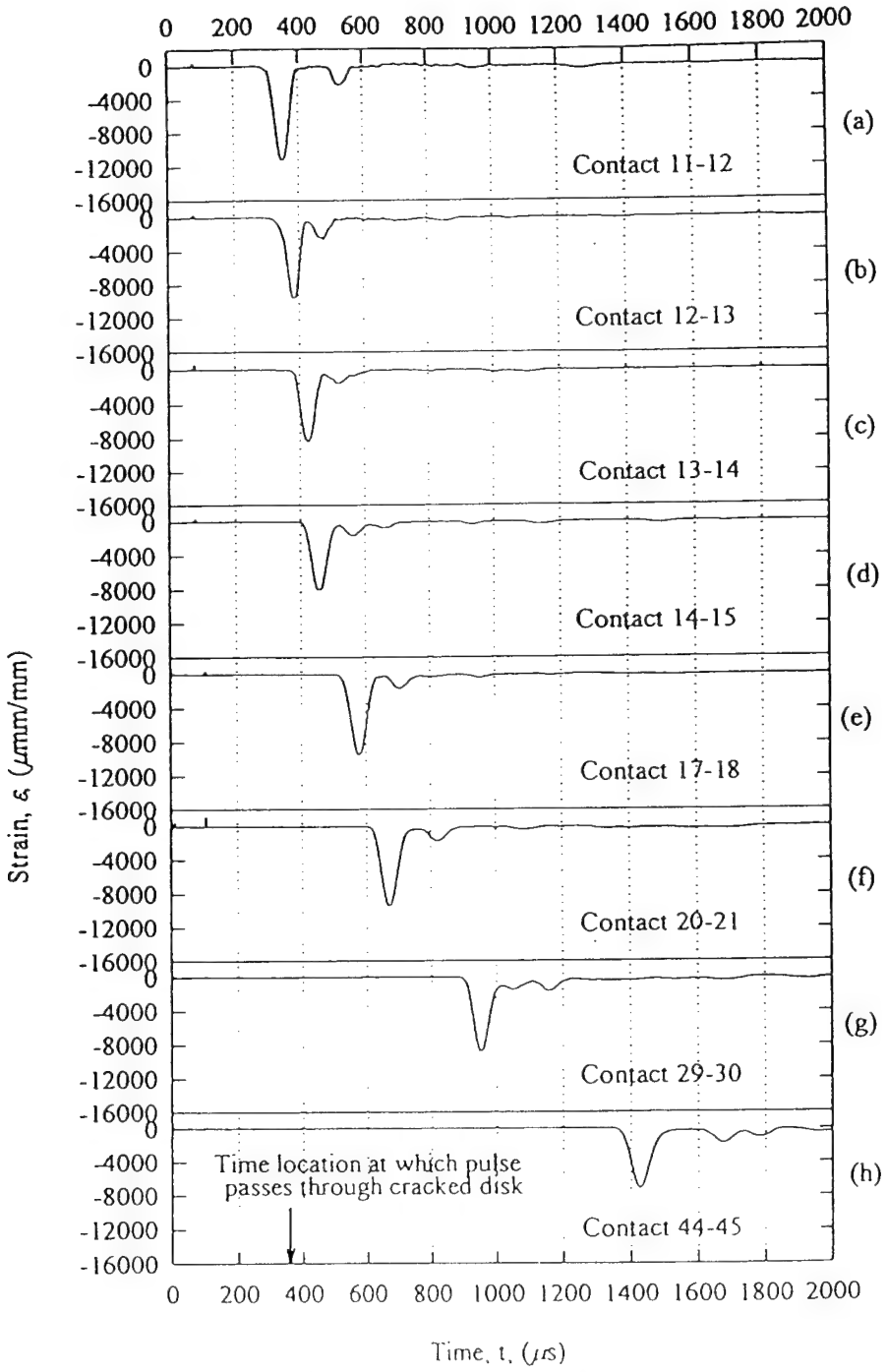

Figure 3.8. Typical strain gage data for a single chain assembly containing a previously fractured disk with a single 50% disk diameter notched open crack oriented -90°.

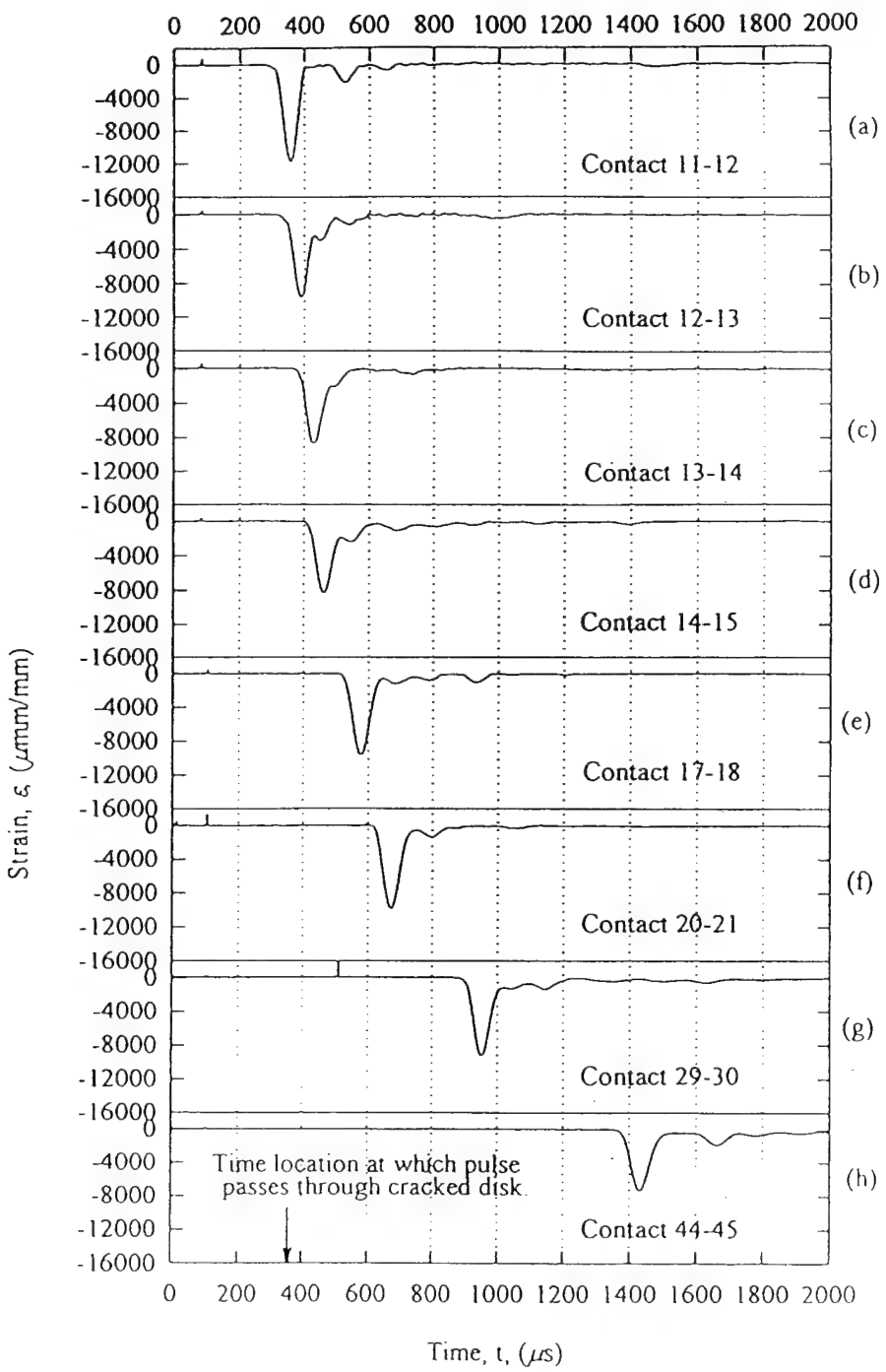

Figure 3.9. Typical strain gage data for a single chain assembly containing a previously fractured disk with a single 50% disk diameter notched open crack oriented +90°.

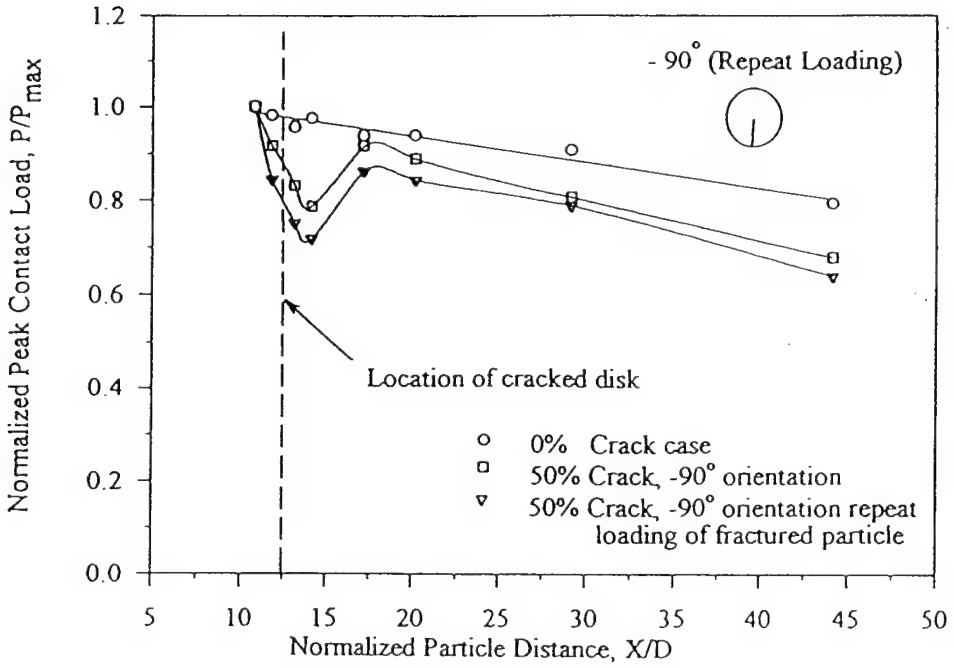

Figure 3.10. Comparison of normalized contact loads as a function of normalized particle distance for -90° notched open crack loading and repeat loading of the fractured particle.

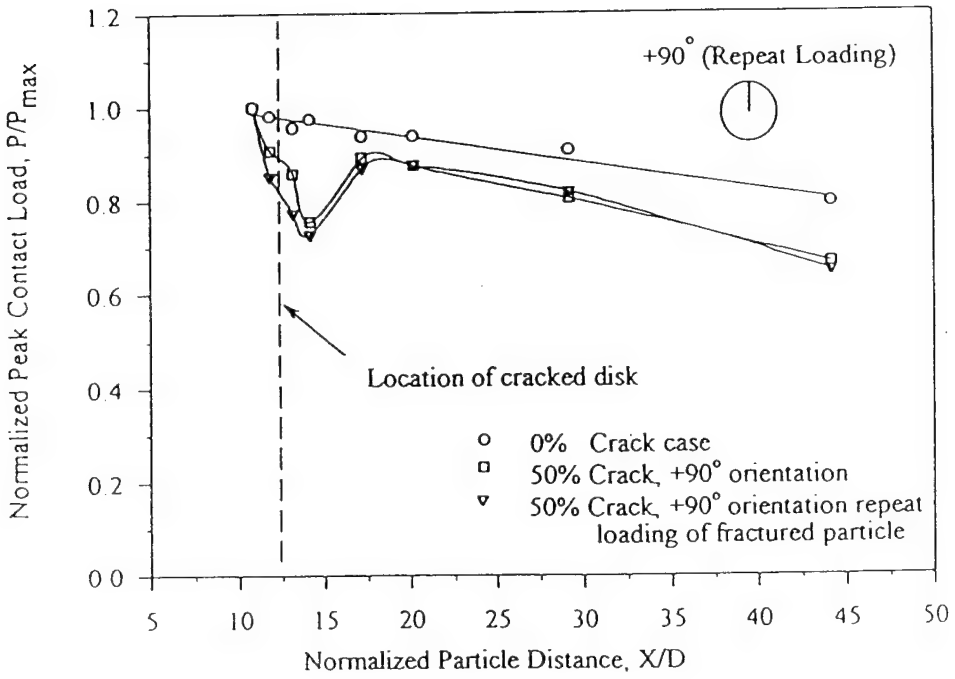

Figure 3.11. Comparison of normalized contact loads as a function of normalized particle distance for +90° notched open crack loading and repeat loading of the fractured particle.

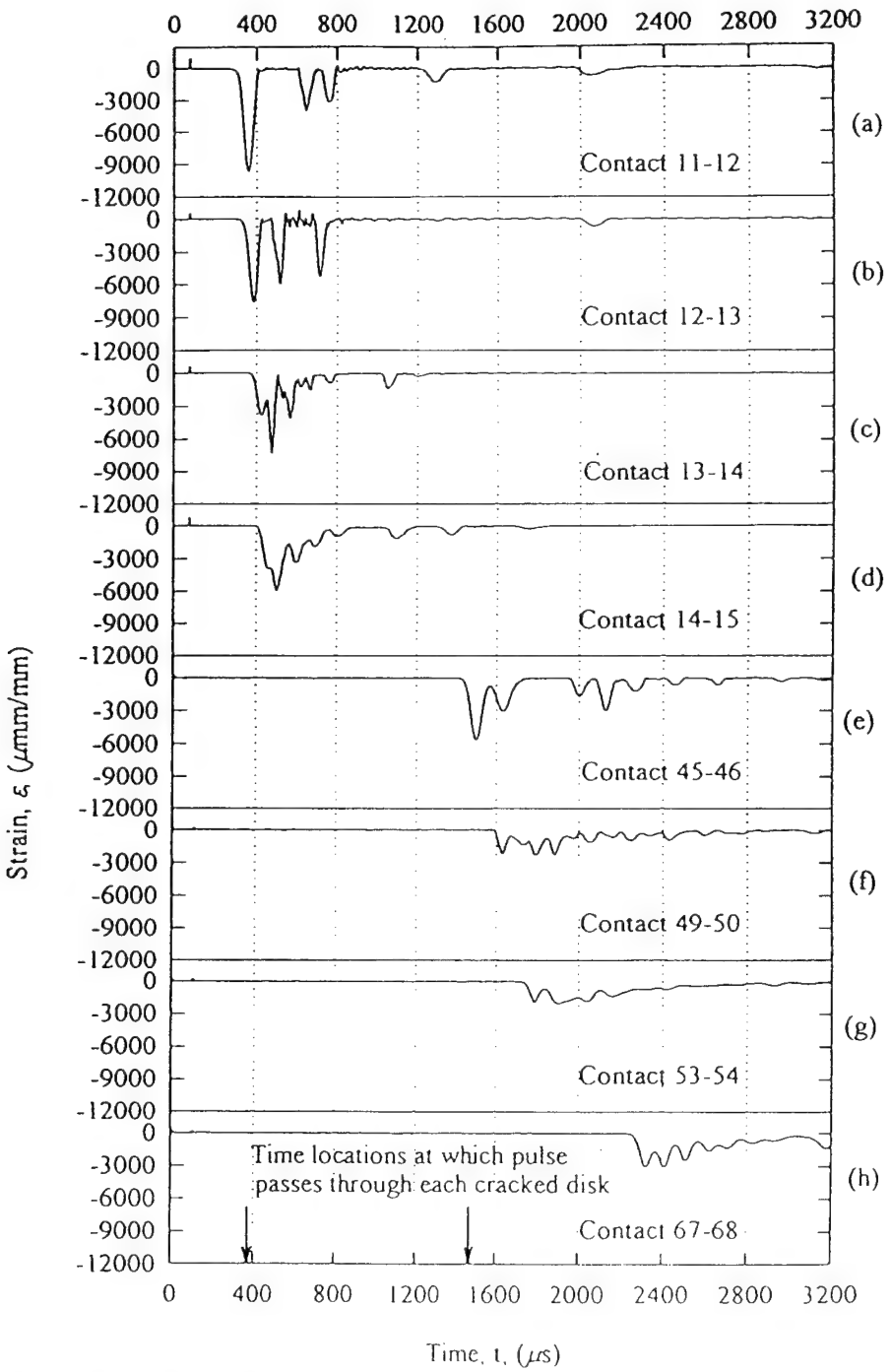

Figure 3.12. Typical strain gage data for a single chain assembly containing multiple spaced flawed particles with single 75% disk diameter notched open cracks.

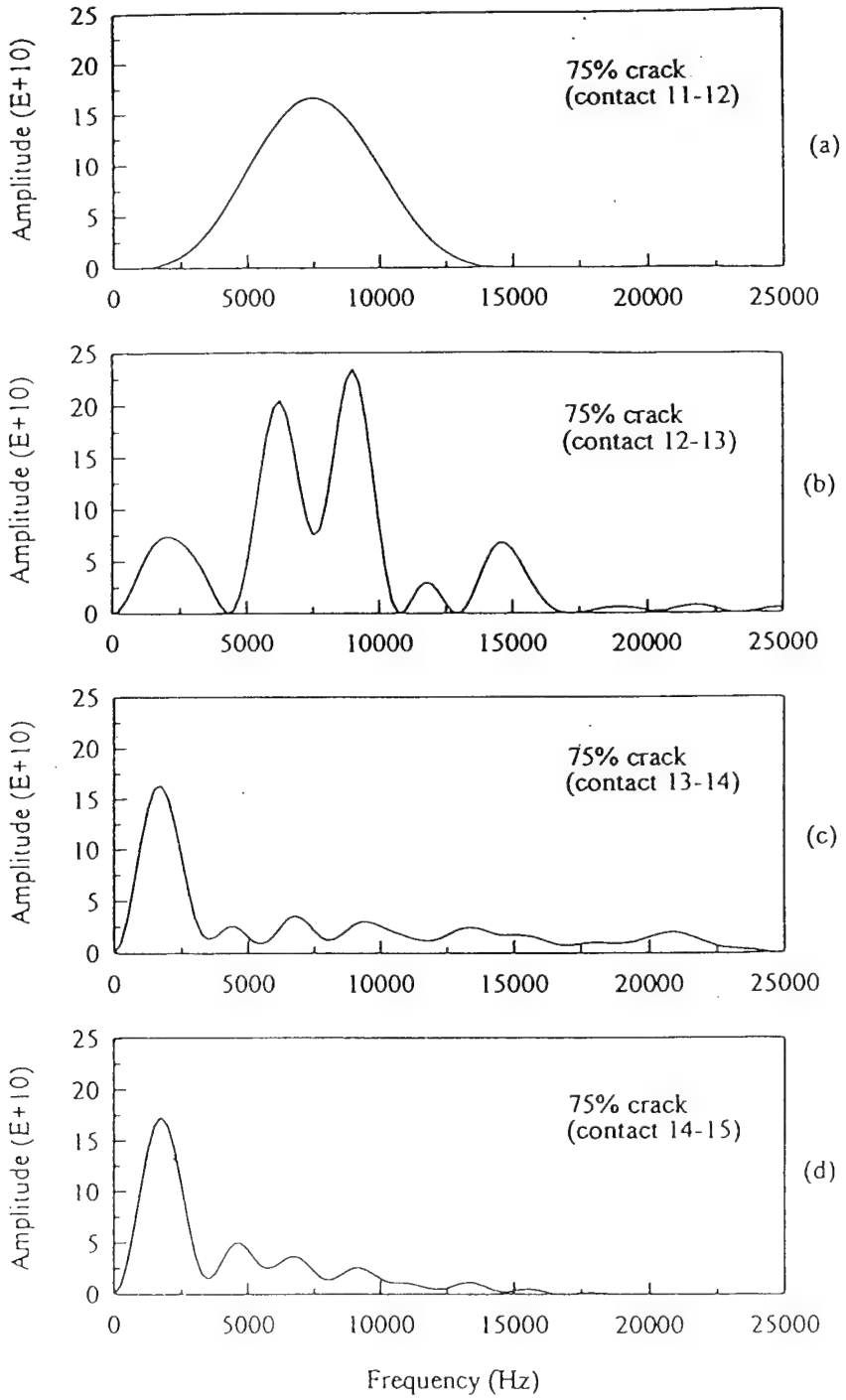

Figure 3.13. Fast Fourier Transform results from experiments on stress wave interactions of multiple (2) spaced 75% notched open cracks in a single chain assembly.

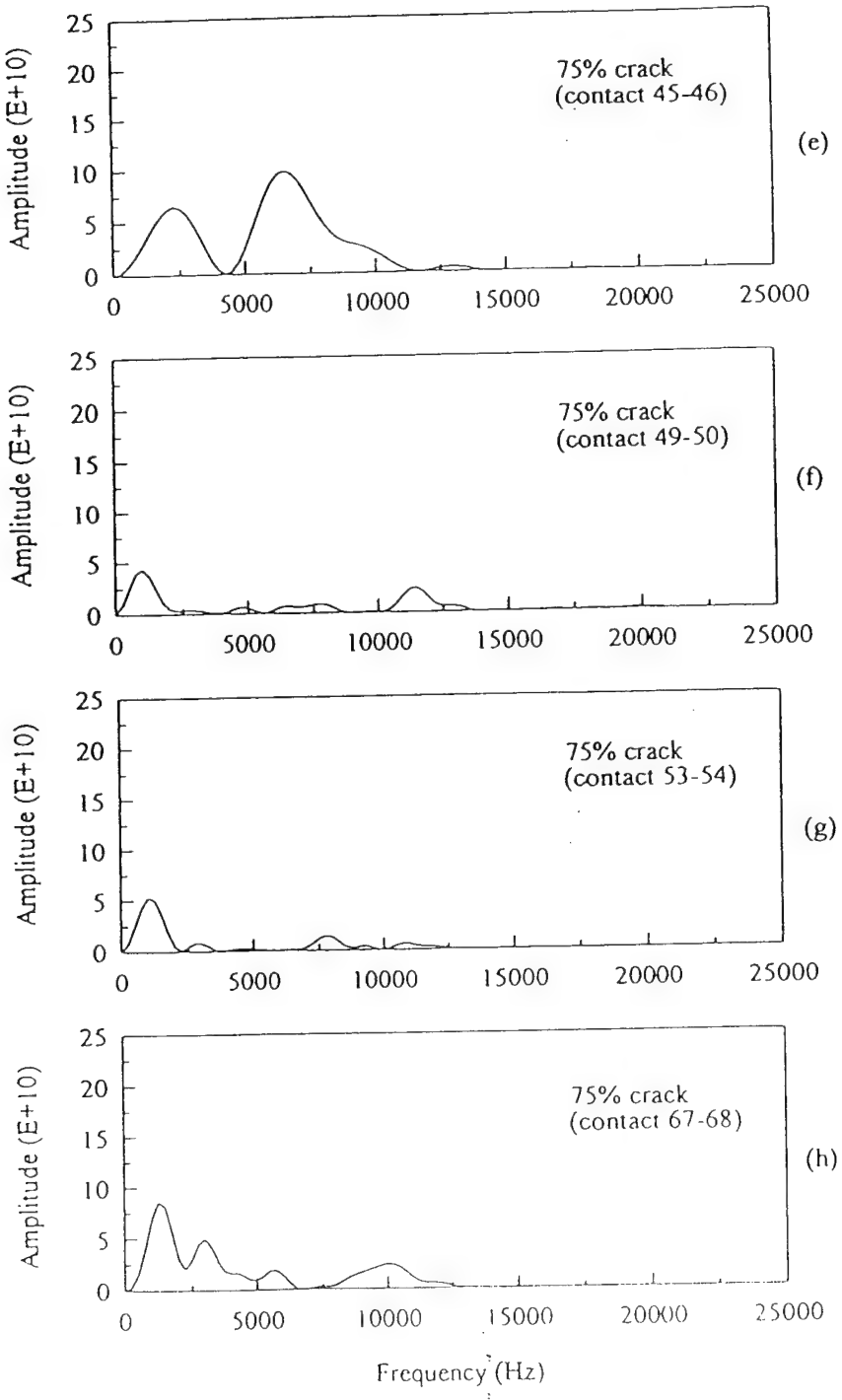
Amplitude (E+10)
25
20
15
10
5
0
0
5000
10000
15000
20000
25000
75% crack
(contact 45-46)
(e)
75% crack
(contact 49-50)
(f)
75% crack
(contact 53-54)
(g)
75% crack
(contact 67-68)
(h)
Frequency (Hz)

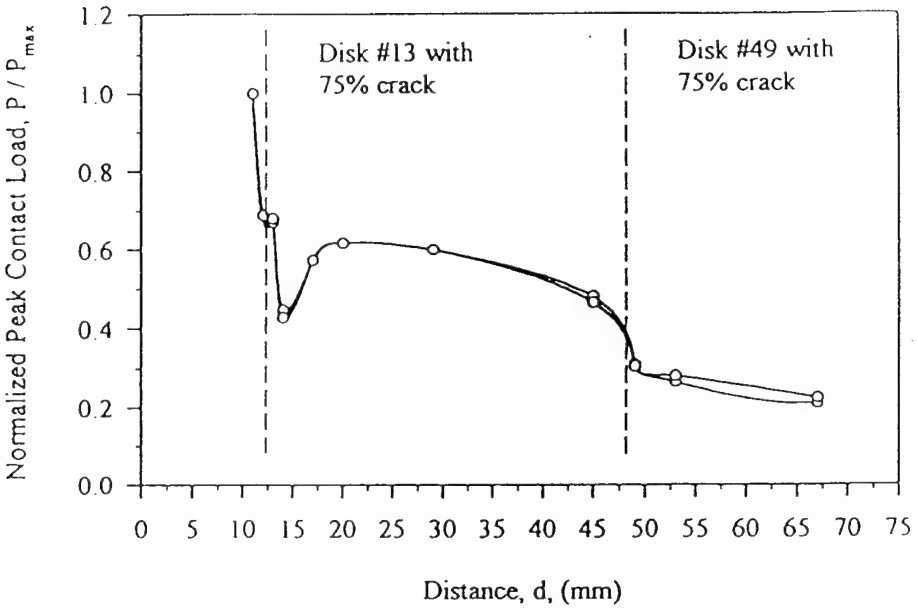

Figure 3.14. Normalized contact load as a function of normalized particle distance for the multiple spaced 75% notched open crack case.

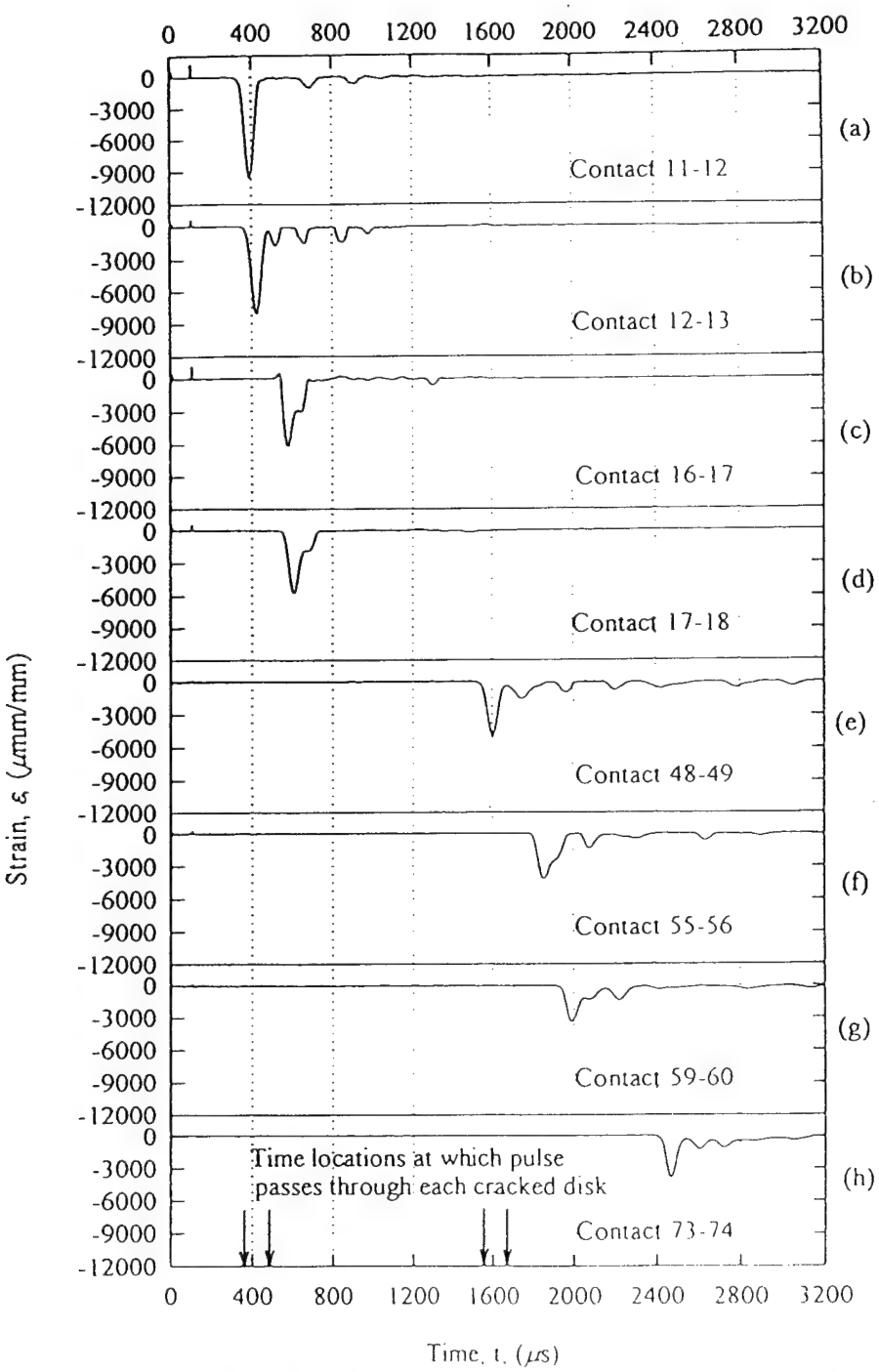

Figure 3.15. Typical strain gage data for stress wave interaction of multiple spaced sectors of staggered flawed particles containing single 50% disk diameter cracks.

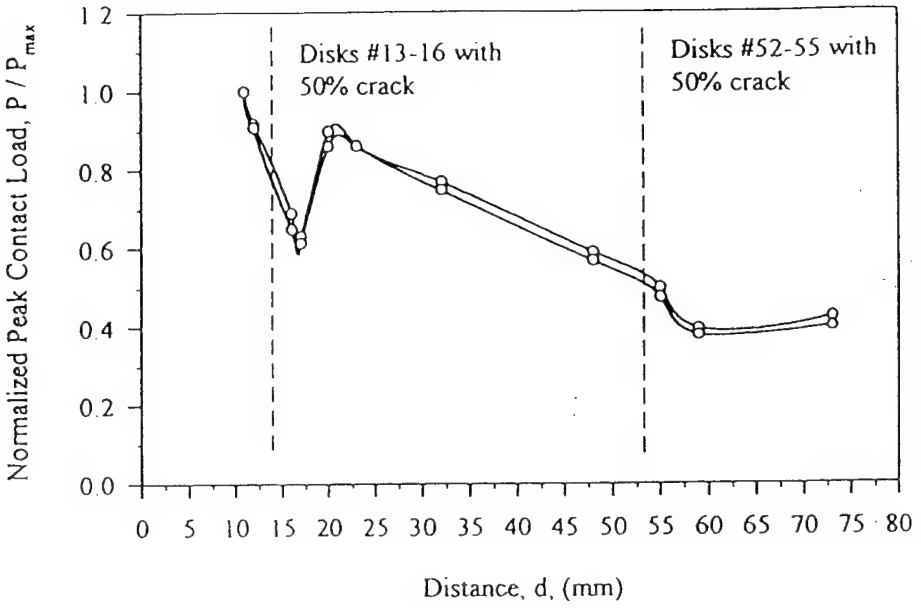

Figure 3.16. Normalized contact loads as a function of normalized particle distance for the case of multiple spaced sectors of staggered multiple flawed particles.

CHAPTER 4

THE EFFECT OF PARTICLE DAMAGE ON WAVE PROPAGATION IN GRANULAR MATERIALS

ABSTRACT

A numerical study is conducted to investigate the effect of particle damage on wave propagation in granular materials. The discrete element method is employed to simulate the dynamic load transfer processes involved during the passage of waves through model granular systems of circular particles. Damage is modeled by incorporating interparticle contact laws which exhibit softening behaviors related to the amount of damage present during the dynamic interaction event. Using a non-linear hysteretic normal contact law, the study establishes a damage threshold and a subsequent softening interparticle contact response. A simple maximum normal stress theory applicable for brittle particles is used to establish the damage threshold for each particle. The softening model allows for a variety of damage behavior to occur, and offers a total softening response for the most severe case.

Discrete element simulation results are conducted on several one and two-dimensional model granular systems using several different damage/softening models. Results generally indicated that the presence of damage leads to significant changes in the wave propagational behavior. Specifically, more severe attenuation occurs in damaged particulate media, and the wave speed is generally reduced.

4.1 INTRODUCTION

In granular media, mechanical loadings are primarily transmitted through interparticle contact. Under sufficiently large loadings, such contact behavior will result in some type of particulate damage. For brittle materials, this damage may be the result of localized contact surface failure cracking or general failure at internal locations within the grains. Results of such damage will be to alter the interparticle load transfer characteristics and generally produce a softening response. This localized change in load transfer behavior will effect the material's wave propagation characteristics.

Considerable work has been reported on fragmentation, fracture and general damage behavior of brittle materials, and some previous studies have investigated such behavior in particulate materials. However, limited research exists on dynamic load transfer processes related to wave propagation in

granular materials exhibiting damage.

With respect to recent work, Gilvarry (1961) developed criteria on a distribution function for fragment size of brittle solids based on Griffith theory. Based on a statistical study, Grady, et al. (1985) also did research on size distributions of fragmented solids produced under dynamic fragmentation processes. Malvern et al. (1989) explored microstructural damage evolution in concrete specimens and found considerable differences under static and dynamic conditions. Toi, et al. (1994, 1995) employed a *mesoscopic* modeling approach whereby a discontinuum damage mechanics theory is developed for brittle materials. A discrete numerical scheme was developed based upon a Voronoi tessellation mesh. Jeulin (1993) developed a micromechanical damage evolution model for heterogeneous materials based on graph theory.

With regard to particle fragmentation, Mitchell (1961) studied the tensile strength of brittle materials by conducting indirect tension tests (diametral-compression) on circular disk specimens, and concluded that fracture of brittle crystalline and cementious materials can be predicted by maximum tensile stress and Mohr failure theories. Rudnick et al (1963) further investigated the diametrical-compression of circular specimens and discussed factors related to various forms of failure (e.g. shear, tension and triple cleft). Jaeger (1967) examined the brittle failure of circular particles under a variety of compressive boundary loadings. Further studies of fracture of loaded disks and spheres were carried out by Kendall and Gregory (1987) and Arbiter et al (1969). Shukla, et al. (1995) conducted experimental dynamic photoelastic studies on wave propagation in model granular materials with flawed or damaged particles.

Investigations of strength and stress-strain behaviors of granular soil during crushing or breakage of soil particles was done by Hardin (1985), Fukumoto (1992), and Hagerty, et al. (1993). Using discrete element modeling, Bruno (1994) studied damage in sedimentary rock modeled as a cemented granular material. Smith and Srolovitz (1994) presented a computer simulation study on brittle fracture behaviors under impact loading. An interesting constitutive theory based on a *critical impact energy* between particles was developed by Richman et al. (1989, 1991) which accounts for grain size reduction in granular flow problems. Applications of such work are made in *comminution* processes in which unrefined granular materials are ground to reduce particle size. Alehossein and Muhlhaus (1994) used Cosserat theory and damage mechanics to develop a continuum model for comminution processes.

In addition to the commonly applied stress and energy methods, some research on

fragmentation has been done by using *fractal fracture mechanics*. Turcotte (1986) conducted such a study and concluded that fragmentation is often a scale invariant process and results in a fractal distribution. Palmer and Sanderson (1991) also observed the scale effect in ice fracture. A new relation for energy size reduction from the fractal concept and Griffith energy criteria was proposed by Naghama and Yoshil (1993).

With regard to the numerical methods, Thornton (1993), Bruno (1991), Meguro (1994) and Chang (1993) used *discrete element methods* to study fracture, fragmentation and failure behaviors of granular and discontinuous materials. Gebara, et al. (1993) have used the so-called *finite block method* developed by Chen and Pan (1991) to simulate penetration problems involving rock rubble materials. Hocking (1992) and Mustoe, et al. (1987) have conducted discrete element simulations of fragmentation behavior of plate-like discontinua subject to flexural cracking. Shi (1993) presented a discrete modeling scheme called the *discontinuous deformation analysis* method which has applications for fragmentation. Other computational approaches include *hybrid discrete/finite element* procedures used by Mansour and Seireg (1983), Munijiza (1995), Ishibashi (1994), Pan (1991) and Barbossa (1990) to investigate the large deformation and fracture behaviors of solids.

Some research on wave propagation in damaged materials has been conducted, e.g. Saka, et al., (1994), Shin and Karr, (1990) and Zhang and Gross, (1992). These studies attempted to correlate the wave propagational characteristics with the current amount of damage present in the material.

The purpose of the present work is to numerically investigate the effect of localized interparticle damage on wave propagation in granular and particulate materials. Of primary concern are the combined effects of the local damage and microstructural fabric on the wave speed and amplitude attenuation. The study is conducted using discrete element numerical simulation incorporating interparticle contact relations which exhibit damage. These new contact relations are developed through modifications of previous contact laws for undamaged materials. Numerical simulations are conducted on several one and two-dimensional model granular systems using several different damage/softening models.

4.2 DISCRETE ELEMENT PROCEDURES

The theoretical modeling used in this study incorporated analytical damage models into a numerical computer scheme based on the *discrete element method*. Originally developed by Cundall et al. (1979), the discrete element method has been successfully used to model the behavior of large

assemblies of disks, spheres, blocks and particles of general shape. The technique makes simplifying constitutive assumptions for each particle (commonly assuming rigid body behavior) and then uses Newtonian mechanics to determine the translational and rotational motion of each particle in assembly system models. Particles are allowed to have contact or other forms of interaction, and interparticle forces develop as a result of particular contact stiffness and damping characteristics. The general concept of the method may be explained by considering a general two-dimensional particulate assembly as shown in Figure 4.1. Isolating attention to the I-th particle and applying Newton's laws yields

$$\sum_{j=1}^{N} F^{ij} + F^{i} = m_i \ddot{x}_i$$

$$\sum_{j=1}^{N} M^{ij} + M^{i} = I_i \ddot{\theta}_i \qquad \textbf{(4.1)}$$

where F^{ij} are the j-contact forces on the I-th particle, F^{I} represents any non-contacting forces on particle I, M^{ij} are the moments (about the particle's mass center) resulting from contact forces F^{ij}, M^{I} is the resultant moment from any non-contacting forces, m_i is the particle mass, and I_i is the mass moment of inertia. With given contact and non-contact forces, the linear and angular accelerations

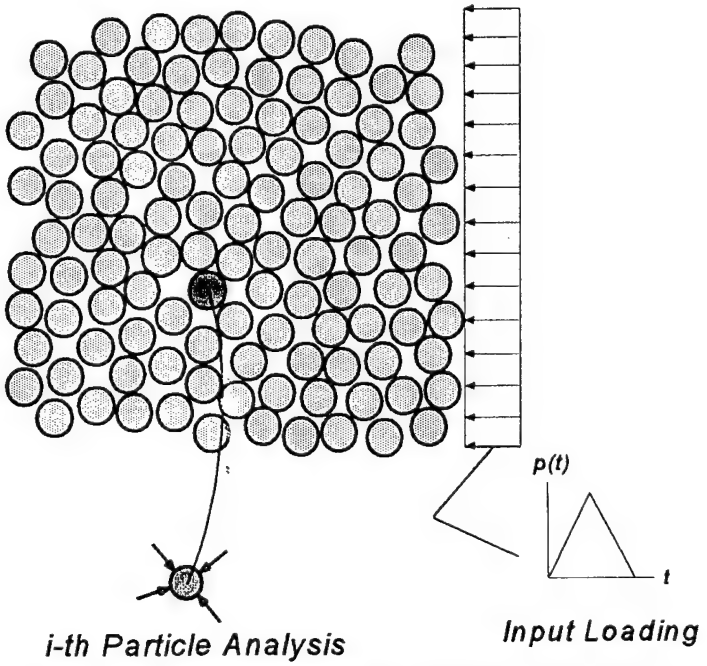

Figure 4.1. Discrete Element Modeling Procedure

of the I-th particle can thus be determined, and the velocities and displacements may be obtained through numerical integration using finite differencing schemes. The new positions and velocities are used to update the previous values, and this allows new contact forces to be determined.

Utilizing this numerical procedure, a discretized time stepping routine is established which determines the particle velocities and positions during each time step. Under the assumptions of nearest neighbor causality, an explicit scheme is developed whereby the resultant force (and thus the acceleration) on any particle is determined solely by its interactions with neighbor contacting particles. For applications involving wave propagation, a time dependent field of particle motions and intergranular contacts are established which result from the propagation of mechanical signals through the medium. Wave motion characteristics of wave speed and amplitude are thus related to the temporal and spatial behavior of the interparticle contact forces.

For the present study the dynamic behavior of model particulate media is simulated using this DEM scheme using and extending our existing computer codes. Numerical results from our previous computer simulations have compared favorably with experimental data from photoelastic and strain gage tests (Sadd, et al. 1989).

4.3 CONTACT DAMAGE LAWS

In order to model granular contact problems associated with damage and fragmentation, new contact law relations must be developed which account for the softening behavior resulting from dynamic damage evolution. Our procedure involves the development of a model to determine the initiation of particle damage and the subsequent post damage contact behavior. This will then be incorporated into our existing discrete element computer codes to simulate dynamic load transfer and wave propagation.

Over the past few years, we have developed several different contact laws appropriate for dynamic load transfer in a variety of granular materials. For dry, uncemented and undamaged materials, we (Sadd et al., 1989) have found that a nonlinear hysteretic law produced simulations which compared favorably with experimental data. This law is shown schematically in Figure 4.2 in which the normal contact force is plotted versus the overlapping normal contact displacement. It seems reasonable to assume that for damage to occur, a threshold must be reached, and that contact behavior below this threshold would correspond to an undamaged response as shown in the figure.

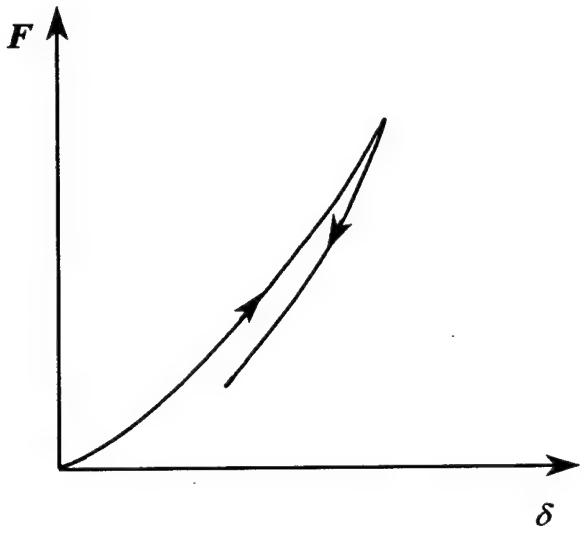

Figure 4.2 Nonlinear Hysteretic Contact Behavior

For brittle materials, particulate damage can be quite variable ranging from small microcracking at the interparticle contacts up to complete fragmentation in which the particle breaks into two or more separate pieces. The probability of damage or fragmentation will depend on the nature of the interparticle contact loadings, the coordination number N, and the strength of the grain material. This behavior could be characterized by a *particle damage/fragmentation function*. It has been demonstrated (Jaeger, 1967) that under equal loading magnitudes particles of equivalent strength will have a higher probability of failure (fracture) under low coordination number conditions.

If damage leads to particle fragmentation, the post fracture shape must be specified with simple geometry so that discrete element modeling can be used to handle the new particles. Thus through damage evolution, one particle may lead to the creation of two or more new particles. Some different approaches can be followed in developing particle fragmentation damage models. One particular approach can be built on the concept of a radius reduction as used by Richman, et al., (1989 ,1991), in which the size (radius) of interacting particles is reduced in relation to an established damage criteria built on impact energy principles. Schonert (1988) also developed an energy damage criteria based on the stored strain energy of particles. Another fragmentation approach could assume the creation of two or more self-similar particles, and this would follow the simple cleavage damage theories work of Mitchell, (1961) and Rudnick, et al., (1963) dealing with the indirect-tension (Brazilian) testing of brittle materials. The present DEM modeling will not address the post fracture behavior, and thus only the initiation and softening contact response will be pursued.

Focusing on granular materials with brittle particles, it would seem reasonable that a maximum tensile stress theory could be applied to develop a damage or fracture initiation criteria. For example, using the work of Rudnick, et al. (1963), it is found for the N = 2 case with diametrical compressive loading, that the maximum tensile stresses are developed normal to the diameter along the loading axis. From elasticity theory, the value of the maximum tensile stress for point boundary loading is given by

$$\sigma_{max} = \frac{2P}{\pi D t} \tag{4.2}$$

where P is the applied load, D is the particle diameter and t is the thickness. If it is assumed that failure occurs according to a maximum normal stress theory, the particle will fail by fracture along the loaded diameter. If the idealized concentrated boundary loading is replaced by a distributed loading acting over a small region (say as predicted by Hertz contact theory), the tensile stresses in the vicinity of the loading with be changed to compression. This effect however, is very local, and most of the loaded diameter will still be subjected to tensile stress given by relation (4.2). For other normal contact loadings at higher coordination number, the region of tensile stress decreases as

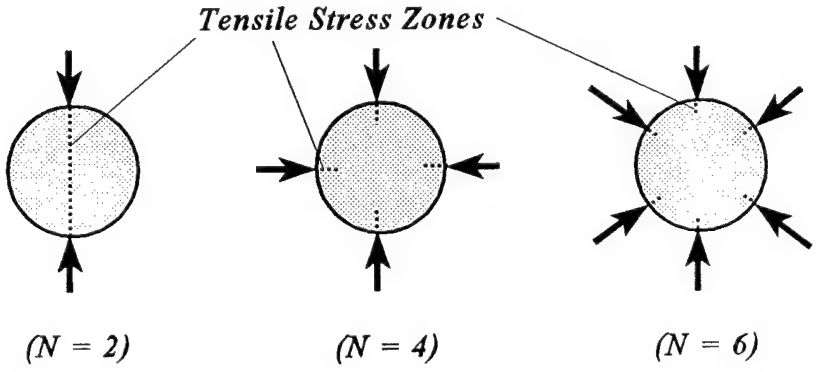

Figure 4.3. Tensile Stress Zones for Particles Under Various Loadings

shown schematically in Figure 4.3. For the case of N = 4, only about 35% of the loaded radii will be in tension. Jaeger (1967) investigated some additional details on the stress distribution in circular particles under coordination numbers of $N = 2$, 3 and 4. Of course in the limit as N becomes large, we approach the case of a circular particle under uniform pressure loading, and the state of stress within the entire grain will be uniform hydrostatic compression with no tensile stress zones.

For a two-dimensional packing of circular particles, the maximum coordination number possible is six. Thus for cases bounded by $N \leq 6$, the maximum tensile stress exists under the loading point, and is equal to the value for the $N = 2$ case given by equation (4.2). Thus as preliminary model, it is proposed that this result be used for all one and two-dimensional granular models to determine the initiation of damage. If σ_f represents the failure tensile stress of the grain material, then relation (4.2) can be used to predict the damage initiation normal contact force as

$$F_f = \frac{1}{2}\pi D t \sigma_f \qquad \textbf{(4.3)}$$

It is expected that if a contacting particle reaches this initiation value during its loading history, the contact law between the particle and its neighbors must be modified to reflect such damage. This type of modification would lead to a softening behavior related to the amount of damage that the contacting particles have undergone. A form which allows for several different softening behaviors is proposed as

$$F = \begin{cases} \alpha \delta^p \ldots\ldots\ldots\ldots \text{if } F < F_f \\ \alpha \delta^p + \alpha_1 (\delta - \delta_f)^r \ldots \text{if } F \geq F_f \end{cases} \qquad \textbf{(4.4)}$$

where α, p, α_1, and r are related to material and geometric properties of the particles. Example behaviors predicted by relation (4.4) are shown in Figure 4.4 for several softening cases. Such a

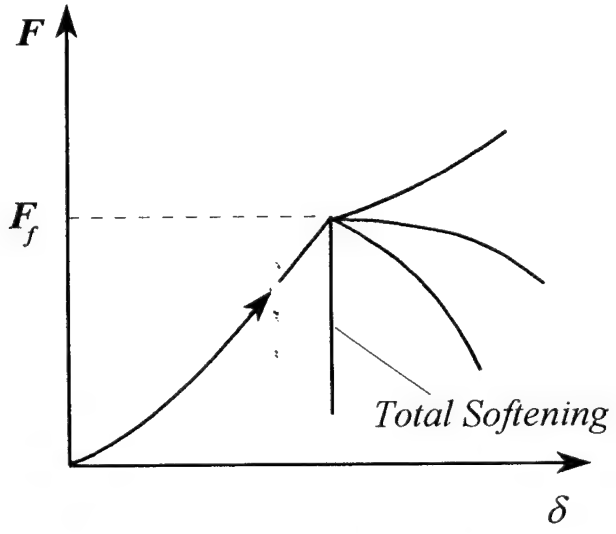

Figure 4.4. Softening Contact Laws

model can be used for a variety of damage ranging from small contact microcracking to complete particle fracture (total softening).

4.4 DEM SIMULATION RESULTS

4.4.1 One Dimensional Models

Using this simple modeling concept, preliminary discrete element simulations have been conducted for a single chain of particles as shown in Figure 4.5. Such an assembly consists of a single array of circular disk particles which are loaded at one end by a dynamic input. Each disk in the assembly is diametrically loaded thus having a coordination number, N = 2. It is assumed that the particle material is brittle with a particular failure stress σ_f, and that each disk particle will fail by the maximum normal stress criteria. The assembly model contained 30 disks, each with 25mm diameter and 6.4mm thickness, and material was chosen as quartz with a mass density of 2650 kg/m^3. The dynamic input consisted of a normal loading of triangular time dependence, with a maximum loading of 7 kN and duration of 60μs. The nonlinear-hysteretic normal contact law with damage as shown in Figure 4.4 was employed in the numerical simulation. For undamaged response the contact law parameters were chosen as p = 1.4 and $\alpha = 1.4 \times 10^9$ N/m$^{1.4}$.

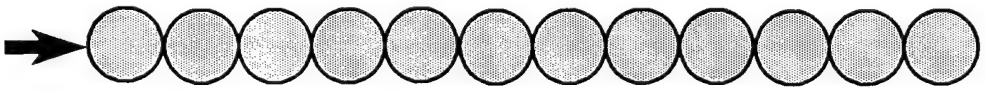

Figure 4.5. Single Chain Particulate Model

The DEM results of the interparticle contact load histories at each of the contact points are shown in Figure 4.6(a). Because the maximum tensile stresses generated by the external loading are smaller than σ_f, no particle damage occurs during wave propagation through the particle chain. The contact load histories thus follow a smooth and continuous rise and fall, and the peak interparticle contact loads attenuate with propagation distance. The average wave speed for this undamaged case is about 1950 m/s.

If however the input loading magnitude of 7 kN is used with a failure stress σ_f = 18 MPa, damage will occur and wave propagation behaviors will change. Figure 4.6(b) illustrates this case using a partial softening contact law shown in Figure 4.4, and equation (4.4) has been used with

p=1.4, $\alpha=1.4\times10^9$ N/m$^{1.4}$, r = 2 and $\alpha_1=2\times10^8$ N/m^2. For this case, the first few particles undergo damage (fracture) thus bringing into play the softening contributions of the contact law. Figure 4.6(b) demonstrates a discontinuous change in the contact load history, and this will produce a corresponding change in wave attenuation. The wave speed for this case is 1600m/s. A third case considered is that with the same input of 7kN and σ_f = 18MPa using the total softening behavior shown in Figure 4.4. DEM simulation results are shown in Figure 4.6(c), and it can be seen that a very significant drop in attenuation is predicted and the wave speed is about 1330 m/s for this particular case. Finally these three cases are compared in Figure 4.7, which plots the peak

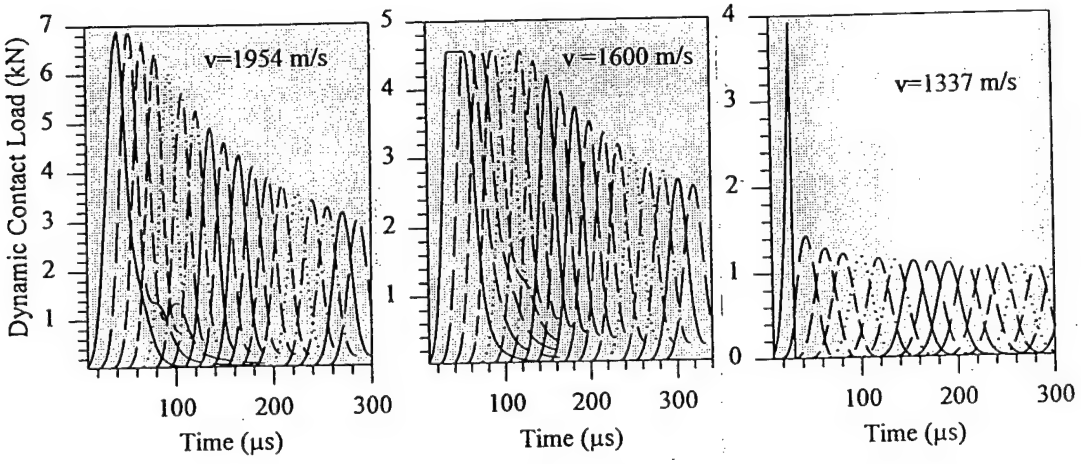

(a) No Damage (b) Partial Damage (c) Total Softening

Figure 4.6. Interparticle Contact Load Histories

contact force verses propagational distance. It is observed that damaged particulate media greatly influences the local wave attenuation behavior leading to significant amplitude decay and softening behavior results in slower wave speeds. Table 4.1 summarizes various DEM simulations by providing wave velocities and peak transmission ratios. The transmission ratio represents the peak amplitude output normalized with respect to the input.

4.4.2 Two-Dimensional Models

The first two-dimensional model to be studied was the hexagonal-closed-packing (HCP) assembly shown in Figure 4.8. The model consisted of 150 particles of identical size as used in

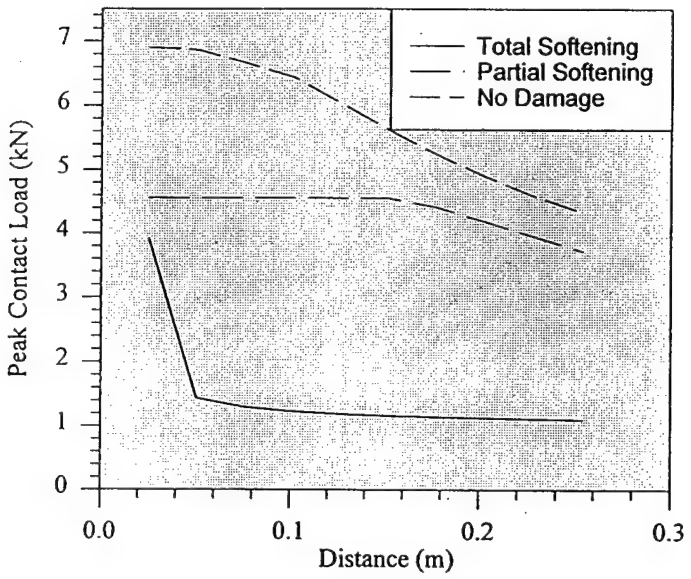

Figure 4.7. Attenuation Comparison of Damaged and Undamaged Behaviors

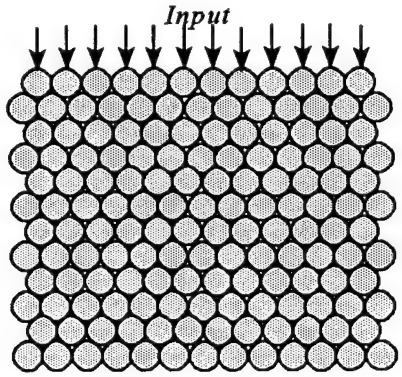

Figure 4.8. HCP Assembly Model

the single chain simulations. The input loading magnitude was 11kN with a duration of 60μs, and was applied as a planar input, loading all particles on the top of the assembly model as shown. Results illustrated in Figure 4.9 represent the average wave transmission behavior. The input signal is the average inter-particle contact behavior between the first and second layers, while the output is the average contact behavior between the last two bottom layers in the assembly. The three cases of no damage, partial softening and total softening are again shown. The effects of damage on the wave characteristics are similar to the one-dimensional case and are summarized in Table 4.1.

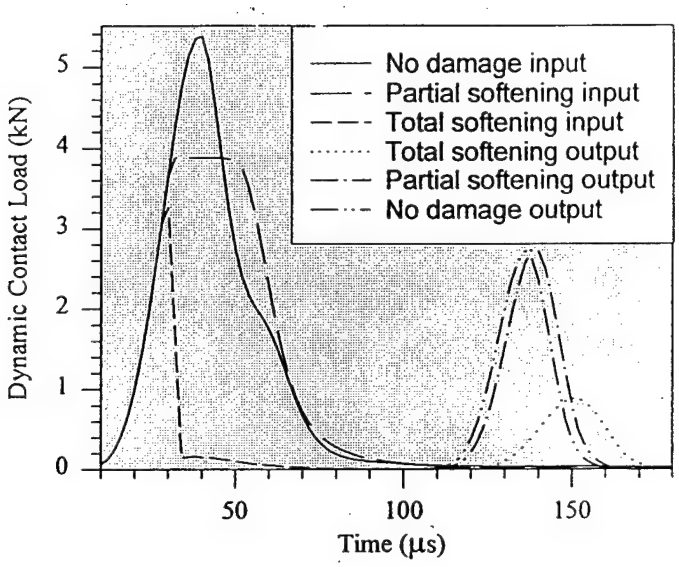

Figure 4.9. Transmission Behavior for the HCP Model

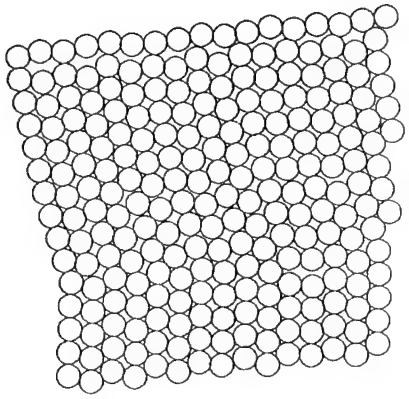

Figure 4.10. Random Assembly Model

A second two-dimensional model under study was a random assembly shown in Figure 4.10. This model was created using one of our numerical random generating codes, and consisted of 240 particles of identical size and type as used previously. The assembly was dynamically loaded by a vertical planar input on the top of the model similar to the HCP case using a magnitude of 7kN with duration 60μs. Again the three cases of no damage, partial softening and total softening are considered and the transmission results are shown in Figure 4.11 and summarized in Table 4.1.

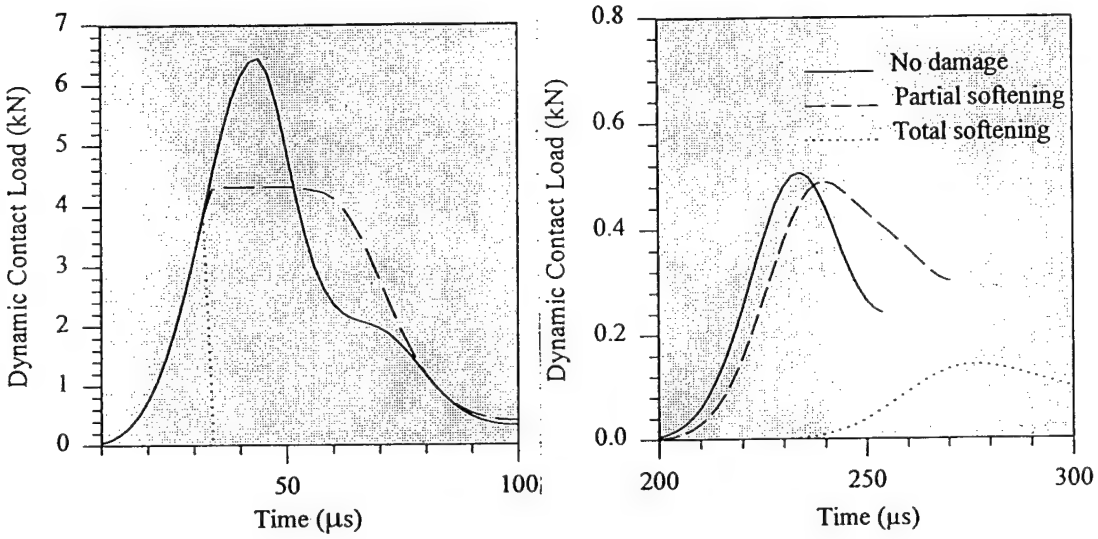

Figure 4.11 Transmission Behavior of the Random Assembly

Table 4.1 Summary of DEM Simulations

Model	Wave Speed (m/s)	Trans. Ratio
S. Chain (No Damage)	1954	0.41
S. Chain (Partial Damage)	1600	0.34
S. Chain (Total Damage)	1337	0.16
HCP (No Damage)	1800	0.25
HCP (Partial Damage)	1630-1930	0.25
HCP (Total Damage)	1440	0.08
Random (No Damage)	1450	0.07
Random (Partial Damage)	1300-1470	0.07
Random (Total Damage)	1110	0.02

4.5 SUMMARY

A preliminary discrete element study of the effect of particle damage on wave propagation in granular materials has been conducted. Damage is modeled through changes of the interparticle contact law between grains in model assemblies. The study assumes brittle particle behavior, and thus uses a maximum normal stress theory to establish a damage threshold for the interparticle contact force. Various softening
damage contact laws are used in a discrete element computer code to simulated wave propagation in several model materials.

Discrete element results for a single straight chain of circular particles indicate that the presence of damage (softening behavior) leads to changes in the wave speed and amplitude behavior. In general more severe wave attenuation occurs for the case with damage. For both partial and total interparticle softening behavior, the local wave amplitude is significantly affected and this leads to a higher attenuation rate. The wave speed is found to locally decrease for the cases with increasing damage. Similar behaviors were also observed in the two-dimensional simulations involving HCP and random assembly models. For the cases with damage, DEM simulations predict a damage zone propagating into the media from the input boundary. Although not considered in this research, this damage propagation could be determined as a function of the input loading, grain properties and the material microstructure.

This research establishes a model with qualitatively appropriate features; however, these preliminary results set the stage for a need of more definitive simulations. Future work is needed in which the damage/softening interparticle response could be experimentally determined for real materials. This could then be used in the DEM code to predict overall damage results in granular systems of such materials.

CHAPTER 5

STRESS WAVE PROPAGATION IN POROUS PARTICLE ASSEMBLIES

ABSTRACT

The effect of micro-structural particle porosity on stress wave propagation was investigated by drilling holes into model particles. Assemblies were subject to compressive stress waves initiated with explosive loading. Three different hole patterns were investigated, namely ring type specimens and rectangular and hexagonal arrays of holes . In all cases, the locations of the holes was fixed and the hole size was increased to increase the porosity. Primarily, the investigation covered the effects that the different types and levels of particle porosity had on group wave velocity and wavelength. The results showed that for all specimens, the velocity shows a monotonic decrease with increasing porosity. The hexagonal array showed a similar behavior to that seen in the ring specimens with a decrease of approximately 30 percent as the particle porosity increased from 0 to 30 percent. Over the same range, the rectangular array showed only a 15 percent drop in group wave velocity.

The characteristic group wavelength behavior differed widely between the three geometries. Most interestingly, the ring specimens showed a decrease of 25 percent in wavelength as porosity increased to about 10-15 percent, and then increased with further increasing porosity. The rectangular array showed the opposite with an increase of 15 percent in wavelength as porosity increased to about 15-20 percent and then a decrease with increasing porosity. The hexagonal array exhibited a continuous increase in wave length with increasing porosity. In general, the experiments showed that the degree of porosity alone is not the dominant factor in determining the effects on dynamic waves.

5.1 INTRODUCTION

The study of stress wave propagation in granular materials is important to many branches of science and engineering including geomechanics and powder metallurgy. Dynamic loads may occur due to earthquake motion, underground explosions, and construction operations. The ability to predict the behavior of structures and foundations necessitates the understanding of wave motion in granular media such as sand, rock, and clay. Granular materials, having spatial discontinuities in their mass density, are modeled here as an array of elastic particles interacting only through contact mechanics, and wave propagation in them is strongly dependent on their micro-structure. A sizeable amount of work has been done to study the wave propagation phenomenon in granular materials from

a micro-structural standpoint. Some of the earliest work is due to Ida, (1939), who used a simple lumped mass-spring model. Contemporary work has proposed new modeling approaches such as the fabric tensor theory (Nemat-Nasser, 1983), the distributed body theory (Goodman and Cowin, 1972), and the distinct element method (Cundall, et al., 1979, and Sadd 1993) in order to predict the behavior of granular media.

Experimental techniques, such as dynamic photoelasticity, have been employed to study the dynamic response of granular materials under explosive loading (Shukla, 1985 and 1992). Later studies by Shukla, et al., (1991) using photoelasticity in conjunction with high speed photography further investigated the effects of particle shape on wave propagation behavior in granular assemblies of elliptic particles. They showed that the wave velocity was dependent on the particle shape. The wavelength of the stress wave pulse showed no change with the particle shape as long as the contact interval (the number of contact points per unit wavelength which was four disk diameters) is kept constant. The load transfer characteristics change with variations in particle shape. However, in most of the past work the granular media was simulated by assemblies of circular or elliptical particles.

An experimental study has been conducted on the dynamic response of granular materials with specific interest in investigating the effect of particle porosity on stress wave propagation characteristics. Particle porosity was achieved by drilling holes in the circular disks. Hole size and the pattern was varied to create different porosity levels as well as various hole distributions. Results indicate that the porosity level alone is not adequate to predict the behavior of a propagating stress wave. The size and distribution of the holes plays a role in the wave propagation behavior.

5.2 EXPERIMENTAL PROCEDURE

Dynamic photoelasticity coupled with high speed photography was used to study the wave propagation process in particulate assemblies. The assemblies were modeled with 25.4 mm diameter circular disks arranged in a single chain assembly (see figure 5.1). A number of the disks in the assembly had holes drilled through them to simulate porosity. The hole size and pattern was varied and the effect on propagating waves were studied. Porosity, η, will be defined as

$$\eta = \frac{area\ of\ holes}{area\ of\ disk} \qquad (5.1)$$

Figure 5.2 shows the various hole patterns studied, as well as the hole sizes. This work also

draws upon previous work by Y. Zhu (1996) which was a preliminary look into these effects utilizing only the ring type specimen. This work extends Zhu's (1996) work but also includes regular rectangular arrays of holes and hexagonal arrays of holes. The disks were machined from Homalite-100, a birefringent polymer, with a coolant running to prevent residual machining induced stresses.

The disk assembly was placed in the optical bench of a high speed Cranz-Schardin camera which provides twenty images of the event at discrete times during the passage of the compressive wave. A small amount of lead azide was detonated at the top of the disk chain to induce a dynamic compressive pulse in the chain. Photographs were taken at a preset delay time from the explosive detonation.

5.3 RESULTS

Figure 5.3 shows six of the twenty frames from a typical experiment with ring type specimens having a hole diameter of 11.5 mm and a porosity of 21 percent. For comparison, figures 5.4 and 5.5 show similar photographs for the hexagonal and rectangular arrays, respectively. Wave front position can be obtained directly from the experimental photographs. The slope of the position / time plot yields average wave front velocity. These position versus time plots were made for each experiment and figure 5.6 shows normalized velocity as a function of porosity for each of the three specimen types. Wave front velocities were normalized with the baseline velocity seen in an assembly of undrilled disks (0 percent porosity).

The plot shows that the ring and hexagonal array specimens exhibited similar behavior. The regular rectangular array specimen showed much less of a decrease in velocity with porosity. It is believed that this type of specimen presented less of a physical barrier to the propagating wave than the other specimens. As the wave propagated through the specimen, there was a clear path of solid material to move through. The ring and hexagonal array specimens presented free surfaces blocking the direct propagation of the wave. As porosity increased for all specimen types, the velocity decreased.

This behavior is similar to that seen by Shukla and Prakash (1990) who studied wave propagation in porous plates. These plates also had hexagonal and rectangular arrays of holes to simulate porosity. Their research showed that wave velocity decreased in the plates with increasing porosity. Also, the rectangular array consistently showed higher wave speeds when compared to the hexagonal array.

In the case of the ring specimens, the decrease in velocity can be attributed to two different mechanisms. First, the stiffness of the system is decreasing with the increasing porosity (hole size). As a general rule, softer systems produce slower wave speeds. Second, the larger the hole, the larger a reflecting surface for the incoming wave. The propagating wave is forced to make multiple reflections within each particle before reaching the opposite contact.

It is not believed that the over all stiffness of the specimens decreased significantly with the addition of the multiple holes. The first of the reasons for decreasing wave velocity in the multi-holed specimens is then not considered to be the major factor in the decreasing wave speed. The second reason is then proposed to be the major factor. It is believed that the increased reflecting surface area are the primary reason for decreasing wave speeds in the multi-holed specimens. This would support the earlier comment that the regular array of holes yields higher wave speeds because it offers a direct propagation path through the center of each particle.

Group wave length was measured directly from the experimental photographs. The distance between the leading and trailing edges was normalized by the wave length in the baseline (0 percent porosity) chain and plotted against the porosity in figure 5.7. Group wave length behaviors were different for each specimen type with the ring type specimens exhibiting the most dramatic behavior. The wavelength drops by as much as 25 percent as the porosity increased to approximately 10 percent. Then the wavelength increases to approximately 10 percent more than the 0 percent porosity case as the porosity is increased to 25 percent.

The other two cases showed more subtle changes in wavelength with increasing porosity. The hexagonal pattern showed a constantly increasing wave length with increasing porosity. The wave length increased approximately 25 percent through the range of porosities tested. The regular array, on the other hand, showed an increase and then a decrease in wave length. The maximum of 115 percent of the baseline occurred at approximately 20 percent porosity.

In order to explain the unusual behavior seen in these experiments it must first be noted that the principle mechanisms governing the propagation of waves in these model particles are scattering, dispersion, and diffraction. We must also note that the observed behavior is a function of the experimental technique being used. Any limitations in the technique will have adverse effects on the results.

Photoelasticity was used to capture full field stresses in the particles. The images are actually fringes, or lines, of constant maximum shear stress. Recall the fundamental relationship between

observed fringes and stress for photoelasticity,

$$\tau_{max} = \frac{N f_\sigma}{2h} \tag{5.2}$$

where N is the observed fringe order, f_σ is the optical fringe constant, and h is the thickness of the specimen. If there is insufficient stress to cause a half order fringe, we observe nearly nothing in the images. For these experiments, using the fringe constant for Homalite-100 and a disk thickness of 6 mm, the stress required to generate a half order fringe is 0.96 MPa.

At this time it is speculated that the observed drop in the wave length is due to a change in the shape of the propagating pulse and an artifact of the resolution capabilities of the experimental technique. Previous research into one dimensional inhomogeneous media (Schreyer, 1977) has shown that discontinuities cause the leading edge of a wave to sharpen and the trailing edge to widen. It is postulated that a similar behavior is being exhibited by these disk chains.

Due to the free surface of the hole, wave energy is being trapped in the particles as the wave propagates down the chain. The leading edge of the pulse is 'stacking up' on its self as it enters a particle and impinges upon the hole. The energy associated with the propagating wave is being spread among more and more particles as the wave propagates down the disk chain due to multiple reflections in each particle.

Figure 5.8 shows a graphical depiction of the proposed hypothesis to explain the observed behavior. The figure shows a series of envelopes which represent the wave shape as a function of particle porosity for the ring-type specimens. Also depicted in the figure is the minimum, or threshold, value of stress required to generate a half order fringe.

For the 0 percent porosity case (solid line) the wave shape is symmetrical about its center point. However, this does not seem to be the case for the ring type specimens. The ring type specimens tend to exhibit a higher fringe order in the leading edge of the wave and a lower fringe order trailing edge. When the particle porosity is low, there is only a small amount of energy left behind in the trailing edge of the wave and the stresses tend to rise more sharply at the leading edge. The wave length appears shorter because wave energy is being trapped in each particle that the wave propagates through. At this point, the energy left behind is not yet significant enough to generate observable stresses. However, as the porosity increases, the energy associated with the trailing edge increases and eventually crosses the observation threshold.

Visual confirmation for a sharpening of the leading edge of the wave is offered in figure 5.3, frame 16. One can easily see that the general magnitude of the observed fringes is much higher in the first two disks while the last two disks have only a half order fringe visible. The fringe magnitude is not symmetric about the perceived center of the wave as is seen in the 0 percent porosity case. Contrasting this to the less dramatic wave length / porosity behavior observed in the multi-holed specimens, the fringes observed in the multi-holed specimens appear symmetric about the center of the propagating wave.

5.4 CONCLUSION

The experiments have shown that particle porosity affects the group wave velocity and the group wave length. The location and size of the holes in the model particles determined the affect on the wave propagation parameters. Holes which block the direct propagation path of the wave through the particle slowed the wave front approximately 25 percent when compared to the baseline case of 0 percent porosity. The rectangular array of holes slowed the wave front only 10 percent for the same change in particle porosity.

The results showed that for all specimens, the velocity shows a monotonic decrease with increasing porosity. The hexagonal array showed a similar behavior to that seen in the ring specimens with a decrease of approximately 30 percent as the particle porosity increased from 0 to 30 percent. Over the same range, the rectangular array showed only a 15 percent drop in group wave velocity.

The characteristic group wavelength behavior differed widely between the three geometries. Most interestingly, the ring specimens showed a decrease of 25 percent in wavelength as porosity increased to about 10-15 percent, and then increased with further increasing porosity. The rectangular array showed the opposite with an increase of 15 percent in wavelength as porosity increased to about 15-20 percent and then a decrease with increasing porosity. The hexagonal array exhibited a continuous increase in wave length with increasing porosity. In general, the experiments showed that the degree of porosity alone is not the dominant factor in determining the effects on dynamic waves.

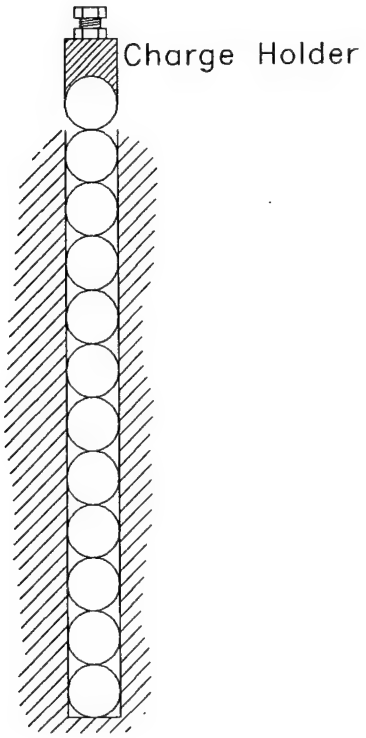

Figure 5.1. Schematic of the single chain of model particles used in dynamic experiments.

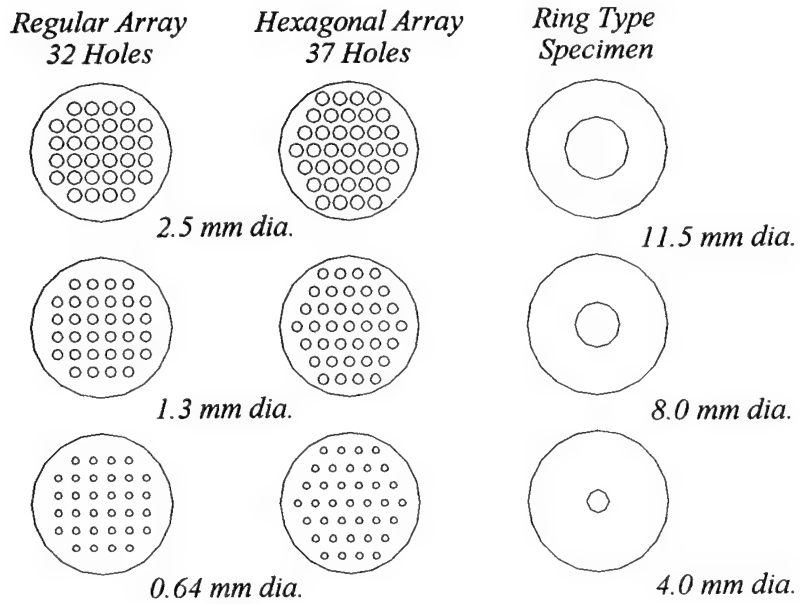

Figure 5.2. Specimen geometry for porous particle experiments.

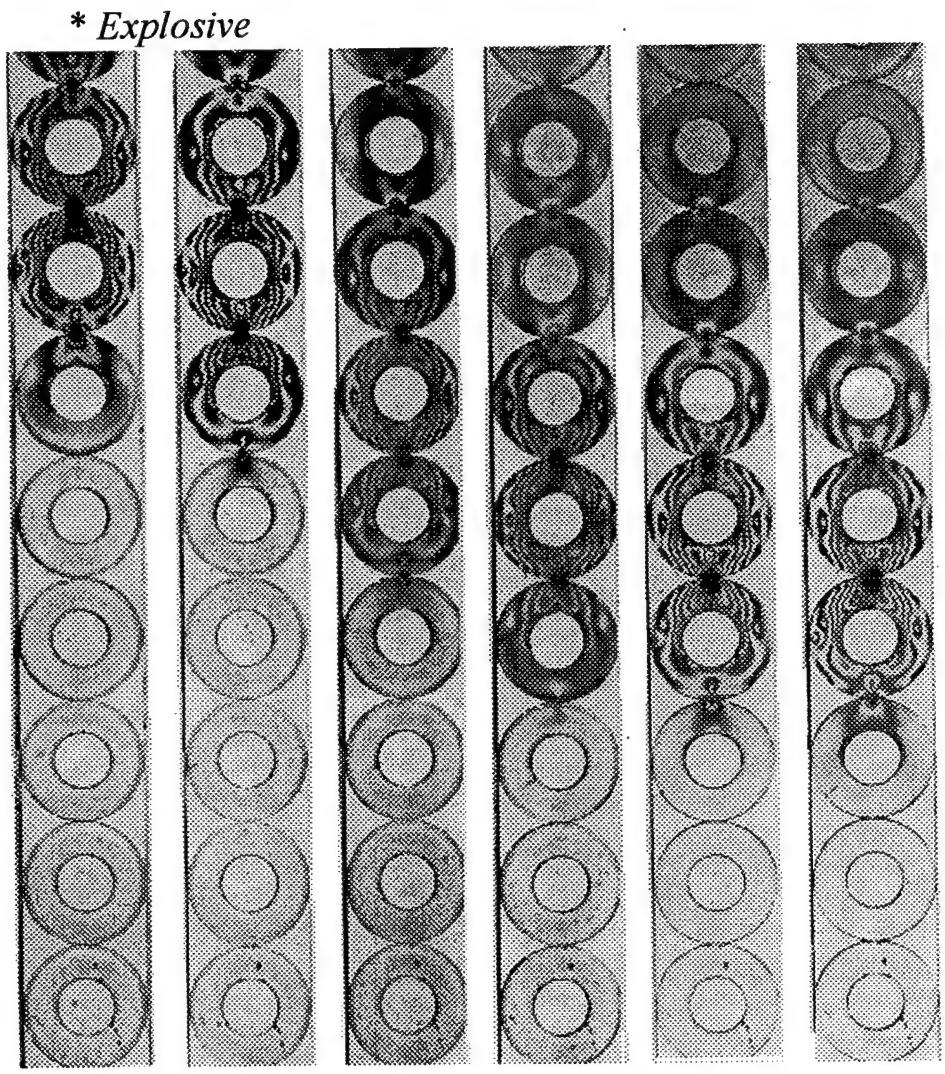

Figure 5.3. Typical isochromatic fringe patterns for the ring-type specimen with a particle porosity of 21 percent.

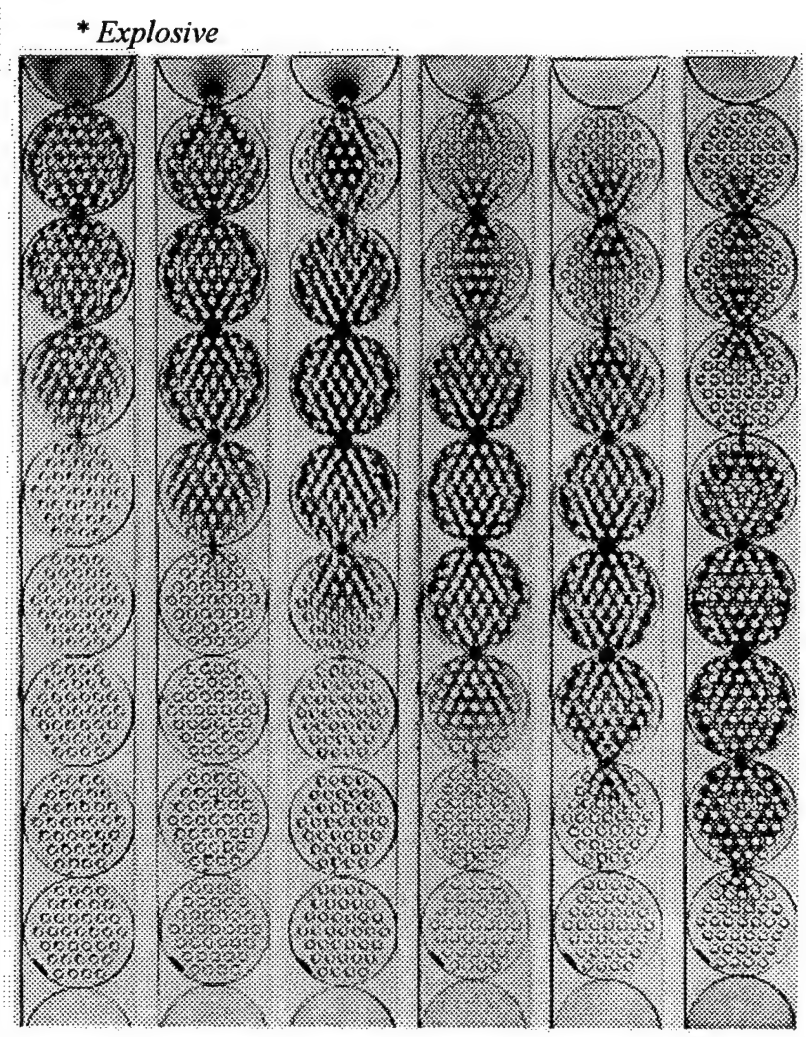

Figure 5.4. Typical isochromatic fringes for the hexagonal array of holes (particle porosity = 21%).

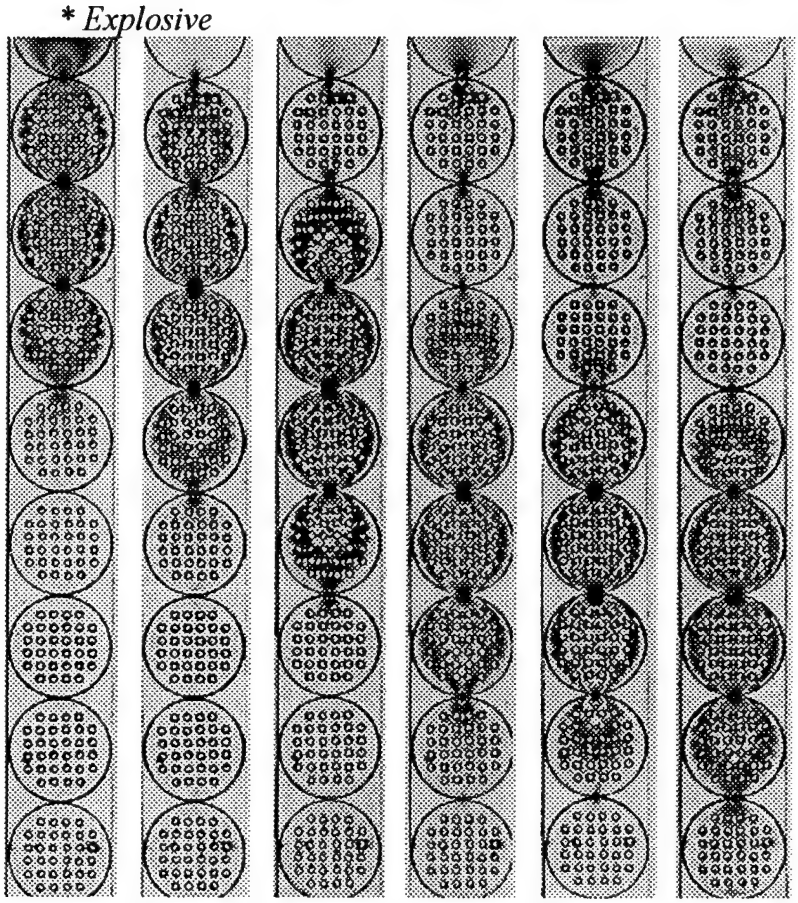

Frame 2 *Frame 6* *Frame 10* *Frame 12* *Frame 14* *Frame 18*
268.5 μs *291.5 μs* *315.5 μs* *346.5 μs* *358.5 μs* *382 μs*

Figure 5.5. Typical isochromatic fringes for the rectangular array of holes (particle porosity = 8%).

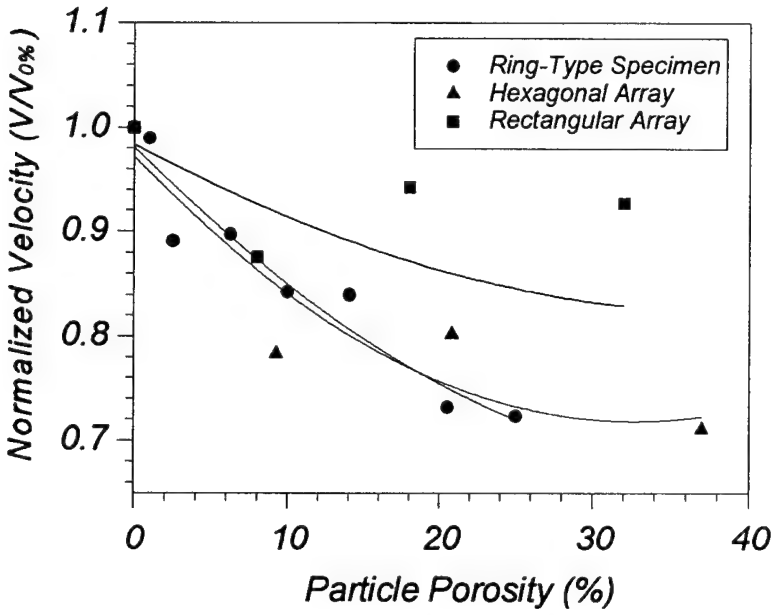

Figure 5.6. Normalized velocity as a function of particle porosity.

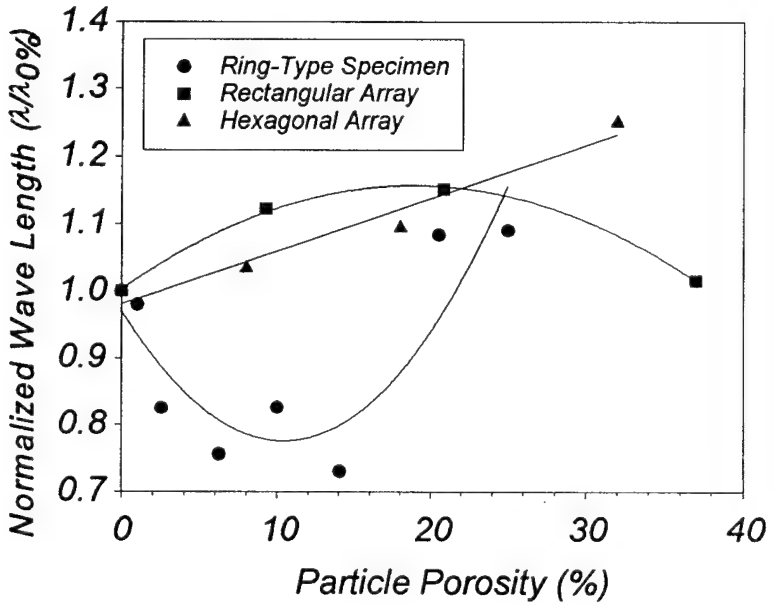

Figure 5.7. Normalized wave length as a function of particle porosity.

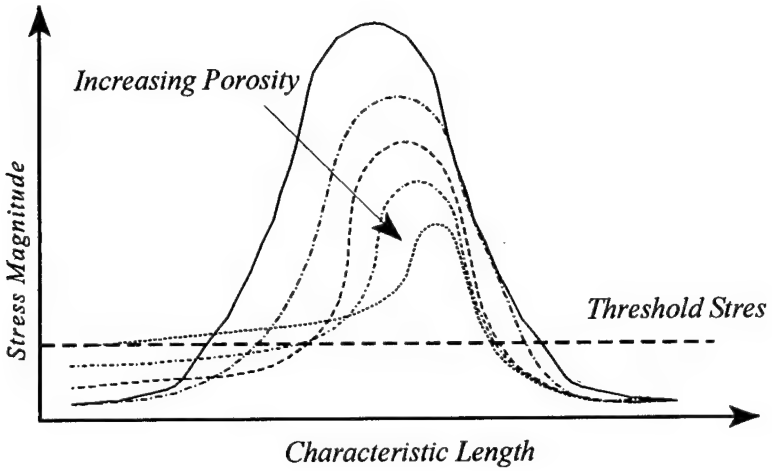

Figure 5.8. Graphical depiction of the change in the propagating wave due to increasing porosity.

BIBLIOGRAPHY

Alehossein, H. And Muhlhaus, H.B., (1994) "An Elastodamage Cosserat Continuum Model for Comminuting Granular Media", *Computer Methods and Advances in Geomechanics, Siriwardane & Zaman (eds), Balkema, Rotterdam.*

Arbiter, N., Harris, C.C., and Stambolitzis, G.A., (1969) "Single Fracture of Brittle Spheres.", *Trans. SME, AIME,* Vol.244, *pp. 118-133.*

Barbosa, R.E., and Haboussi, J.G., (1990) "Discrete Finite Element Method for Multiple Deformable Bodies", *Finite Elements in Analysis and Design,* Vol.7, *pp. 145-158.*

Bruno, M.S., (1991) "Microstructural Analysis of the Inelastic Behavior of Sedimentary Rock", *Mechanics of Materials,* Vol.12, *pp. 95-118.*

Bruno, M.S., (1994) "Micromechanics of Stress-induced Permeability Anisotropy and Damage in Sedimentary Rock", *Mechanics of Materials,* Vol.18, *pp. 31-48.*

Chang, C.S., (1993) "Micromechanical modeling of deformation and failure for granulates with frictional contacts", *Mechanics of Materials,* Vol.16. *pp. 13-24.*

Chen,W.F., and Pan,A.D., (1991) "Finite Element and Finite Block Methods in Geomechanics," *Proc. of 3rd Int. Conf. on Const. Laws Eng. Matls.*

Cundall, P.A. and Strack, O.D.L. (1979) "A Discrete Numerical Model for Granular Assemblies," *Geotechnique,* Vol.29, *1, pp.47-65.*

Fukumoto, T. , (1992) "Particle Breakage Characteristics of Granular Soils", *Soils and Foundations,* Vol. 32, *pp. 26-40.*

Gebara, J.G., Pan, A.D., and Anderson, J.B., (1993) "Finite Block Analysis of the Impact of High Kinetic Energy Penetrators into Rock Rubble", *Proceedings of the 2nd Int. Conf. on DEM , MIT, pp. 301-313.*

Gilvarry, J.J., (1961) "Fracture of Brittle Solids. I. Distribution Function for Fragment Size in Single Fracture (Theoretical)" , *J. App. Phys.* Vol.32 *.pp. 391-399.*

Grady, D.E., and Kipp, M.E., (1985) "Geometric Statistics and Dynamic Fragmentation", *J. Appl. Phys.* Vol.58 *,, pp. 1210-1222.*

Gross, D., and Zhang, C.H., (1992) "Wave Propagation in Damaged Solids", *Int. J. Solids Structure,* Vol. 29, *pp. 1763-1779.*

Hardin, B.O., (1985) "Crushing of Soil Particles", *J.Geotech. Eng., Vol.*111, *pp. 1177- 1192.*

Hagerty, M.M., Hite, D.R., Ullrich, C.R., and Hagerty ,D.J., (1993) "One-Dimensional High-Pressure Compression of Granular Media" , *J. Geotech. Eng. Vol.119 ,pp. 1-18.*

Hocking, G. , (1992) "The Discrete Element Method for Analysis of Fragmentation of Discontinua", *Engineering Computations, Vol.9, pp. 145-155.*

Ishibashi, I., Agarwal, T.K., and Wang, Y., (1994) "Hybrid Finite Element/Discrete Element Model for Large Deformation Geotechnical Engineering Problems", Computing in Civil Engineering. No.1, pp. 857-864.

Jaeger, J.C., (1967) "Failure of Rocks under Tensile Conditions", *Int. J. Rock. Mech. Min. Sci.*, Vol 4, pp 219-227.

Jeulin, D., (1993) "Damage Simulation in Heterogeneous Materials from Geodesic Propagations", *Eng. Computations, Vol.10, pp. 81-91.*

Kendall ,K., and Gregory, R.D., (1987) "Fracture of Radially Edge-cracked Discs", *J. of Mat. Sci. Vol.22, pp. 4514-4517.*

Malvern, L.E., Jenkins, D.A., Tang, T., and Gong, J., (1989) "Dynamic Testing of Concrete with the Split Hopkinson Pressure Bar," *Proc. Fourth Int. Symposium on the Interaction of Non-nuclear*

Munitions with Structures, Panama City Beach,Florida, *April 17-21, pp. 296-301.*

Mansour, A. and Seireg, A., (1983) "A Computer-Based Simulation of Ice-Breaking by Impact", *J. Energy Res. Tech. Trans. of the ASME, Vol.105 , pp. 448-453.*

Meguro, K., and Hakuno, M., (1994) "Application of the Extended Distinct Element Method for Collapse Simulation of a Double-deck Bridge", *Structural Engineering/Earthquake Engineering Vol.10, pp. 175s-185s.*

Mustoe, G.G.W., Williams, J.R., Hocking, G., and Worgan, K. J., (1987) "Penetration and Fracturing of Brittle Plates under Dynamic Impact", *NUMETA '87*, Swansea, UK

Mitchell, N.B., (1961) "The Indirect Tension Test for Concrete", *Mat. Res. & Standards, pp. 780-788.*

Munjiza, A., Owen, D.R.J. and Bicanic, N., (1995) "A Combined Finite-Discrete Element Method in Transient Dynamics of Fracturing Solids", *Eng. Com.,, Vol.12, pp. 145-174.*

Nagahama, H., and Yoshii , K., (1993) "Fractal Dimension and Fracture of Brittle Rocks", *Int. J. Rock Mech. Min. Sci. & Geomech. Abstr. Vol. 30, pp. 173-175.*

Palmer, A.C., and Sanderson, T. J. O., (1991) "Fractal Crushing of Ice and Brittle Solids", *Proc. R. Soc. Lond. A, Vol. 433, pp. 469-477.*

Pan, X.D., and Reed, M.B., (1991) " A Couple Distinct Element -Finite Element Method for Large Deformation Analysis of Rock Masses", *Int. J. Rock Mech. Min. Sci. & Geomech. Abstr. Vol.28, pp. 93-99.*

Richman, M.W. and Oyediran, A.A., (1991) "Grain Size Reduction in Granular Flows of Spheres: The Effects of Critical Impact Energy ", *J. of Applied Mechanics, Trans. of the ASME, No.91-WA/APM-20, pp. 1-6.*

Richman, M.W., and Chou, C.S., (1989) "A Theory for Grain-Size Reduction in Granular Flows of Spheres", *J. App. Math. and Phys.,Vol. 40, pp. 883-898.*

Rudnick, A., Hunter,A.R., and Holden. F.C., (1963) "An Analysis of the Diametral-Compression Test", *Mat. Res. & Standards. pp. 283-289.*

Sadd, M.H., Shukla, A., and Mei, H., (1989) "Computational and Experimental Modeling of Wave Propagation in Granular Materials",*Proc.4th Int. Conf. Comp. Meth. and Exp.Italy. pp. 325-334.*

Sadd, M.H., Tai, Q.M., and Shukla, A., (1993) "Contact Law Effects on Wave Propagation in Particular Materials Using Distinct Element Modeling",*Int. J. Non-linear Mech.,Vol. 28, pp. 251-265.*

Saka, M., Ohba, S., Aizawa, N., and Abe, H., (1994) "Analysis of Nonlinear Wave Propagation and Shock Wave Formation in Quasi-brittle Material", *JSME Int. J. Series A, Vol. 37, pp. 421-427.*

Schonert, K., (1988) "A First-Survey of Grinding with High-Compression Roller Mills", *Int. J. Miner Process.*, Vol 22, pp. 401-412.

Schreyer, H.L. (1977), "One-Dimensional Elastic Waves in Inhomogeneous Media," *J. Engng. Mech. Div., Proc. Am. Soc. Civil Engineers*, **103**(EM5), 979-989

Shi, G. H., (1993) *Block System Modeling by Discontinuous Deformation Analysis, Topics in Engineering, Vol. 11, Comp. Mech., Southampton, U.K.*

Shin, J. G., and Karr , D.G., (1994) "Propagation of Continuum Damage in a Viscoelastic Ice Bar ", *J. Offshore Mech. and Arctic Eng.,Trans. of ASME, Vol. 116, pp. 109-113.*

Shukla, A., Singh, R. and Zervas, H., (1995) "A Effect of Flaws on Stress Wave Propagation in Particulate Aggregates: Near and Far Field Observations", *Intl. J. Solids and Structures, Vol 32, pp. 2523-2546.*

Smith, R.W., and Srolovitz, D.J., (1994) "Simulation of Dynamic Fracture of an Impact-loaded

Brittle Solid". *Modelling Simul. Mater. Sci. Eng. Vol.2, pp. 1153-1170.*

Thornton, C., Kafui, D.K., and Yin,K.K., (1993) "Application of DEM to Impact Fracture/ Fragmentation", *proceedings of the 2nd int. conf. on DEM conference. MIT, pp. 265-273.*

Turcotte, D.L., (1986) "Fractals and Fragmentation", *J. of Geophys Research, Vol.91, pp. 1921-1926.*

Toi, Y., and Che, J.S., (1994)"Computational Damage Mechanics Models for Brittle Microcracking Solids Based on Mesoscopic Simulations", *Eng. Frac. Mech., Vol.48, pp. 483-498.*

Toi, Y., and Kiyosue, T., (1995) "Damage Mechanics Models for Brittle Microcracking Solids Based on Three-dimensional Mesoscopic Simulations", *Eng. Frac. Mech., Vol.50, pp.11-27.*

Zhu, Y. (1996), "Particle shape effects on dynamic load transfer in granular media," Ph.D. Dissertation, University of Rhode Island.

SUMMARY OF PUBLICATIONS AND THESES/DISSERTATIONS

All of this previous work has resulted in several journal publications, conference presentations and thesis and dissertations as listed below.

Publications

1. "Dynamic Response of Damaged Particulate Media," *Proceedings of the 1993 SEM 50th Anniversary" Spring Conference on Experimental Mechanics,* June 1993, pp. 1119-1128.
2. "Effect of Flaws on the Stress Wave Propagation in Particulate Aggregates: Near and Far Field Observations," *International Journal of Solids and Structures,* 32(17/18), 1995, pp. 2523-2546.
3. "Explosively Generated Pulse Propagation Through Particles Containing Natural Cracks," *Mechanics of Materials*, 23, 1996, pp. 255-270.
4 "The effect of Particle Damage on Wave Propagation in Granular materials", with J. Y. Gao, *Mechanics of Deformation and Flow of Particulate Materials*, pp. 159-173, Ed. C. S. Chang, A. Misra, R. Y. Liang and M. Babic, Proc. of McNu Conference, Trans. ASCE, Northwestern University, June 1997.

Theses and Dissertations

1. Dr. Harry Zervas, Title of Dissertation: "Study of Stress Wave Propagation in Damaged Particulate Media," Ph.D., 1995.
2. Mr. Frank Sienkiewicz, Title of Dissertation: "Influence of Cementation and Moisture on Load Transfer in Particulate Materials," Ph.D., 1997.

Other Graduate Participants

Dr. Raman Singh, J. Y. Gao

Interactions/Transitions

During the past year we have had several interactions with other civilian and DOD laboratories. In addition, several presentations of our work have been made at national meetings.

We presented an overview of our research at the *Workshop on Mechanics and Statistical Physics of Particulate Materials* hosted by the *Institute for Mechanics and Materials* at the University of California - San Diego, June, 1994.

We have interacted with the Naval Undersea Warfare Center at Newport, RI. *Mr. Harry Zervas,* a senior engineer at NUWC, worked on his doctorate on this project. He is a co-author on our papers on damaged particles.

Our work has been presented at the Spring Conference of the Society of Experimental Mechanics at Baltimore, MD, 1995.

Interaction with *Dr. Jack Dvorkin* of Stanford University's Department of Geophysics, Stanford, California, has continued throughout the course of this project.

September, 1995, we presented an overview of our research work on wave propagation in granular materials to a NRL workshop on *Shock Wave Propagation Prediction* organized by Mark Emery at NRL, Washington, DC.

Results of our work on particle shape effects were presented at the ASME *Particulate Mechanics Symposium,* June, 1996, at John's Hopkins University.

Results of our work were presented at Texas A&M University Department of Mechanical Engineering in a seminar given by A. Shukla, April, 1995.

Results of our work were presented at California Institute of Technology Department of Aeronautics and Mechanics, May, 1995.

Results of our work were presented at McNu Conference, Northwestern University, June 1997.

HONORS/AWARDS

Professor Arun Shukla was elected *Fellow* of the *Society of Experimental Mechanics, 1994.*

Professor A. Shukla was elected Fellow of the American Society of Mechanical Engineers.

Mr. Frank Sienkiewicz received the First Prize for a Technical Paper Presentation at the National SEM Conference on Experimental Mechanics, 1993.

Mr. Frank Sienkiewicz received an Outstanding Paper Award at the Northeast Graduate Student Symposium on Mechanics, at the University of Rhode Island, 1997.